

Advances in Membranes from Microporous Materials for Hydrogen Separation from Light Gases

Nicholaus Prasetya* , I Gede Wenten, and Bradley Paul Ladewig*

With the pressing concern of the climate change, hydrogen will undoubtedly play an essential role in the future to accelerate the way out from fossil fuel-based economy. In this case, the role of membrane-based separation cannot be neglected since, compared with other conventional process, membrane-based process is more effective and consumes less energy. Regarding this, metal-based membranes, particularly palladium, are usually employed for hydrogen separation because of its high selectivity. However, with the advancement of various microporous materials, the *status quo* of the metal-based membranes could be challenged since, compared with the metal-based membranes, they could offer better hydrogen separation performance and could also be cheaper to be produced. In this article, the advancement of membranes fabricated from five main microporous materials, namely silica-based membranes, zeolite membranes, carbon-based membranes, metal organic frameworks/covalent organic frameworks (MOF/COF) membranes and microporous polymeric membranes, for hydrogen separation from light gases are extensively discussed. Their performances are then summarized to give further insights regarding the pathway that should be taken to direct the research direction in the future.

1. Introduction

With the pressing concern of global climate change, hydrogen will undoubtedly play an essential role as the main source of clean energy carrier in the future. Within the context of hydrogen economy, the main advantages of using hydrogen are primarily to reduce the concentration of the greenhouse gases in the atmosphere and also to eliminate the dependency fossil fuel-based economy that continuously aggravates the environmental issues.^[1,2] It is then expected that such energy transition will significantly contribute in mitigating the climate change

N. Prasetya

Institute of Functional Interface (IFG), Karlsruhe Institute of Technology, Hermann-von-Helmholtz-Platz 1, 76344, Eggenstein-Leopoldshafen, Germany
E-mail: nicholaus.prasetya@partner.kit.edu


N. Prasetya, Prof. B. P. Ladewig

Paul Wurth Chair, Faculty of Science, Technology and Medicine, University of Luxembourg, 2, Avenue de l'Université, L-4365, Esch-sur-Alzette, Luxembourg

E-mail: bradley.ladewig@uni.lu

Prof. I. G. Wenten

Department of Chemical Engineering, Institut Teknologi Bandung, Jalan Ganesha 10, Bandung 40132, Indonesia

 The ORCID identification number(s) for the author(s) of this article can be found under <https://doi.org/10.1002/eam2.12843>.

DOI: 10.1002/eam2.12843

issues, particularly if the hydrogen can be fully produced from renewable resources and by utilizing clean energy.

Despite its potential as a promising energy carrier and its abundance, the hydrogen does not come naturally as a gas and is always in combination with other elements. Therefore, there are a number of common ways to produce hydrogen such as by hydrocarbon reforming.^[2] Up to now, hydrogen production from steam methane reforming (SMR) combined with water gas shift (WGS) reaction can still be considered as the most economically viable and therefore cannot be neglected from the perspective of hydrogen economy, although it still depends on the fossil fuels.^[2,3] In the case, the syngas containing H₂ and CO is firstly produced and the CO will be further converted into CO₂ through WGS reaction. The separation of H₂ from the CO₂ and unconverted CH₄ in this case becomes crucial so the H₂ can be further used for power generation.^[4,5]

Hydrogen can also be obtained by recovering the purge gases from various industries such as from the ammonia plant, iron and steel industry in the form of coke oven gas or off-gas from refineries.^[6–8] In the case of ammonia plant, for example, the hydrogen is firstly produced mostly through natural gas reforming to synthesize ammonia which is mainly further used in fertilizer industries. About 96% of the ammonia is still currently produced through the conventional energy-intensive Haber–Bosch process and therefore contributes to around 1.4–1.8% of the global CO₂ emission while also utilizing around 2% of the global energy production.^[9,10] Considering the vast amount of the hydrogen required to produce ammonia, it is then also released in a significant amount from an ammonia plant. It is estimated that a stream of up to 180–240 Nm³ per ton of ammonia has to be purged containing large quantities of hydrogen (up to 67% of H₂, 25% of N₂ and a mixture of other gases).^[11] The hydrogen in this stream is has a huge potential to be recovered as an energy carrier once it can be effectively and efficiently separated from the rest of the stream components. Another example can also be seen in the post-combustion gaseous stream from the production of carbon black consisting of approximately 60.5% N₂, 17.9% CO, 16.4% H₂, and 5.3% CO₂.^[12] Once this flue gas is further used for power generation by converting to CO₂, water, and heat, the remaining flue gas still consists of low concentration of hydrogen that could potentially be recovered from the nitrogen as the major component.

Another scenario can also be seen in the future regarding the planning to transport the hydrogen. Taking into account that transporting

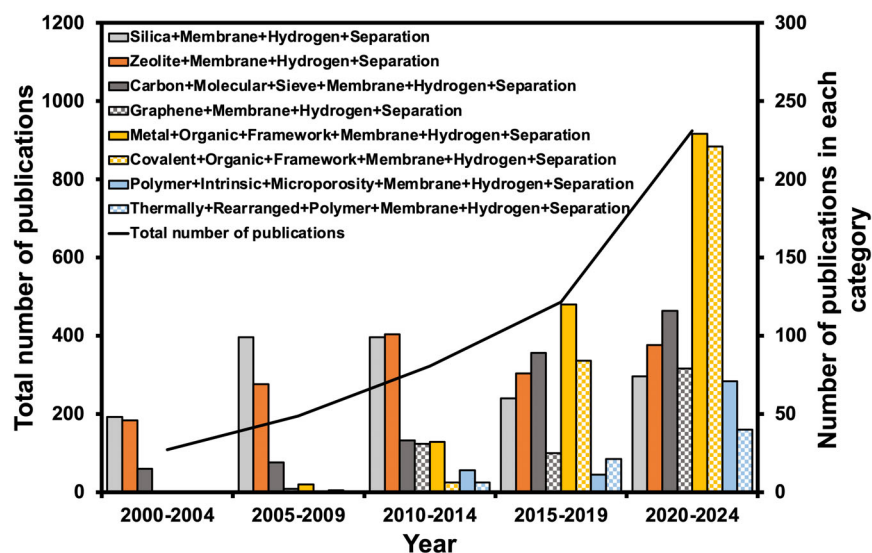


Figure 1. Number of publications of microporous materials membrane for hydrogen separation based on Scopus.

hydrogen through the pipeline is the lowest cost alternative, there is a possibility to utilize the existing network of the natural gas pipeline to co-transport hydrogen with natural gas.^[13] Depending upon the gas grid infrastructure, hydrogen might be blended with the concentration between 5% and 20%.^[14] If such a scenario can be fully implemented in the future, one of the main challenges is then to find a reliable technology that can effectively and efficiently purify the hydrogen from methane at the desired locations.

Up to now, the separation process of hydrogen from these light gases can be carried out by employing several techniques such as through liquid absorption, pressure swing adsorption (PSA), or cryogenic separation.^[7,15–17] However, because of a number of disadvantages associated with these processes, particularly the relatively high-energy demand, membrane technology could be a better alternative in the future. This is because, in comparison to other conventional separation technologies, membrane technology could offer various advantages such as higher energy efficiency, smaller footprint, ease of operation, and lower investment and operational cost.^[18–20]

The use of membrane for hydrogen purification is indeed not a new technology. Various polymers have then been investigated to be used as a membrane material for hydrogen separation from various gases. In 2008, these studies have then been nicely summarized by Robeson by indicating the existence of the upper bound encountered in polymeric membranes for hydrogen separation.^[21] Based on this study, it can be clearly seen that there exists a permeability-selectivity trade-off encountered in polymeric membranes. A polymeric membrane with high hydrogen permeability such as poly(1-trimethylsilyl-1-propyne) (PTMSP) usually exhibits a low hydrogen selectivity and vice versa.

Considering the trade-off issue encountered in the polymeric membranes, the use of dense metallic membranes is also very attractive and therefore have also been investigated as a promising membrane material for hydrogen separation. In this case, palladium (Pd) and its alloys are probably the most common metallic membrane material investigated for hydrogen purification. The use of palladium to separate hydrogen has then been reported as early as 1866,^[22] which has become the foundation of various studies and discussions about this material and its

alternative in the 1950–1960.^[23–25] In general, palladium is a promising membrane material for hydrogen separation since it can offer almost an infinite selectivity toward hydrogen and thus a pure hydrogen flow at the downstream side can be obtained. Despite their high effectiveness, these metallic membranes suffer from a number of disadvantages. Firstly, palladium is a rare earth metal. This causes the production cost of a palladium membrane to be more expensive than a polymeric membrane. In order to reduce the production cost of a palladium-based membrane, it has to be fabricated instead as a thin layer on a porous substrate. Secondly, a palladium membrane can also suffer from the hydrogen embrittlement when operated below 300 °C which could lead to the mechanical deformation of the membrane.^[26,27] Therefore, palladium must be alloyed, either to form a binary alloy or a ternary alloy, with other metals to address the embrittlement problem and also to improve its chemical resistance.^[26,28]

Addressing the above issues, a number of researches have then been directed to investigate other promising materials for hydrogen purification, particularly microporous materials. In this case, the employment of microporous materials has gained an increased interest because they could offer high productivity and selectivity and thus surpassing the upper bound limit. As can be seen in **Figure 1**, there is an increasing trend in the publications related to various microporous materials for hydrogen separation. Such a possibility is particularly driven by the possibility to rationally tailor the pore structure of these materials for selectively permeating hydrogen while rejecting other impurities. For example, as can also be seen in **Figure 1**, there is an increasing trend from around 2010 in research and development in the field of metal organic frameworks, covalent organic frameworks, and microporous polymeric membranes (polymer of intrinsic microporosity and thermally rearranged polymer) whose architecture can be rationally designed by selecting appropriate building blocks. This review then intends to highlight the recent advances of these promising materials in the field of hydrogen separation, which could then be used as a guidance to choose the next membrane materials for hydrogen purification.

2. Gas Transport in the Microporous Materials

The gas transport occurring through a membrane can usually be described through solution–diffusion mechanism as illustrated in **Figure 2a**. In this case, the gas permeation occurs through three steps: (i) adsorption and dissolution of the gas into the membrane matrix, (ii) diffusion of the gas across the membrane matrix, and (iii) desorption at the downstream side. The selectivity is therefore determined both by the solubility and diffusivity of the gas molecules in the membrane material. The gas transport of the membranes fabricated from polymeric materials can usually be described by this phenomenon. However, it should also be noted that this phenomenon might only occur in the ideal scenario where the polymeric membranes are dense, symmetric, and defect-free. Therefore, in a non-ideal situation, for example, in the presence of defective sites, the gas transport of the polymeric

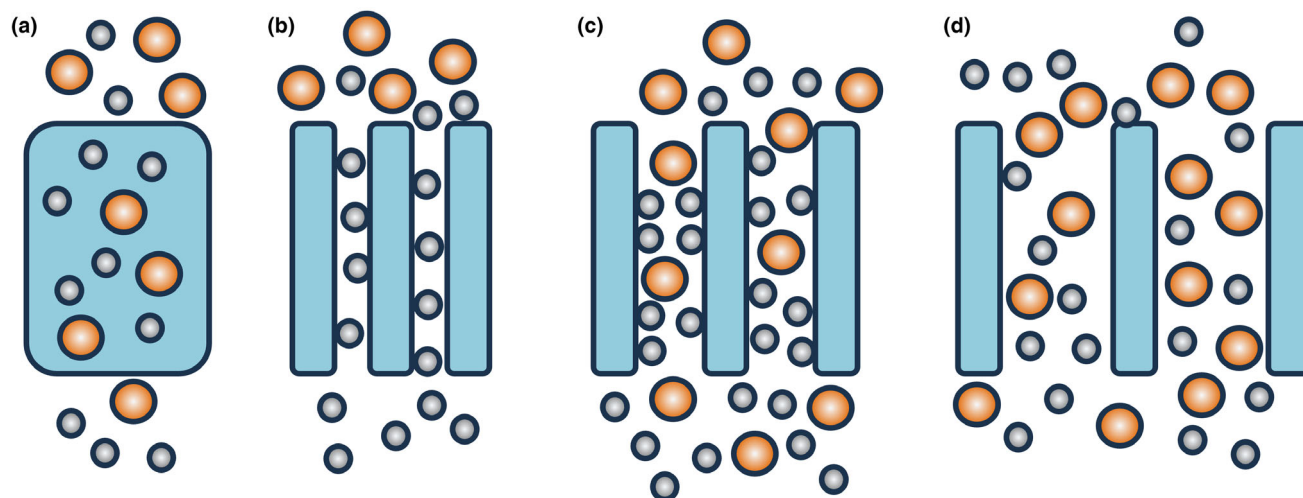


Figure 2. A schematic of the possible gas transport phenomenon through a microporous membrane: a) solution–diffusion, b) molecular sieving, c) surface diffusion, and d) Knudsen diffusion.

membranes might no longer be governed by the solution–diffusion mechanism.

Meanwhile, in a microporous material with a more complex and porous structure, the gas transport mechanisms could be governed by a combination of different mechanisms.^[29,30] There are at least three phenomena that could also occur when the gas molecules are transported across the membrane. In the ultra- or micropores region, the gas molecular sieving can occur, as illustrated in Figure 2b. In this case, the membrane selectivity is governed by the ability of a certain gas molecule to pass through the pores. When the pores in a microporous membrane become larger and falls within the range of 0.3–1 nm, the gas transport can now be governed by surface diffusion, as illustrated in Figure 2c. Lastly, the Knudsen flow can also govern the gas transport process across a microporous membrane, as illustrated in Figure 2d, when the pore size in the membrane falls in range between 1 and 50 nm. This occurs when the mean free path of a gas molecule is much larger than the pore diameter. All of these gas transport could then occur simultaneously in a microporous membrane. For instance, when a microporous membrane contains some large pores or defective parts, the gas transport occurring through these defective sites might be governed by both surface and Knudsen diffusion, while the rest might be molecularly sieved by the non-defective sites of the membrane. Moreover, the ability for a certain gas molecule before being transported across the membrane could also be affected by the adsorption of the molecule on the membrane, which in the case of microporous polymeric membranes corresponds to the material's solubility.

3. Microporous Membrane Materials for Hydrogen Separation

3.1. Silica-Based Membranes

The use of silica-based membrane for hydrogen purification has been studied as early as 1989 where the decomposition of tetraethoxysilane (TEOS) was used as a silica precursor and an inorganic porous glass was used as the support.^[31] From this early study, it was found that the

H₂/N₂ selectivity of the silica membrane is about twice higher than the selectivity of the porous support. In silica-based membranes, the separation is governed based on the molecular sieving phenomenon. This is in contrast to the separation of their support layer which is normally governed by the Knudsen diffusion. Therefore, a defect-free silica-based membrane could exhibit a very high hydrogen permselectivity toward light gases.

In general, as illustrated in Figure 3, a microporous silica-based membrane can be fabricated either by a sol–gel^[32–54] or chemical vapor deposition (CVD) method.^[55–85] In a sol–gel technique, a porous substrate is usually firstly dipped in a silica colloidal precursor containing silica nanoparticles. This is then followed by drying and sintering the coated substrate to obtain a porous silica structure.^[86] This process can be repeated several times to obtain a defect-free silica membrane. Three approaches, namely (i) silica polymers, (ii) particulate-sol, and (iii) templating, can then be used to fabricate a silica membrane based on the sol–gel method and various factors might affect the membranes properties and their hydrogen separation performance.^[20]

A study comparing TEOS and three different silica precursors, namely 1,1,3,3-tetraethoxy-1,3-dimethyldisiloxane (TEDMDS), bis(triethoxysilyl)ethane (BTESE), and hexaethoxy disiloxane (HEDS), has revealed that the TEOS-derived silica membrane gives the best H₂/N₂ selectivity around 340 with the lowest H₂ permeance around $3 \times 10^{-7} \text{ mol m}^2 \text{ s}^{-1} \text{ Pa}^{-1}$ (895 GPU, GPU = gas permeation unit and $1 \text{ GPU} = 3.35 \times 10^{-10} \text{ mol m}^2 \text{ s}^{-1} \text{ Pa}^{-1}$) as it results in the membrane with the smallest pore size.^[47–49] Meanwhile the order of the pore size of the rest is HEDS < BTESE < TEDMDS-derived silica membrane. All the silica membranes fabricated using these precursors have exhibited low H₂/N₂ selectivity in the range of 7–20 because of their looser pore structure with the TEDMDS-derived silica membrane shows the lowest H₂ permeance around $1 \times 10^{-6} \text{ mol m}^2 \text{ s}^{-1} \text{ Pa}^{-1}$ (2985 GPU) because of the presence of the impermeable pendant groups in its network. Another investigation has also indicated that there is a difference between the silica membrane prepared from acid-catalyzed polymeric silica sol and base-catalyzed colloidal silica sol.^[38] The former leads to the formation of low-branched silica particles leading to interpenetration and denser thin film while the latter

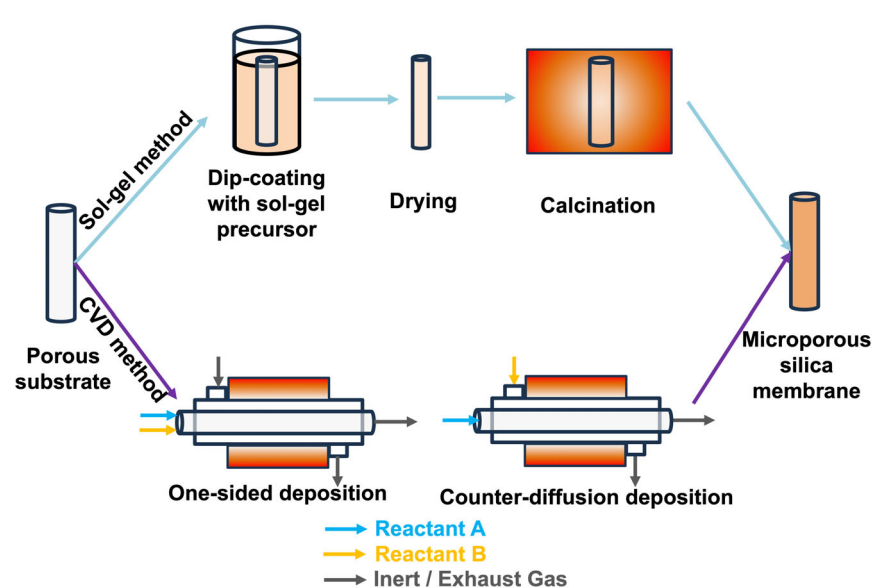


Figure 3. A schematic diagram of the microporous silica membrane prepared on a tubular/hollow fiber substrate.

results in highly branched silica particles that cannot interpenetrate because of the steric hindrance. As a result, the latter pathway produces better and applicable silica membrane as the former produces an almost non-permeable silica membrane. For the silica polymers pathway, carefully controlling the clusters condensation rate during the silica network polymerization is essential to obtain a defect-free silica membrane.^[87] In the case of templating method, for example, the selection of the correct templating agent is crucial to obtain a silica membrane with narrow pore distribution. It has been observed that the use of methacryloxypropyltrimethoxysilane (MOTMS) as a templating agent can increase the micropore volume and narrow down the pore distribution of the membrane and thus resulting in almost 40 times increase of hydrogen permeance than the membrane fabricated without MOTMS.^[36]

One of the main challenges related to the sol-gel process is the required time for the calcination since this may take up to 12 h including the ramping up to the target temperature and the holding time.^[88] In this respect, a 1-hour calcination step with the ramping up step of more than $100\text{ }^{\circ}\text{C s}^{-1}$ has not just managed to reduce the calcination time but also to produce a good silica membrane with H_2 permeance and selectivity against N_2 around $1 \times 10^{-7}\text{ mol m}^2\text{ s}^{-1}\text{ Pa}^{-1}$ (298.5 GPU) and 40, respectively.^[45] Another study has also shown the possibility to use a hot plate at $550\text{ }^{\circ}\text{C}$ for calcination.^[44] With just 1 h calcination time, a silica membrane with H_2 permeance around $1 \times 10^{-7}\text{ mol m}^2\text{ s}^{-1}\text{ Pa}^{-1}$ (298.5 GPU) and selectivity against CO_2 , N_2 , and CH_4 around 17, 250, and 250, respectively, can be obtained. However, contamination from the environments must be fully avoided to obtain a defect-free membrane.

Differing from the sol-gel method, a CVD technique relies on the reaction of the silica precursor in the gas phase occurring around the pores of the substrate in order to modify them.^[89] Such a reaction can then be accelerated by various factors including the presence of the catalyst in the precursor such as tetraisopropyl titanate^[63] and the presence of opposing reactants such as water vapor that also contributes in

reducing the fabrication temperature.^[73] Meanwhile, the quality of the silica membrane produced with CVD method is often influenced by various reaction parameters such as the flow direction of the reactants, reaction temperature and time, and the presence of other components. In this case, a defect-free silica membrane can usually be obtained by prolonging the reaction time leading to lower hydrogen permeance and higher hydrogen permselectivity as the pore of the substrates become smaller.^[56,57,59,60] In order to obtain a homogeneous silica membrane, it has also been observed that flowing the two reactants on different sides of the porous substrate (outer and inner sides) yields a more uniform silica membrane with better hydrogen permselectivity.^[62] This is because the formation of a uniform silica film within the substrate pores will be more promoted rather than being accumulated on the surface of the substrate that can lead to film cracking as the thickness increases. Meanwhile, to obtain a thinner silica membrane to increase the hydrogen permeance, introducing a barrier on the pore surface of the porous substrate such as by introducing temporary carbon layer^[67] or by firstly coating a silica sol-gel layer on the barrier will limit the active region of the CVD and thus helping to assist in obtaining a thinner silica membrane.

Moreover, choosing the correct silica precursor is also crucial to obtain a silica membrane with excellent hydrogen separation performance. For example, the use of TEOS as silica precursor might result in a silica membrane with higher hydrogen permeance than the one fabricated from SiCl_4 when using Vycor glass as the support.^[65] This is because TEOS diffuses slower than SiCl_4 into the support pores because of its molecular size and thus considerable pore blocking might be resulted when SiCl_4 is used as the precursor. In another study, the use of three different silica precursors, namely tetramethoxysilane (TMOS), phenyltrimethoxysilane (PhTMS), and 3-aminopropylmethyldiethoxysilane (APMDES) has been investigated and the membranes were fabricated using the CVD method.^[55] It was observed that the H_2/N_2 selectivity follows the order of TMOS-deposited (1265) > PhTMS-deposited (633) > APMDES-deposited (100) silica membrane. This is caused by the fact that TMOS-deposited silica membrane has the smallest pore size distribution than the others and thus has shown an excellent H_2 selectivity, even though this also means that it has the slowest H_2 permeance compared to the rest of the membranes. In addition, the selection of the support material is also crucial to obtain a silica membrane that can combine excellent hydrogen permeance and selectivity. For example, comparative studies employing Vycor glass and alumina as a support have indicated that the H_2/CO_2 and H_2/CH_4 selectivity of the former is about four to five times higher than the latter (up to more than 10 000).^[56,57] This is because the $\text{SiO}_2/\text{Vycor}$ glass membrane has more constricted pores than the $\text{SiO}_2/\text{alumina}$ and thus more effective in hindering the adsorption of gases with kinetic diameter of more than 0.3 nm. However, this must also be compensated by the slower hydrogen permeance, which was found about one order of magnitude lower. Another study using alumina as the support has also shown that by firstly coating the alumina substrate with boehmite sol as an

intermediate layer can produce an ultrathin silica membrane with thickness less than 50 nm and increase its hydrothermal stability.^[58,72] Moreover, both the hydrogen permeance and the H₂/CO₂ and H₂/CH₄ of this silica membrane has also been improved from its uncoated counterpart for about 60% to be around $1.6 \times 10^{-7} \text{ mol m}^{-2} \text{ s}^{-1} \text{ Pa}^{-1}$ (477.6 GPU) and about two to three times to be around 590 and 940, respectively.^[58] This is because the intermediate layer coated on the support gives a finer microstructure and a membrane with fewer defects can be obtained. The advantages of using of boehmite as the intermediate layer can then be further enhanced by applying differential pressure when the silica membrane is fabricated using a counter-diffusion approach as it can more effectively deposit the film in the pores of this intermediate layer.^[84] As a result, the H₂/CO₂ and H₂/CH₄ selectivity of this membrane can reach as high as 1200 and 24 000, respectively. In another study, coating the alumina substrate with an intermediate layer from silica is also possible. In this case, a looser silica membrane from phenyltriethoxysilane before the deposition of the selective silica layer made from TEOS is also found to be very effective to significantly enhance the hydrogen permeance up to around $3.6 \times 10^{-6} \text{ mol m}^{-2} \text{ s}^{-1} \text{ Pa}^{-1}$ (10 746 GPU) while maintaining satisfactory H₂/CH₄ selectivity around 30.^[82]

A silica-based membrane for hydrogen separation can also be modified by embedding the membrane with various metals or metal oxides such as cobalt,^[33,34,41,45] nickel,^[35,40] niobium,^[50] palladium,^[53] and zirconia^[43] to improve its separation performance and structural stability. The incorporation of metal or metal oxides inside the silica membrane is expected to improve its hydrothermal stability by increasing its resistance against densification when operated at high temperature. This could then result in an excellent H₂/CO₂ selectivity around 1500 even when the membrane was operated at 600 °C and 600 kPa.^[33] In addition, in comparison with the non-doped silica membrane, the hydrogen permeation activation energy of the metal-doped silica membrane is also lower and thus indicating the significant reduction of the dense structure in the metal-doped silica membranes.^[34,35] Despite its proven efficacy, the metal-loading inside the membrane must also be optimized. For instance, in a zirconia-doped silica membrane, increasing the zirconia content in the silica sol from 10% to 50% results in a silica membrane with lower hydrogen permeance and selectivity.^[43] The hydrogen permeation activation energy also increases from 3.4 to 44 kJ mol⁻¹ and thus indicating the densification of the SiO₂-ZrO₂ network structure. The silica membrane with the lowest zirconia content also performs better after hydrothermal treatment giving H₂/N₂ selectivity around 190 compared to around 15 found in the silica membrane with the highest zirconia content. Similarly, if a silica membrane is doped with more than 50% niobium, structural densification occurs leading to low H₂ permeance and H₂/CO₂ selectivity around $3 \times 10^{-9} \text{ mol m}^{-2} \text{ s}^{-1} \text{ Pa}^{-1}$ (8.9 GPU) and 15, respectively, after a hydrothermal treatment.^[50] When the content of the niobium is less than 50%, after hydrothermal treatment, the H₂ permeance and H₂/CO₂ selectivity of the membrane can still be maintained around $3.1 \times 10^{-8} \text{ mol m}^{-2} \text{ s}^{-1} \text{ Pa}^{-1}$ (92.5 GPU) and 207, respectively. Moreover, high metal doping might also lead to structural instability of the silica membranes.^[35]

There are also other non-conventional approaches to introduce metal into the silica membrane. A silica membrane can be binary doped such as with palladium-cobalt^[32] and palladium-niobium.^[52] A synergistic effect can be seen in the case of Pd-Nb BTESE-derived silica membrane, as illustrated in Figure 4a–c, where the niobium contributes in creating

a denser silica membrane structure to improve the membrane selectivity while the Pd contributes in enhancing the H₂ permeance through preferential adsorption.^[52] As a result, the H₂ permeance and H₂/CO₂ selectivity of the Pd-Nb silica membrane can reach up to $1.1 \times 10^{-7} \text{ mol m}^{-2} \text{ s}^{-1} \text{ Pa}^{-1}$ (328.4 GPU) and 107, respectively, which is significantly higher than bare BTESE-derived silica membrane. The introduction of the metal can also be carried out after the fabrication of the silica membrane as studied in the impregnation of palladium nanoparticles in the silica membrane through vacuum method as can be seen in Figure 4d–f.^[42] In this case, the Pd nanoparticle might contribute in plugging the membrane defects. As a result, the H₂ permeation is more activated in the Pd-impregnated silica membrane as indicated by higher activation energy at 6.32 kJ mol⁻¹ in comparison to 4.22 kJ mol⁻¹ observed in the non-modified one because of its denser structure. Consequently, this results in lower H₂ permeance of the Pd-impregnated silica membrane that is found to be around $2.3 \times 10^{-8} \text{ mol m}^{-2} \text{ s}^{-1} \text{ Pa}^{-1}$ (68.7 GPU) than the non-impregnated counterpart that falls around $3.4 \times 10^{-8} \text{ mol m}^{-2} \text{ s}^{-1} \text{ Pa}^{-1}$ (101.5 GPU). However, the H₂/N₂ selectivity of the former is about four times higher than the latter and reaches 115.

Operating the silica membrane at higher temperature could be more beneficial for hydrogen separation.^[37,41,42,60,75] This has been exemplified by a study showing that the H₂/N₂ selectivity of the silica membrane can be improved from around 20 to be around 102 by increasing the temperature from 423 to 873 K.^[37] In another study, the H₂/CO₂ of a cobalt-silica membrane can also be improved from 45 to 160 by elevating the operating temperature from 100 to 250 °C.^[41] In these cases, the increase of hydrogen selectivity is mainly attributed to the fact that the permeation activation energy of the hydrogen molecule in the silica membranes is higher than the other light gases. Therefore, as the operating temperature is elevated, the increase of the hydrogen permeance is higher than the other light gases and thus resulting in higher hydrogen selectivity.^[37,41,75]

3.2. Zeolite Membranes

In the perspective of the hydrogen separation, employing zeolite membranes is actually quite promising as it can offer a number of advantages such as well-defined pore size and better physical and chemical properties. They can also be operated at high temperature like a silica membrane since they are inorganic materials. As illustrated in Figure 5, a number of zeolite membranes fabricated from different zeolites such as AIPO-18,^[90] CHA,^[91] DDR,^[92–98] DD3R,^[99] FAU,^[100–103] LTA,^[104–113] Si-CHA,^[114,115] silicalite 1,^[116,117] silicalite 2 MEL,^[118] MFI,^[119–125] NaA,^[126–129] SAPO 17,^[130] SAPO 34,^[131–140] SSZ 13,^[115,139,141–147] STT,^[148,149] titanosilicate AM-3,^[150,151] titanosilicate-umbite,^[152,153] and ZSM 5^[154–158] have been investigated for this purpose. They can be fabricated through two main routes, namely in situ crystallization by hydrothermal reaction, microwave-assisted or ionothermal reaction^[101,102,104–107,109,110,119,121,125,134] or seeding followed by secondary growing.^[92,111–115,117,118,126–129,131–133,136,138,142,145–147] Moreover, a stronger attachment between the zeolite and the support layer can also be achieved through substrate functionalization such as with 1,4-diisocyanate,^[108] 3-aminopropyltriethoxysilane,^[102,106,107,129] 3-chloropropyltrimethoxysilane,^[104] polyethyleneimine,^[128] and polydopamine.^[103,105] By doing this, both the physical and covalent bond of the zeolite and the support layer can be greatly improved.

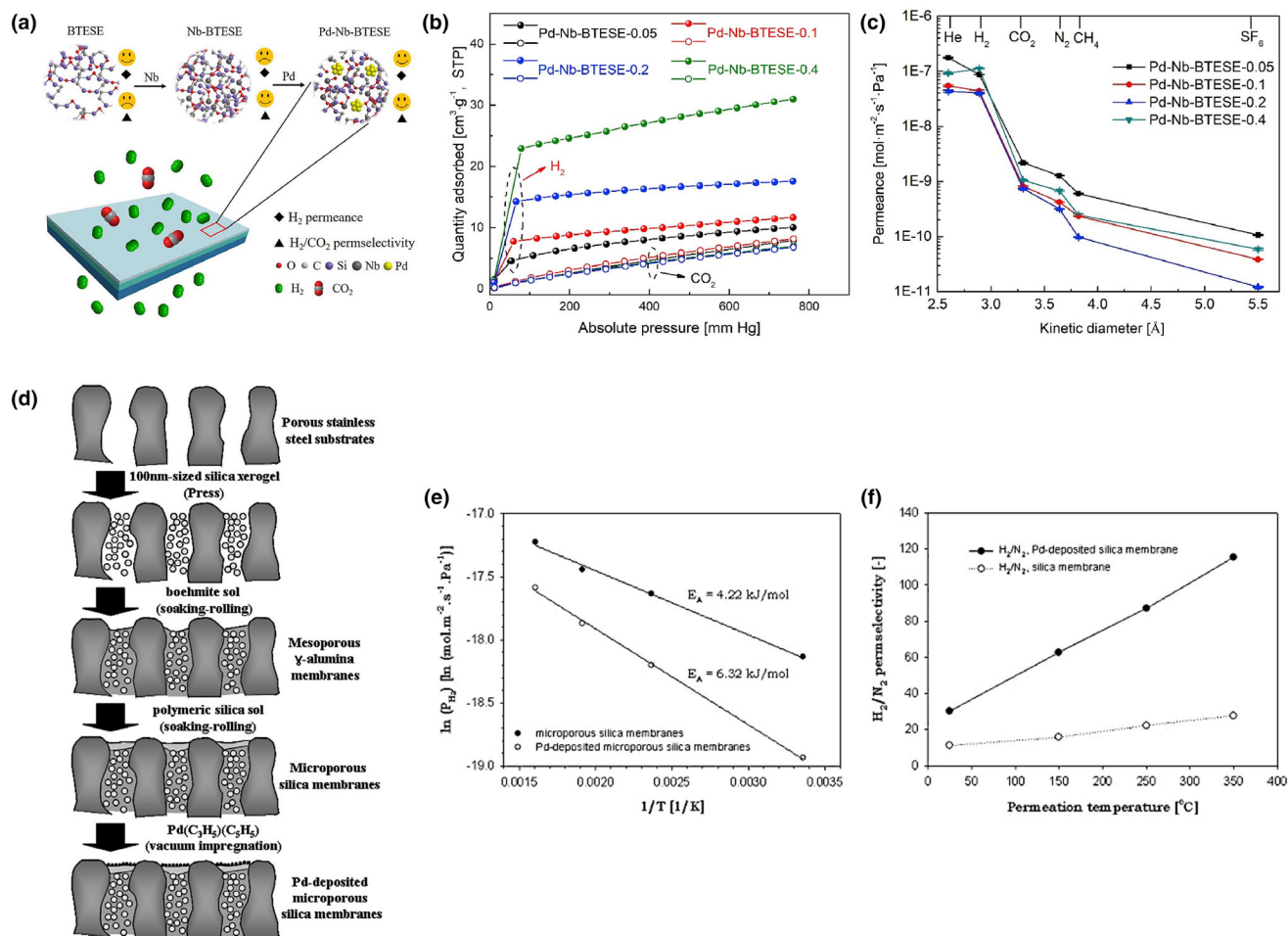


Figure 4. Illustration of the synergistic effect of a) the Pd-Nb-BTESE silica membrane and b) the impact of Pd-Nb loading on hydrogen adsorption and c) gas separation performance. d) Illustration of the palladium-impregnated silica membrane through vacuum-assisted method and e) its impact on the hydrogen permeation activation energy and f) H₂/N₂ selectivity. Figures a–c^[52] and Figures d–f^[42] are reproduced with permission. Copyright 2020 and 2008, respectively, Elsevier.

Figure 5 shows the crystal structures of six zeolite types: CHA, DDR, FAU, LTA, and MFI. Below the structures is a table of their pore characteristics.

Zeolite type	CHA	DDR	FAU	LTA	MFI
Pore diameter (nm)	0.737	0.766	1.124	1.105	0.636
Pore aperture (a, b, c) (nm)	0.372; 0.372; 0.372	0.365; 0.365; 0.263	0.735; 0.735; 0.735	0.421; 0.421; 0.421	0.47; 0.446; 0.446

Figure 5. Some examples of zeolites used as a membrane material for hydrogen separation with their corresponding pore diameter and pore aperture. The pore diameter and aperture data are obtained from the International Zeolite Association (IZA).

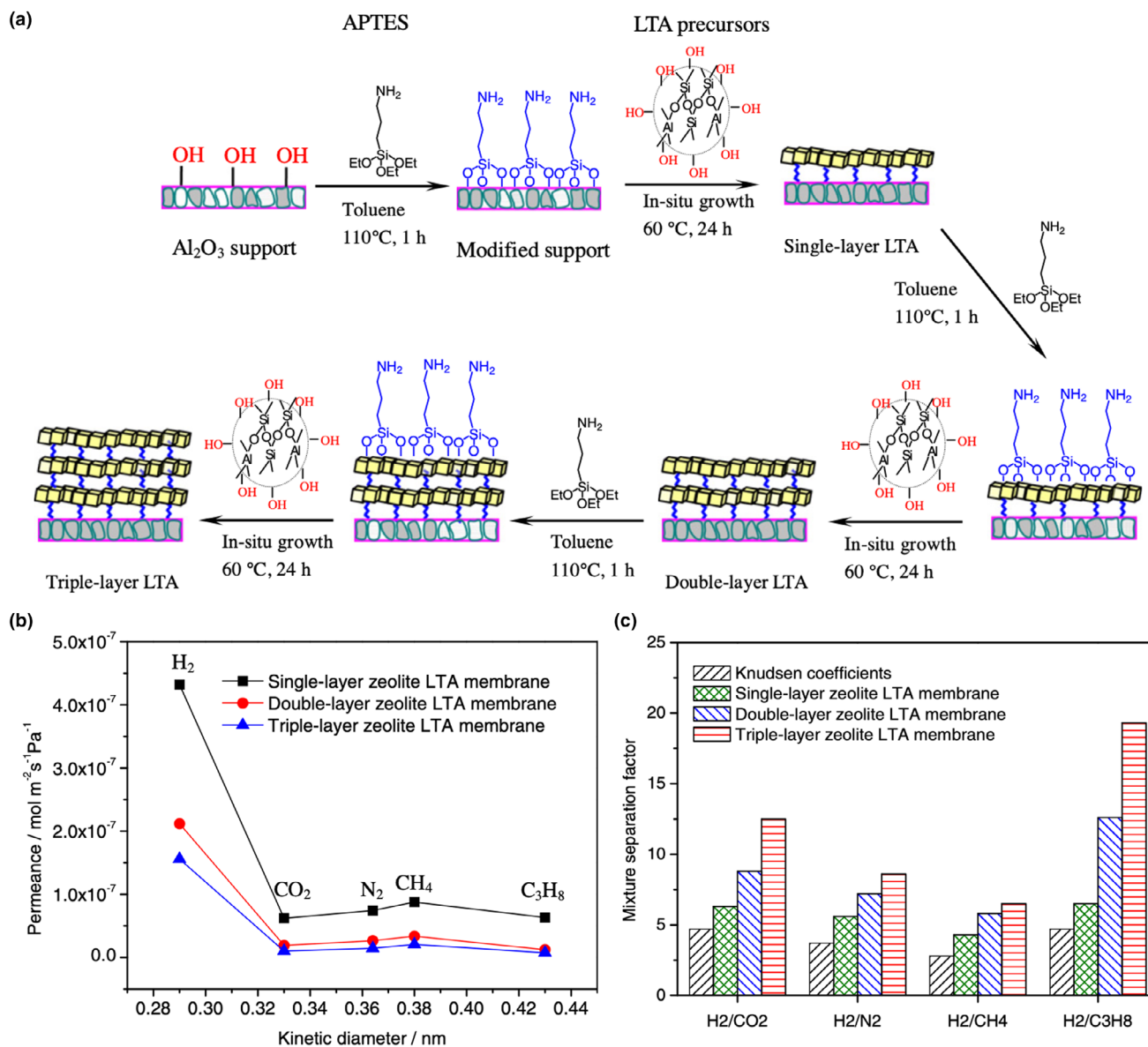


Figure 6. a) An illustration to fabricate a multi-layer LTA zeolite membrane functionalized with APTES at the interlayer and b, c) the comparative gas separation performance of the resulting zeolite membranes with different layers. Reproduced with permission.^[107] Copyright 2012 Elsevier.

In addition to a conventional single-layer membrane, a zeolite membrane can also be fabricated as a multi-layer membrane such as in the case of FAU-LTA,^[159] ZSM-5-silicalite-1^[154] and multi-layer LTA.^[107] In this case, functionalization with 3-aminopropyltriethoxysilane at the zeolite interlayer seems necessary to act as a protective barrier for the existing layer when it undergoes the next synthesis step.^[159] One of the main functions of this strategy is then to heal the defects existing in the first layer such as observed in the case of triple-layer LTA zeolite membrane, as illustrated in **Figure 6a,b**, where the H_2 separation factor from CO_2 , N_2 and CH_4 can be increased from 7; 5.8 and 4.9, respectively, observed in the single layer LTA zeolite membrane to be 12.5; 8.6 and 6.5, respectively in the triple-layer LTA zeolite membrane.^[107] The application of this multi-layer approach can then also be widened

by using other materials as the intermediate layer such as palladium.^[160] Apart from its role to separate the hydrogen from nitrogen, the zeolite layer also contributes to protect the palladium layer against cracking in the event of drastic operating temperature changes. As a result, the H_2/N_2 separation performance of the zeolite-palladium composite membrane can be stably maintained at around 300 when the operating temperature is periodically cycled between 350 and 500°C . Meanwhile, almost 300% drop in H_2/N_2 selectivity is observed in the pure palladium membrane during this cycling.

Despite these numerous investigations, it should also be noted that not all of the investigated zeolite membranes have shown promising performance for hydrogen separation as the employment of a zeolite with pore aperture around 0.3 nm is required to only allow the

hydrogen permeation whose kinetic diameter is around 0.289 nm. Therefore, zeolite membranes such as FAU with pore size around 0.7 nm^[100] or silicalite 2 MEL with pore size around 0.55 nm^[118] might not be suitable for this purpose because their hydrogen molecular sieving capability will be limited.

It does not mean, however, that zeolite with larger pore size should be completely excluded to be applied for hydrogen separation purpose. One strategy to utilize this particular zeolite is to do a modification or a post-treatment process to reduce its pore size in order to enhance the hydrogen separation performance by using silica. For example, the zeolitic pore of the MFI^[119–124] and ZSM 5^[131,154] can be reduced by using methyl-diethoxysilane (MDES) which is decomposed at high temperature to produce amorphous SiO₂. In another study, tetraethylorthosilicate (TEOS) can also be used as a silica precursor to modify the pore of a DDR zeolite membrane.^[95] The effectiveness of this deposition process can also be improved by increasing the number of acidic sites in the zeolite such as through ion exchange process.^[123]

This modification process can then significantly improve the hydrogen separation performance of a zeolite membrane. For example, in the case of MFI zeolite membrane, the H₂ selectivity against CO₂, N₂, and CH₄ can be improved significantly from Knudsen selectivity value to be around 141, 63, and 180, respectively with only about 25% loss on the hydrogen permeance.^[124] In another case, although the untreated ZSM 5 shows almost no H₂/CO₂ separation, the H₂/CO₂ selectivity can be increased to be around 47 after the modification. However, this must be compensated with lower H₂ permeance that decreases about one order of magnitude to be around 1×10^{-7} mol m⁻² s⁻¹ Pa⁻¹ (298.5 GPU).^[131] A similar result is also obtained with the DDR membrane. After modification, up to one order of magnitude lower H₂ permeance is observed to be around 2×10^{-8} mol m⁻² s⁻¹ Pa⁻¹ (59.7 GPU) but the H₂/CO₂ selectivity can be significantly improved from 2.6 to be around 33.^[95]

However, it should be noted that this strategy cannot be generally applied toward all types of zeolite membrane since it must be ensured that the modifier fits into the zeolite pore and the membrane has a relatively good quality with low intercrystalline defects.^[119] In the case where the modifier cannot go inside the zeolitic pore, however, there is still a chance that such a modification can bring a beneficial impact by modifying the non-zeolitic pores or healing the membrane defective sites. This has been investigated to modify the SAPO 34 membrane.^[131] In this case, the modifier does not modify the SAPO 34 pore but rather modifies the non-zeolitic pore because of the difficulty of the MDES to go into the SAPO 34 pores. After the modification, the H₂/CH₄ selectivity can be increased to 59 from 39 without any significant loss on the H₂ permeance since the H₂ mostly goes through the zeolitic pore. In another study using DDR zeolite membrane, the membrane is modified using tetramethoxysilane to heal the defective sites.^[98] As a result, compared to the unmodified membrane, the H₂ permeance of the modified membrane falls to 1.36×10^{-7} mol m⁻² s⁻¹ Pa⁻¹ (406 GPU), which is around one order of magnitude lower, but its H₂/CH₄ selectivity can be significantly improved from around 3 to be around 45.

Another strategy to use zeolite with relatively large pore size is, as has also been briefly mentioned above, to fabricate it as a composite zeolite membrane to exploit the synergistic effect originated from its constituents. For example, in the case of FAU-LTA composite zeolite membrane, the pore aperture of FAU is around 0.74 nm.^[159] Despite this, its combination with the LTA can create a new composite membrane with higher hydrogen selectivity (10.6; 8.6 and 7.1 against CO₂,

N₂, and CH₄, respectively) than the membrane fabricated solely from the FAU (8; 7.2 and 5.6 against CO₂, N₂, and CH₄, respectively) which could be contributed from the synergistic effects between the two zeolites and their interlayer structure.

In addition to the pore size adjustment, the hydrogen separation performance of a zeolite membrane can also be improved when it is operated at higher temperature.^[120,121,131,139,154] For example, at 150 °C, the H₂/CO₂ separation of a ZSM-5/silicalite-1 bilayer membrane is found to be around 14 which then increases to be around 24 as the temperature is elevated to 450 °C because of the reduced adsorption affinity of the zeolite to CO₂.^[154] A similar trend has also been observed for MFI zeolite membrane where the H₂/CO₂ separation factor can be increased about three times to be around 21 where it is operated at 300 °C rather than at 150 °C.^[120] However, one cannot neglect the fact that a contrasting situation might also be observed as reported in a number of cases. For example, the H₂/CH₄ selectivity of a modified SAPO 34 zeolite membrane decreases from around 59 at 25 °C to be around 28 at 250 °C.^[131] In another study, a Ti-silicate zeolite membrane has also shown a decrease in H₂/N₂ selectivity from around 47 at 40 °C to be around 31 at 150 °C.^[152] Si-CHA zeolite membrane has also shown a decreasing trend in the H₂/CH₄ selectivity from 85 to be around 77 as the operating temperature increases from 25 to 150 °C that is mainly caused by lower H₂ permeance at higher temperature.^[114] Therefore, evaluating this trend case by case is particularly crucial since this behavior depends strongly upon a number of factors such as the effect of the adsorption of the permeating gases and the permeation activation energies through the zeolite membranes, whose differences might also be more strengthened when each gas permeates through different pores in the zeolite membrane.^[114,152]

Some zeolite membranes such as AIPO-18,^[90] DD3R,^[99] SAPO-34,^[140] and Si-CHA^[114] have also shown a negative hydrogen separation performance trend with increasing operating pressure. For instance, when the operating pressure drop increases from 0.2 to 1 MPa, the H₂ permeance in the AIPO-18 membrane recues almost half to be around 0.6×10^{-7} mol m⁻² s⁻¹ Pa⁻¹ (179.1 GPU) and its H₂/CH₄ selectivity drops from around 25 to 19.^[90] In another study employing Si-CHA, the H₂/CH₄ selectivity drops from 85 to be around 50 as the pressure drops increases from 0.2 to 1 MPa.^[114] Such cases might be attributed because of the hydrogen coverage in the zeolite does not linearly increase with increasing pressure because of the weak hydrogen adsorption resulting in the hydrogen permeance reduction and thus renders the membrane for being ineffective to inhibit the permeation of other light gases.^[90,99]

3.3. Carbon-Based Membranes

In the area of carbon-based membranes, there are two material classes that could be promising for hydrogen purification, namely carbon molecular sieve (CMS) membrane and graphene-based membranes. Both materials are very attractive to be applied for this purpose since they can exhibit a sharp molecular sieving ability to produce a highly selective membrane.

3.3.1. Carbon Molecular Sieve (CMS)-Based Membranes

CMS membrane is a carbon-based membrane that is produced through pyrolysis of polymeric precursors. Because of this reason, it can be

easily inferred that one of the most important aspects in producing a high-quality CMS membrane for hydrogen separation is the selection of the polymers. Various polymers have then been investigated as a precursor for CMS membranes, either as a self-standing or a supported CMS membrane, applied for hydrogen separation including cellulose or regenerated cellulose,^[161–166] cross-linked polyester,^[167] Kapton^[168] lignin-based or lignin-derived polymers,^[169–171] Matrimid,^[172,173] novolac polymer (phenol-formaldehyde),^[174–178] phenolphthalein-based cardo poly (arylene ether ketone),^[179] polyamides,^[180] polybenzimidazole (PBI),^[181–183] polydopamine,^[184] polyetherimide,^[185–187] polyfurfuryl alcohol,^[188–192] polyhedral oligomeric silsesquioxanes (POSS),^[193] poly(phthalazinone ether sulfone ketone),^[194] polyimide,^[187,195–203] polyimide/azide,^[204] polymer of intrinsic microporosity (PIMs),^[205] polypyrrolone,^[206] poly(siloxane imide),^[207] Tröger's base polymer,^[208–210] wood tar^[211] or a blend of polymers such as poly(2,6-dimethyl-1,4-phenyleneoxide) (PPO)–polyvinylpyrrolidone (PVP),^[212] poly styrene sulfonic acid-Tröger's base polymer,^[209] polyimide-polyvinylpyrrolidone,^[213] PBI-Matrimid,^[182,214] PBI-P84,^[182,214] and PBI-Torlon.^[182,214]

Considering the huge possibilities of the precursors, selecting the correct precursor for a CMS membrane becomes crucial. For example, in a systematic study involving four different polyimides with different groups (aromatic, phenyl ether, (CH₃)₂, and (CF₃)₂) results in four different polyimides with four different chain structures: rod-like, curved, helical, and helical with higher fractional free volume.^[201] As expected, a CMS membrane with the highest H₂ permeability around 1673 Barrer is obtained from the precursor with helical-chain structure and high free volume, which is constructed from 4,4'-(hexafluoroisopropylidene) bis(*p*-phenyleneoxy) dianiline (BDAF) and pyromellitic dianhydride (PMDA), while the CMS membrane constructed from the rod-like structure, namely *p*-phenylenediamine (PPD) and PMDA, shows the lowest H₂ permeability around 366 Barrer. This is because the pendant groups in the helical-chain polyimide contributes in sterically hindering the orderliness of the graphite-like sheets packing leading to a more open micropore structure after the pyrolysis. However, the H₂/N₂ selectivity of the former is only found to be around 12. Meanwhile, the PPD-PMDA-derived CMS membrane shows H₂/N₂ selectivity around 73 and thus exhibiting a more enhanced molecular sieving for hydrogen separation.

Once an appropriate polymer has been chosen, the pyrolysis process of these precursors can be conducted in the absence of oxygen and the temperature is usually set to be around 400–1000 °C, which has to be optimized as this will affect the sp³/sp² ratio in the CMS membranes. In this case, a CMS membrane with high quantity of sp³ type of defects usually exhibits high hydrogen permeance and thus controlling the conversion of the sp³ to sp² hybridized carbon is crucial to obtain a CMS membrane with excellent molecular sieving property.^[162,195] Therefore increasing the pyrolysis temperature of the precursor can usually bring a positive impact to increase the number of ultramicropores and also the sp² hybridized carbon resulting in the enhanced hydrogen molecular sieving of the CMS membranes but optimization is also necessary in order to avoid the shrinkage of the pores resulting in a defective CMS membrane.^[162,171–173,179,180,205,208,211,212] For instance, when using aromatic polyamide as the carbon precursor for the CMS membrane, increasing the pyrolysis temperature from 550 to 925 °C results in a significant increase of H₂/CO₂ selectivity more than 150 times to be around 366, although the H₂ permeability also decreases from around 687.4 to 9.1 Barrer. This could be attributed to the generation of ultra-microporous regions in the CMS membrane that

might exclusively allow hydrogen to be adsorbed and passed through the membrane resulting as indicated by the enhancement of both the diffusive and sorption selectivity, as illustrated in **Figure 7a,b**.^[180] A similar situation is also observed when employing PIM as the carbon precursor.^[205] By increasing the pyrolysis temperature from 600 to 800 °C the H₂/N₂ and H₂/CH₄ selectivity increases from around 28 and 40, respectively, to be around 128 and 363, respectively, without significant reduction of the H₂ permeability which can be maintained around 2177 Barrer.^[205] In another study, by increasing the carbonization temperature of phenolphthalein-based cardo poly (arylene ether ketone) from 700 to 900 °C, the interlayer spacing of the graphitic-like crystallite in the CMS also decreases resulting in an increase of the H₂/CH₄ selectivity from 311 to 1859, even though this has to be compromised with the reduction of the hydrogen permeance from around 4.6 × 10⁻⁷ (1373.1 GPU) to be around 2 × 10⁻⁷ mol m⁻² s⁻¹ Pa⁻¹ (597 GPU).^[179] In another investigation using cellulose hollow fiber as precursor, increasing the pyrolysis temperature from 500 to 850 °C also brings down the sp³/sp² ratio of the CMS membrane from 0.73 to 0.36 resulting in a decrease of H₂ permeance from 466.8 GPU to 148.2 GPU but significantly enhancing the H₂/CO₂ selectivity from 11.1 to 83.9.^[162] In addition to the appropriate pyrolysis temperature selection, the dwelling time at this particular temperature could also crucially affect the performance of the resulting CMS membrane. For example, as investigated using cellophane as the precursor, by prolonging the dwelling time at the final pyrolysis temperature to 240 minutes, more ultramicroporous regions in the CMS membrane can be generated.^[166] As a result, the H₂ permeability only slightly decreases from 148 to 109 Barrer but the H₂/CO₂ and H₂/N₂ selectivity can be more than doubled to be around 22 and 1086, respectively.

The hydrogen separation performance of the CMS membranes can then be improved by employing various strategies. This can be done, for example, by adding various metals such as aluminum,^[176] copper,^[163] iron,^[169] ytterbium,^[181] and zinc^[200] to the precursor. For instance, in addition to lowering the pyrolysis temperature, the use of iron as an additive to the precursor also contributes in maintaining the neck structure of the CMS membrane to improve the hydrogen selectivity.^[169] At the same pyrolysis temperature, the hydrogen permeance of the iron-added CMS is not markedly different from the non-added one, namely 132 versus 124 × 10⁻⁹ mol m⁻² s⁻¹ Pa⁻¹ (394 vs. 370 GPU), respectively, but the H₂/CH₄ and H₂/N₂ selectivity in the iron-added CMS membrane can be significantly improved from its non-added counterpart from 54 and 32, respectively, to be 584 and 293, respectively.^[169] Similarly, when using zinc as the additive, the H₂ permeability and the H₂/CH₄ selectivity of the resulting CMS membrane constructed from polyimide can be significantly increased from 5852 to 6768 Barrer and from 84.3 to 370, respectively, as the presence of Zn²⁺ ion might help in molecularly sieve the larger gas molecules and barely affect the hydrogen permeation.^[200] In another investigation using ytterbium as the dopant, compared with the pristine CMS membrane, the H₂ permeability of the metal-doped polybenzimidazole-derived CMS membrane can be increased from 519 to 1556 Barrer while its H₂ selectivity against CO₂, N₂, and CH₄ can be almost doubled to be around 12, 411, and 1532, respectively.^[181] In this case, the ytterbium can establish a coordination bonding with the imidazole precursor resulting in tightened interchain packing of the precursor. As a result, after carbonization, more ultramicropores regions can be formed which are responsible to enhance the hydrogen molecular sieving.

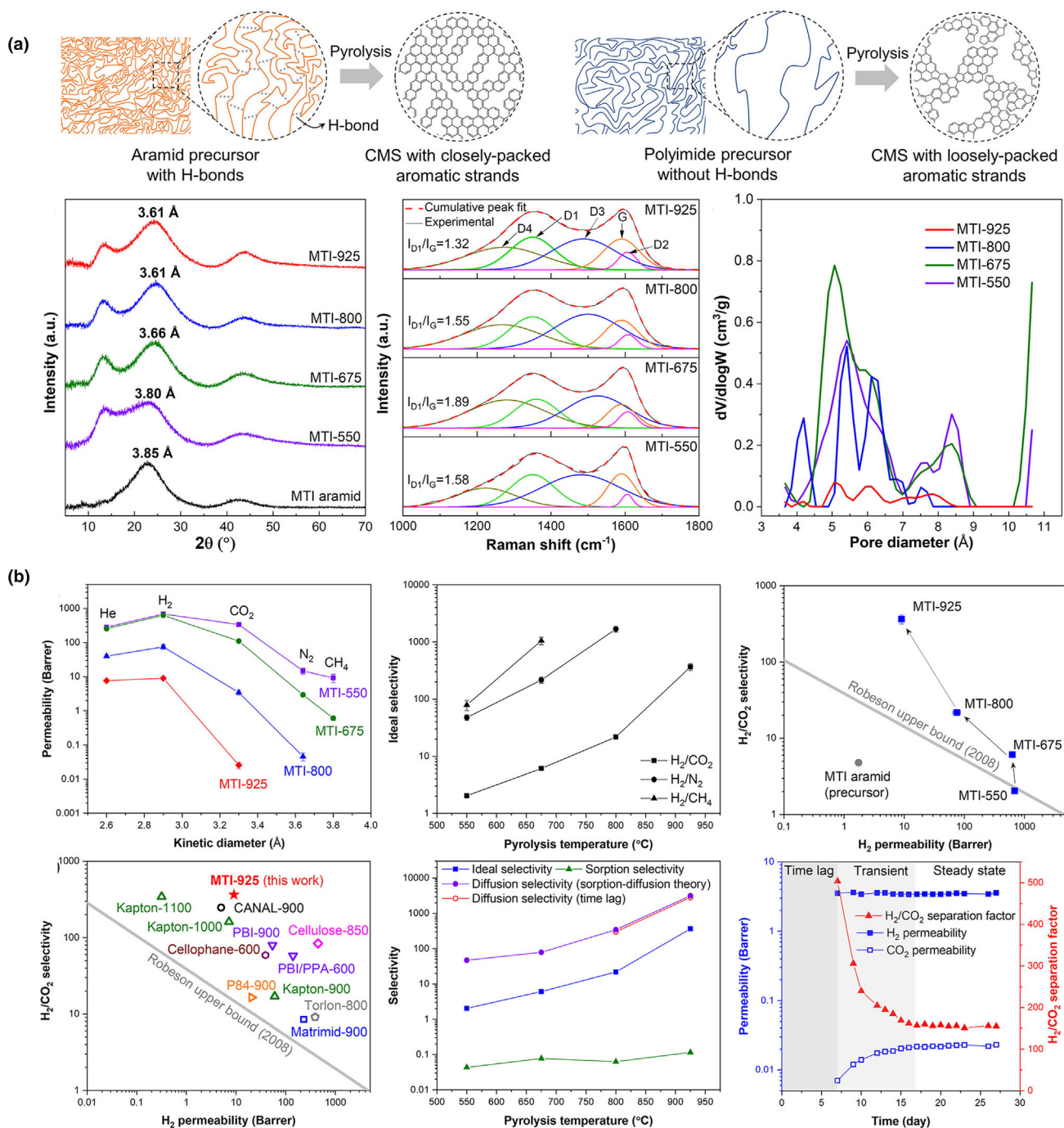


Figure 7. a) The illustration and the trend of the ultra-microporous generation through pyrolysis at different temperatures of an aromatic polyamide as a precursor of CMS membrane and b) the hydrogen separation performance of the resulting CMS membranes pyrolyzed at different temperatures. Reproduced with permission.^[180] Copyright 2022, American Chemical Society.

In addition to metal doping, the CMS precursor can also be mixed with other materials such as glycerol,^[164] micro-nanocrystalline cellulose,^[215] propylene glycol,^[164] pyrophosphoric acid,^[183] TiO_2 ,^[189] and zeolite.^[189,216–218] The beneficial aspect of having this composite is the possibility of the additive to tailor the porous structure of the resulting CMS membranes and rendering them to be more

suitable for hydrogen separation.^[164,215,218] For instance, by using around 1 wt% of propylene glycol as the additive, the H_2/CH_4 selectivity of the cellulose-derived CMS membrane can be increased to 3498 from 684 observed in the CMS membrane fabricated without additive.^[164] This performance does not have to be compromised with low hydrogen permeability since it can be maintained around 500

Barrer. In another study using zeolite as an additive at 7.5 wt%, the H_2 permeability in the 10X zeolite-doped CMS membrane can be improved to 1709 Barrer with H_2/N_2 and H_2/CH_4 selectivity of 105 and 551, respectively.^[216] The additive such as pyrophosphoric acid can also act as a cross-linking agent for polybenzimidazole.^[183] By using the cross-linked polybenzimidazole as a CMS precursor, a CMS membrane containing sub 0.33 nm ultramicropores, which is crucial for the hydrogen molecular sieving ability, can be fabricated by pyrolyzing the precursor at relatively low pyrolysis temperature around 600 °C. As a result, a CMS membrane with H_2 permeability up to 140 Barrer and H_2/CO_2 selectivity around 58 can be obtained.

Alternatively, the hydrogen separation performance of a CMS membrane can also be improved through post-modification strategy. This has been investigated, for example, by post-modifying the pore of the polyimide and polyetherimide-derived CMS membranes with a carbon layer formed from the carbonization of poly(*p*-phenylene oxide).^[187] Compared with the pristine CMS membranes, the H_2 permeability of the post-modified CMS membranes can be increased almost three times to be around 1450 and 812 Barrer for poly(*p*-phenylene oxide)/polyimide and poly(*p*-phenylene oxide)/polyetherimide, respectively. More remarkably, the H_2/N_2 and H_2/CH_4 selectivity for both CMS membranes can also be significantly improved from the range of 9–17 to be around 172 and 18–24 to be around 136 for poly(*p*-phenylene oxide)/polyimide and poly(*p*-phenylene oxide)/polyetherimide, respectively. This has been attributed to the formation of the carbon layer from poly(*p*-phenylene oxide) that can simultaneously improve the hydrogen molecular sieving by reducing the pore size of the polyimide and polyetherimide-derived CMS membranes and also enhance their gas sorption.

As the gas transport through the CMS membranes are also an activated process, the hydrogen selectivity of this material can also be affected by the operating temperature. In this case, operating the membrane at higher temperature might result in an increase in hydrogen selectivity^[161,162,195,208] even though a number of studies have also observed the contrasting trend.^[163,174,179,198] Higher operating temperature usually leads to the faster diffusion of the hydrogen. Meanwhile, the impact of the sorption of other gases also becomes lower resulting in an increase of hydrogen selectivity.^[162] However, when the hydrogen permeation across the CMS membranes is less affected by the change of the temperature compared with other gases, as usually indicated through the permeation activation energy, the reverse situation might occur, namely lower selectivity at high temperature.^[163,174] It has also been reported that higher operating pressure might help to increase the CMS membrane hydrogen selectivity.^[208] An increase of around 20% in H_2/CO_2 and H_2/N_2 selectivity and 50% in H_2/CH_4 selectivity has been reported as the operating pressure is increased from 2 to 4 bar as the H_2 permeability barely changes compared to other gases.^[208]

One of the most crucial issues encountered in the CMS membrane is the aging phenomenon which is caused by sorption of oxygen and water molecules.^[162,169,207,218] For instance, it has been observed that after 400 days storing in ambient condition, almost half of the hydrogen permeance is lost.^[169] In another study, 50 days of storage leads to the reduction of H_2 permeance and H_2/CO_2 selectivity about 40% and 10%, respectively.^[162] Regarding this phenomenon, it seems likely that, when the aging is reversible, the membrane performance might be partially brought back through heat treatment.^[162] For instance, it has been observed that up to 74% of the H_2 permeability can be recovered after heat-treating the aged CMS membrane.^[218] However, it can

also happen that the physisorption or chemisorption occurring in the CMS membrane is already irreversible and thus heat treating the CMS membrane does not help to gain back its initial performance.^[163,169] Therefore, in order to make the CMS membrane performance more stable and predictable, a high temperature treatment in the air atmosphere might then be carried out to fasten the aging. It has been observed that this process can half the aging time of a CMS membrane from 28 to 14 days before the hydrogen permeability stabilizes.^[207]

3.3.2. Graphene-Based Membranes

Graphene is a 2D nanomaterial of a carbon allotrope where the carbon atoms are arranged in a hexagonal lattice. Although a perfect graphene membrane is impermeable to any gases, its defective counterparts could be used in a gas separation process. In the field of hydrogen purification, this has been demonstrated by using graphene with exceptionally high hydrogen permeance (in the order of $10^{-2} \text{ mol m}^{-2} \text{ s}^{-1} \text{ Pa}^{-1}$, around 3×10^7 GPU) with satisfactory H_2/CO_2 selectivity around 8 when its thickness can be controlled within the atomic scale.^[219,220] The graphene membrane can also be modified using ozone to simultaneously control its defective sites to improve the hydrogen permeance and selectivity up to around 300% and 150%, respectively.^[221] The pores in the graphene material can also be artificially fabricated such as by employing focused ion beam, which can then be further modified by depositing nickel microislands responsible to enhance the CO_2 adsorptive property and thus hindering its permeation.^[222] As a result, a graphene membrane with H_2 permeance H_2/CO_2 selectivity around 20 000 GPU and 26, respectively, can be obtained. However, most studies are more directed toward the use of its derivatives, namely graphene oxide (GO) and reduced graphene oxide (rGO). Differing from graphene, GO is not a completely 2D material and therefore can be non-uniformly stacked to become permeable to small gases, as long as the energy barrier of gas permeation can be surpassed.^[223]

A defect-free GO membrane for hydrogen separation can be prepared through different methods such as vacuum filtration,^[224–237] spin coating,^[223,227,238] and spray-evaporation.^[239] Regardless of the chosen method, the GO membrane fabrication is usually initiated by preparing a GO suspension. In order to obtain a good GO membrane, the steps involved in this phase, such as centrifugation and dilution, need to be optimized.^[224] Once a good GO suspension is obtained, the next crucial step is to obtain a smooth GO membrane with less wrinkle sites and excellent interlayer stacking resulting in an optimum *d* spacing between the GO nanosheets that is sufficient to molecularly sieve hydrogen from other light gases. In this step, modifying the substrate with Silicalite-1 to improve the interfacial adhesion of the GO membrane,^[237] synthesizing the GO with Brodie instead of Hummer method,^[232] having a large GO nanosheets, which can be obtained through repeated freeze–thaw method^[227] or pre-cross-link the GO nanosheets with cations,^[235] ethylenediamine,^[228] or cysteamine^[234] have been proven to be helpful to control the *d* spacing of the GO membrane so it can perform well for hydrogen purification. In the case of spin-coating, directly spin-coating a GO solution on a polyethersulfone substrate, rather than firstly contacting the substrate to the air-liquid interface of the GO suspension, can produce a GO membrane with interlocked layer structure exhibiting molecular sieving ability.^[223] In another study, spinning polyethyleneimine as an intermediate layer between GO nanosheets, as can be seen in **Figure 8c,d**, might also help to reduce the electrostatic repulsive force between two

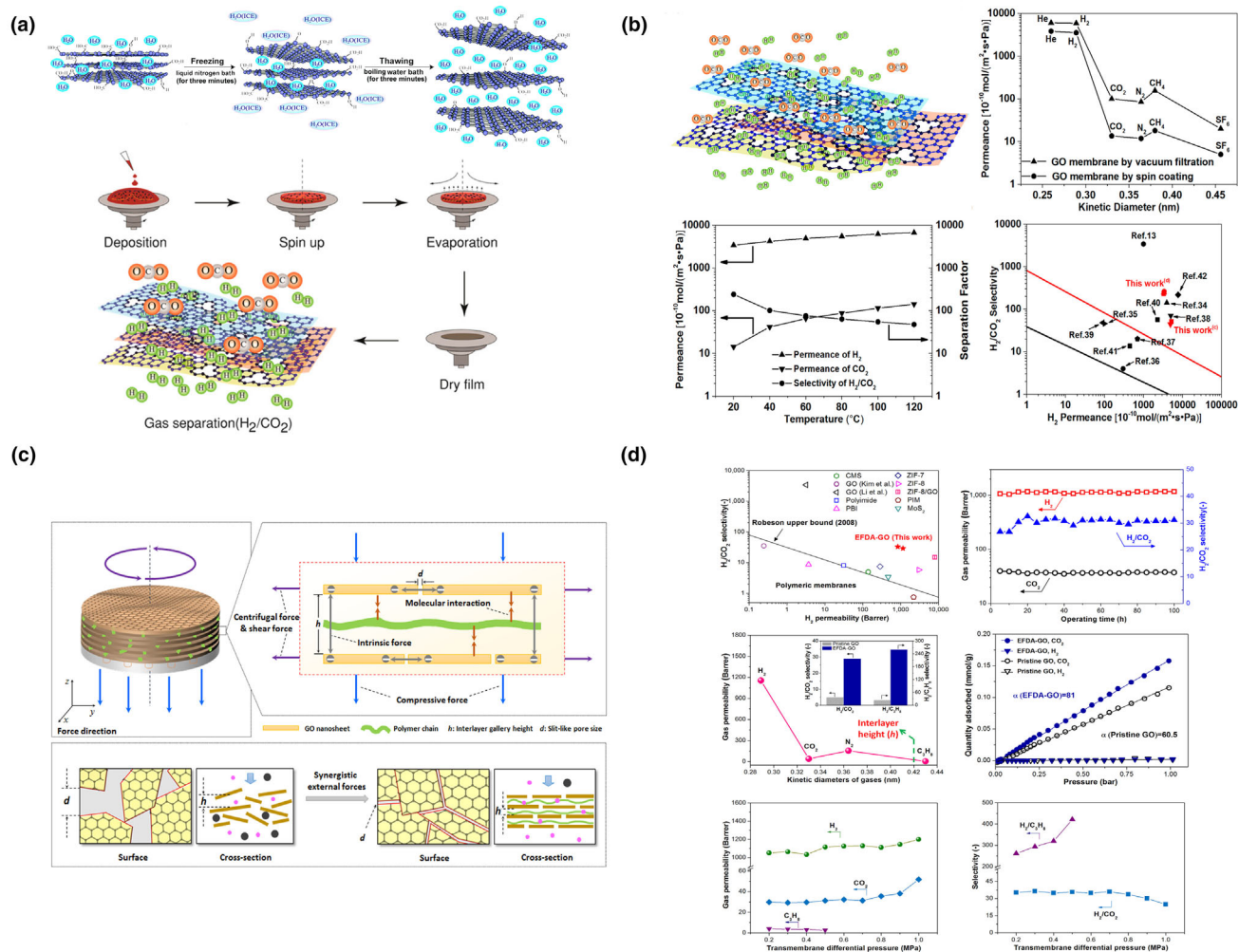


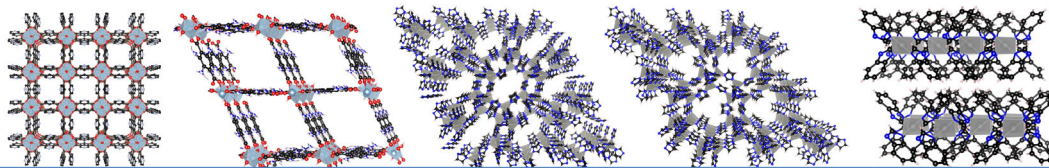
Figure 8. a) Illustration of the strategy to fabricate a GO membrane with freeze-thaw approach and c) PEI as an intermediate layer and their corresponding hydrogen separation performance shown in (b, d), respectively. Figures a, b^[227] and Figures c, d^[238] are reproduced with permission. Copyright 2016, American Chemical Society.

GO nanosheets and thus resulting in a more homogeneous interlayer GO stacking.^[238] When compared with the normal GO membrane prepared without PEI as the intermediate layer, the H₂/CO₂ selectivity of the latter is about six times higher reaching about 30 with H₂ permeability around 1200 Barrer. Meanwhile, in the case of self-standing GO membrane, Even though most of the GO membranes for hydrogen separation are fabricated on a porous support, using a slow filtration rate during the collection of the GO nanosheets is crucial to produce a good GO membrane exhibiting a molecular sieving capability as faster filtration leads to a more haphazard arrangement of the GO stacks and thus producing a looser membrane.^[240]

The hydrogen separation performance of a GO membrane can then be influenced by a number of factors but the gas pathways in a GO membrane is considered to be mainly influenced by the interlayer spacing of the GO sheets and the structural defects.^[223] The interlayer spacing of a GO membrane can then be reduced by reducing it into an rGO membrane.^[241] However, this strategy barely positively impacts the hydrogen separation performance of the modified membrane.^[225] Therefore, controlling the structural defects of a GO membrane might

be a more effective way to obtain a GO membrane with excellent hydrogen separation performance. In this case, it has been observed that the hydrogen permeance in a GO membrane decreases exponentially as the membrane thickness increases.^[224] It is then hypothesized that the hydrogen and other small gases permeate through the structural defects of the GO membrane with molecular sieving ability. Therefore, by optimizing the membrane thickness down to 9 nm, a GO membrane with H₂/CO₂ and H₂/N₂ selectivity of around 3400 and 900, respectively, can be obtained.^[224]

Moreover, the hydrophilicity of the GO membrane and the presence of various functional groups in the GO membrane can also influence the hydrogen separation performance. It has been observed that a GO membrane might show a CO₂-philic transport property in its pristine state where CO₂ is the fastest gas transported across the membrane.^[223] However, this condition can be reversed by thermally annealing and operating the membrane at elevated temperature to open up the GO pore and renders it to be less CO₂-philic and thus resulting in H₂/CO₂ selectivity around 40. However, it should also worth to note that, even though the hydrogen permeance of a GO membrane can be enhanced



MOF name	CAU-10-PDC	MIL-53(Al)-NH ₂	ZIF-7	ZIF-8	Zn ₂ (bim) ₄
Pore size (nm)	0.295 – 0.415	0.75	0.3	0.34	0.21

Figure 9. Some examples of MOFs used as a membrane material for hydrogen separation with their corresponding pore size.^[248,261,268,285,314]

at high temperature, operating the GO membrane at elevated temperature might also result in the reduction of its initial selectivity.^[223,229,231,233,236] For example, when operated at 120 °C, although the hydrogen permeance increases up to three times compared to the room temperature operation, the H₂/CO₂ selectivity of a GO membrane has been observed to get lower from around 240 to 47.^[227] In another study, the H₂/N₂ selectivity of a surfactant-modified GO operated at 100 °C also reduces to be around 10 from 30 when operated at room temperature.^[231] This might then be caused by various factors including the faster diffusion process of the gas transport at high temperature and also because the GO membrane becomes more porous.^[223,231]

3.4. Metal Organic Frameworks (MOF)- and Covalent Organic Frameworks (COF)-Based Membranes

3.4.1. Metal Organic Framework-Based Membranes

In the last two decades there is a growing interest in the research and development in the field of metal organic frameworks (MOFs) as a promising next generation of porous materials that can be used for various purposes such as environmental remediation,^[242] water purification,^[243] sensor,^[244] and also gas separation.^[245] As the name indicates, MOF is constructed from metal clusters which are connected by organic linkers. In addition to its high surface area and porosity, one of the main selling points of MOFs is their tailorable architecture, which means that one can rationally design a MOF for a specific purpose and this possibility is principally endless.

Various MOFs, as illustrated in **Figure 9**, have then been investigated to be achieved this objective such as CAU-1,^[246] CAU-10-H,^[247] CAU-10-PDC,^[248] CuBTC,^[249–258] MIL-53(Al),^[259] MIL-53(Al)-NH₂,^[260,261] MOF-74(Mg),^[262] MOF-74(Ni),^[263] UiO-66,^[264,265] UiO-66-NH₂,^[266] ZIF-7,^[267–270] ZIF-8,^[257,267,270–298] ZIF-9,^[299,300] ZIF-67,^[300–302] ZIF-78,^[303] ZIF-90,^[304–306] ZIF-95,^[307–309] and ZIF-100.^[310] As in the case of the zeolite membrane, there are two main routes that can be used to fabricate a MOF membrane for hydrogen separation, namely in situ crystallization^[247,254,256,267,270,274,276,280,299] and seeding followed by crystal growing.^[248,253,257,260,263,265,266,268,277–279,285,286,303,308] However, in the case of MOF membranes, there are more rooms to be explored as this material offers a different chemistry than zeolite. One of the strategies that are often explored is by separately preparing the metal and ligand solution which can then be brought in contact through different methods. For example, a substrate can be firstly covered by metal hydroxide nanostrand, metal oxide, or metal sol to

be later converted into MOF once exposed to the ligand precursor either in the solution or in a vapor-assisted mode as exemplified in the case of CuBTC^[251,258] and ZIF-8.^[283,293,297] Another strategy is by employing a layer by layer assembly method where the substrate is exposed consecutively to the metal and ligand precursor.^[255,273,275,301] Counter-diffusion is also another method to produce a MOF membrane where the metal and ligand precursor are located on the different side of the substrate so the substrate acts as a porous barrier between the two precursors. This method has been used to produce ZIF-8 membrane.^[271,288] A rather rapid MOF membrane can also be fabricated through an evaporation-induced crystallization,^[249] electrospray deposition,^[269] or crystallization using sustained precursor method^[294] which can significantly reduce the production time of the MOF membranes. Moreover, MOF membranes can also be produced with a certain orientation to improve its hydrogen molecular sieving effect. This is exemplified in the case of ZIF-95 where the presence of MOF seeds and MOF building block on a porous substrate can be converted into *c*-oriented dense membrane through vapor-assisted process.^[309]

The substrate for the MOF membranes can also be firstly modified before the MOF is grown on its surface. In the case of inorganic substrates, they can be firstly coated or modified by various methods such as immersing in the ligand solution,^[272] oxidation,^[256] coating with various molecules such as 3-aminopropyltriethoxysilane,^[286,299,304,307] 3-aminopropyltriethoxysilane-TiO₂,^[289] chitosan,^[253] cobalt nanosheets,^[302] gelatin containing metal hydroxide nanostrands,^[279] layered double hydroxide (LDH),^[281] LDH-ZnO,^[276] metal gels,^[291] poly(methyl methacrylate) (PMMA) which is followed by hydrolysis process,^[254] polydopamine,^[310] polydopamine-modified carbon nanotube,^[290] and ZnO.^[274,280,282,284,295,300] Meanwhile, in the case of a polymeric substrate, hydrolysis,^[250] ammoniation^[252,261] or coating with other materials with similar property as the MOF, such as metal phenolic networks,^[292] metal ions,^[250] or ZnO array,^[270] can also be an option to increase the MOF attachment to the support.

In the first development of a MOF membrane for hydrogen separation, a number of researches have been devoted to CuBTC since this MOF is relatively simple to be prepared. However, considering its relatively big pore aperture, the separation factor might not be too satisfactory. Addressing this issue, zeolitic imidazolate frameworks (ZIF) family MOF which possesses the properties of both zeolite and MOF,^[311] such as ZIF-7, ZIF-8, ZIF-9, ZIF-95, and ZIF-100 might offer a more promising separation performance since their pore aperture usually lies around 0.3 nm. Using a microfluidic approach, a ZIF-7 membrane has exhibited H₂ permeance around 22 × 10⁻¹⁰ mol m⁻² s⁻¹ Pa⁻¹ (6.6 GPU) and H₂ selectivity against N₂

and CH₄ around 35 and 34, respectively.^[267] In another investigation, a ZIF-7 membrane with higher H₂ permeance about $4.5 \times 10^{-8} \text{ mol m}^{-2} \text{ s}^{-1} \text{ Pa}^{-1}$ (134 GPU) can be obtained with H₂ selectivity against CO₂, N₂, and CH₄ around 13.6; 18 and 14, respectively.^[268] In the case of ZIF-8, up to around 23 and 78 in H₂/N₂ and H₂/CH₄ selectivity, respectively, with H₂ permeance $1.4 \times 10^{-8} \text{ mol m}^{-2} \text{ s}^{-1} \text{ Pa}^{-1}$ (41.8 GPU) has been reported.^[276] Even though the ZIF-8 framework is reported to be flexible and its pore aperture is a little bit bigger than ZIF-7, such a high hydrogen selectivity could be associated with the reduction of the ZIF-8 grain size and the suppression of the ZIF-8 framework flexibility when it is grown in the confined environment of ZnO nanocrystals. Using the same idea of a confined growing of ZIF-8, an ultrathin ZIF-8 membrane with thickness around 550 nm can also be produced using a counter-diffusion approach employing polydopamine-wrapped single-walled carbon nanotube as the interlayer.^[271] The resulting membrane shows H₂ permeance around $6.3 \times 10^{-7} \text{ mol m}^{-2} \text{ s}^{-1} \text{ Pa}^{-1}$ (1880 GPU) and H₂ selectivity against CO₂, N₂, and CH₄ around 43, 20, and 38, respectively. A good separation performance has also been exhibited by ZIF-9 membrane that has H₂ permeance and H₂/CO₂ separation factor around $1.1 \times 10^{-7} \text{ mol m}^{-2} \text{ s}^{-1} \text{ Pa}^{-1}$ (328.4 GPU) and 22, respectively.^[299] Using a secondary growing strategy by utilizing the ZIF-95 nanosheet geometry as the seed, a defect-free ZIF-95 membrane can also be grown on an alumina substrate showing a promising H₂ separation performance.^[308] The H₂ permeance of the membrane is reported to be around $1.7 \times 10^{-7} \text{ mol m}^{-2} \text{ s}^{-1} \text{ Pa}^{-1}$ (507.5 GPU) and its H₂ selectivity against CO₂, N₂, and CH₄ is found to be around 42, 37, and 40, respectively. When the orientation of the ZIF-95 can be controlled, a slightly better performance with H₂ permeance around $7.9 \times 10^{-7} \text{ mol m}^{-2} \text{ s}^{-1} \text{ Pa}^{-1}$ (2358.2 GPU) and H₂/CH₄ selectivity around 54 can also be obtained.^[309] In the case of ZIF-100, it has been found that the H₂/CO₂ selectivity of this MOF membrane can reach 70 with H₂ permeance around $5.8 \times 10^{-8} \text{ mol m}^{-2} \text{ s}^{-1} \text{ Pa}^{-1}$ (173.1 GPU).^[310] Even though its pore aperture is slightly larger than the kinetic diameter of CO₂, its high separation performance is attributed to the strong CO₂ adsorption within the framework resulting in the retardation of CO₂ permeation.

In order to further improve the hydrogen separation performance, the MOF membranes can also be post-modified such as through functionalization. For instance, a ZIF-67 membrane can be post-modified by introducing ethylenediamine into its pores.^[302] Even though the H₂ permeance decreases more than twice to be around $6.5 \times 10^{-7} \text{ mol m}^{-2} \text{ s}^{-1} \text{ Pa}^{-1}$ (1940.3 GPU), the H₂/CO₂ selectivity can be significantly improved from around 17 to 30. Using the same molecule, the pore of MOF-74(Mg) has also been successfully modified to improve its H₂/CO₂ separation from around 11 to be 28 while maintaining H₂ permeance around $1.2 \times 10^{-7} \text{ mol m}^{-2} \text{ s}^{-1} \text{ Pa}^{-1}$ (358.2 GPU).^[262] In addition to the pore narrowing effect, the presence of the amine group from ethylenediamine in a MOF with big pore aperture such as MOF-74(Mg) can also hinder the CO₂ passage through the adsorption effect. Post-modification can also be carried out by exploiting the functional group in the MOF such as with the aldehyde group of ZIF-90 which can be functionalized through imine condensation with ethanolamine^[305] or with organosilica.^[306] Compared with the non-modified membrane, the H₂ permeance of the ethanolamine-functionalized ZIF-90 only drops around 16% to be around $2 \times 10^{-7} \text{ mol m}^{-2} \text{ s}^{-1} \text{ Pa}^{-1}$ (597 GPU) but the H₂ selectivity against CO₂, N₂, and CH₄ significantly improves to be around 15, 16, and 19, respectively. A more significant improvement, however,

is obtained for the organosilica-modified ZIF-90, as illustrated in **Figure 10a**, which shows H₂ selectivity against CO₂ and CH₄ to be around 20 and 71, respectively. Post-modification can also be carried out with rapid thermal treatment as exemplified in ZIF-8.^[298] By thermally treating the ZIF-8 at 360 °C for less than 10s, the lattice flexibility of the ZIF-8 can be significantly reduced and thus resulting in a ZIF-8 membrane with H₂/N₂ and H₂/CH₄ selectivity of more 200, which is more than 10-fold improvement than the pristine ZIF-8 membrane and also significantly higher than most of the ZIF-8 polycrystalline membranes.

As in the case of zeolite membrane, a MOF membrane for hydrogen separation can also be fabricated from two different MOFs constructed as double layer, as studied in ZIF-90/ZIF-8,^[294] ZIF-8/ZIF-9,^[312] and ZIF-67/ZIF-9.^[312] In the case of ZIF-8/ZIF-9 and ZIF-67/ZIF-9, the main rationale to exploit the hydrogen molecular sieving property from ZIF-9 that has smaller pore size than ZIF-8 and ZIF-67.^[312] Meanwhile, both ZIF-8 and ZIF-67 contributes in reducing the CO₂ preferential adsorption. Using this strategy, the H₂ permeance of the ZIF-8/ZIF-9 and ZIF-67/ZIF-9 at 150 °C is found to be around $83.9 \times 10^{-9} \text{ mol m}^{-2} \text{ s}^{-1} \text{ Pa}^{-1}$ (250.4 GPU) and $53.3 \times 10^{-9} \text{ mol m}^{-2} \text{ s}^{-1} \text{ Pa}^{-1}$ (159.1 GPU), respectively, and its H₂/CO₂ selectivity is found to be around 9. In another investigation, a double layered MOF membrane of ZIF-8/ZIF-67 and ZIF-67/ZIF-8 have been studied for hydrogen separation.^[301] Compared with the ZIF-67 membrane, the H₂ selectivity against CO₂, N₂, and CH₄ can be improved almost twice to be around 13, 10, and 11, respectively. This might be attributed to the increase of the surface smoothness when growing the second layer of the MOF resulting in a MOF membrane with less defect densities.

One of the strongest performing MOFs for the hydrogen separation probably comes from the employment of nanosheet architecture. In this case, a study using 2D CuTCPP membrane which is grown in the *c*-orientation has shown a promising H₂ permeance and H₂/CH₄ selectivity around $2.4 \times 10^{-7} \text{ mol m}^{-2} \text{ s}^{-1} \text{ Pa}^{-1}$ (716.4 GPU) and 55, respectively.^[313] Even though the pore aperture of this MOF is quite large around 1 nm, by growing the MOF as a highly oriented membrane, the AB stacking of the MOF can be established resulting in a reduction of the pore aperture and thus imparting the hydrogen molecular sieving ability. A different situation is encountered, however, in the case of Zn₂(bim)₄ because its pore aperture is already very tight around 0.21 nm and thus can potentially only allow hydrogen to pass through while rejecting all other light gases.^[314] It has been successfully fabricated as a 1 nm thickness membrane through drop casting method on a hot surface. The H₂ permeance of this membrane is reported to be as high as 2700 GPU with around 291 H₂/CO₂ selectivity. Using the same strategy others sub-10-nm 2D MOFs such as Zn₂(bim)₃ MOF membrane, as illustrated in **Figure 10b,c**, with H₂ permeance and H₂/CO₂ selectivity around $65.1 \times 10^{-8} \text{ mol m}^{-2} \text{ s}^{-1} \text{ Pa}^{-1}$ (1943 GPU) and 128, respectively^[315] and [Cu₂Br(IN)₂]_n with H₂ permeance around 600 GPU and H₂/CO₂ and H₂/CH₄ selectivity around 190 and 290, respectively, can also be produced^[316] and thus demonstrating the versatility of this approach to fabricate a 2D MOF membrane with excellent hydrogen separation performance. In another study, an ultra-thin ZIF-L nanosheet membrane with a membrane-interlocked-support (MIS) architecture has also been developed by confining the grow of the nanosheets inside the voids of the porous support.^[317] As a result, a MOF membrane with high H₂ permeance around 4033 GPU and a very good H₂/CO₂ selectivity of around 321 can be obtained because the membrane intercrystalline

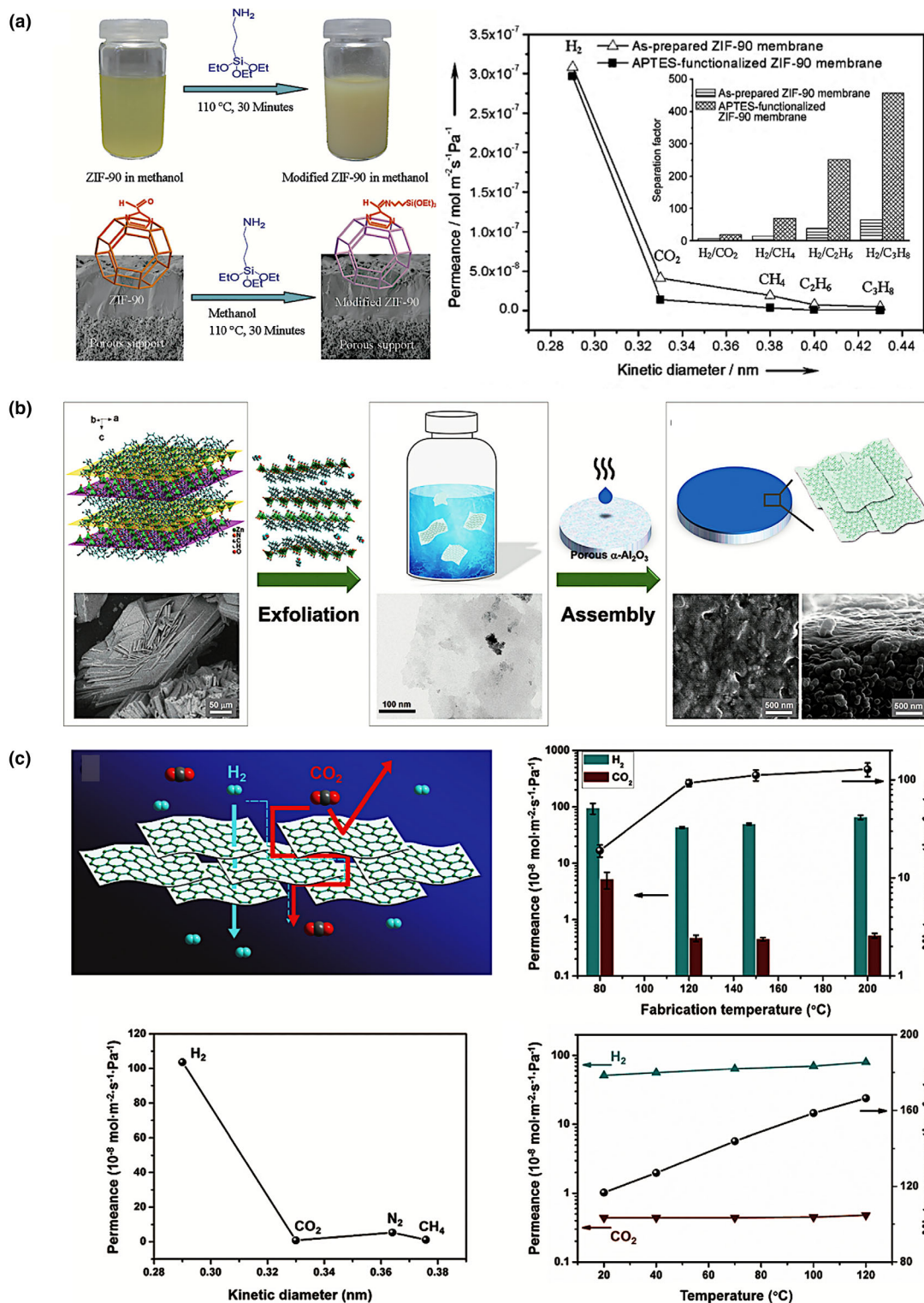


Figure 10. a) The illustration of the ZIF-90 pore modification using organosilica and the impact of the modification process on the hydrogen separation performance. b) The illustration of the fabrication process of 2D Zn₂(bim)₃ MOF membrane through exfoliation and drop-casting on a hot substrate and c) its hydrogen separation performance. Figure a^[306] and Figures b, c^[315] are reproduced with permission. Copyright 2012 (a) and 2017 (b, c) John Wiley and Sons, Inc.

structure is significantly reinforced. One of the most interesting features related to the 2D MOF membrane is the inverse relationship that could occur between membrane thickness and selectivity. In the case of $\text{Zn}_2(\text{bim})_4$, stacking the nanosheets more than a few layers can reduce the H_2/CO_2 selectivity from 291 up to 53.^[314] Similarly, in the case of $\text{Co}_2(\text{bim})_4$ 2D membrane which is fabricated using ligand–vapor phase transformation of a cobalt gel, increasing the membrane thickness from 57 to 750 nm results in the decrease of the H_2/CO_2 selectivity from 58.7 to around 10.^[318] This phenomenon then suggests the dependency of the gas selectivity on the nanosheet stacking behavior (i.e., misalignments or orderliness) which could lead to the generation of non-selective voids in the nanosheet stacking resulting in the reduction of gas selectivity.

Advancement in this field has also revealed the possibility to utilize the competing permeating gas to further enhance the gas selectivity. For instance, the performance of a CAU-10-PDC membrane has been observed to be significantly affected by the CH_4 molecule since it can induce the conformational change in the crystal lattice of the MOF.^[248] During the initial period of separation, the H_2 permeance is found to be 3326 Barrer with H_2/CH_4 selectivity around $2 \times 10^{-8} \text{ mol m}^{-2} \text{ s}^{-1} \text{ Pa}^{-1}$ (59.7 GPU). After more than 1300 minutes equilibration time, the H_2 permeance drops almost one order of magnitude lower but the H_2/CH_4 selectivity increases to be around 101. This could be attributed to the change of the pore limiting diameter of the MOF from 0.415 to 0.295 nm upon exposure to CH_4 . Another case is also observed in the amino-modified $\text{Zn}_2(\text{bim})_4$, which is synthesized through a mixed ligand strategy by mixing benzimidazole and 5-aminobenzimidazole.^[319] The H_2 permeance of the resulting nanosheet membrane is around 1966 GPU with a very high H_2/CO_2 selectivity around 985, which could be caused by the CO_2 molecules that are physisorbed at the interlayer of the nanosheets during permeation and thus contributing to regulate and stabilize the nanosheet stacking resulting in a significant improvement of the molecular sieving capability of the membrane.

In addition to the 2D MOF, another promising approach can also be seen in the direction of the employment of MOF-glass membrane. This has been investigated by using ZIF-62 because it has the glass-forming ability.^[320] The MOF-glass membrane is obtained by melt-quenching process where it is subjected to the melting temperature before being cooled down to form the glass. The advantage of this approach is, during the melting process, the MOF is in the liquid phase and thus has the ability to penetrate the porous support and also heal its intercrystalline defects generated during the polycrystalline membrane fabrication. In addition, the resulting MOF glass can still maintain its microporous structure and thus able to separate hydrogen from the light gases. The H_2 permeability of this membrane has been reported to be around 4600 Barrer with selectivity against N_2 and CH_4 to be 53 and 60, respectively.

For some of the MOF membranes, increasing the operating temperature does seem to benefit the hydrogen separation performance. This is evidenced, for instance, in the case of ZIF-7 membranes where the H_2/CO_2 selectivity increases at higher operating temperature.^[267–269] In one study, this value can improve remarkably to 13.6 from 5.4 as the operating temperature increases from 50 to 220 °C.^[268] In the case of ZIF-95 membrane, the H_2/CO_2 separation factor also increases from around 19 to be around 42 as the temperature goes up from 50 to 200 °C.^[308] The H_2/CO_2 selectivity of a 2D MOF membrane $\text{Zn}_2(\text{bim})_3$ has also shown the same trend where it increases from around 120 to be 160 as the operating temperature increases from 20

to 120 °C.^[315] In these cases, higher temperature will considerably enhance the H_2 diffusion compared to other gases, as can be indicated through the permeation activation energy. In addition, the adsorption of other gases might also be hindered as the temperature increases.

A contrasting trend, however, is also reported as can be seen in the selectivity trend of a CuBTC,^[250] MIL-53(Al)- NH_2 ,^[261] MOF-74(Mg),^[262] amine-modified MOF-74(Mg),^[262] ZIF-9^[299] and ZIF-100.^[310] For instance, the H_2/CO_2 selectivity of a ZIF-9 membrane reduces from around 22 at 25 °C to be around 15 at 125 °C. Such a decrease in the selectivity can also be more pronounced in a MOF membrane with high affinity toward CO_2 . For instance, the amine-modified MOF-74(Mg) experiences a drop in H_2/CO_2 selectivity from 28 to around 10 as the operating temperature increases from 25 to 100 °C.^[262] Meanwhile, its non-modified counterpart only exhibits a slight drop from 10.5 to be around 10. In these cases, the diffusion of the competitor gases is more affected by the change of the operating temperature, as can be indicated by their activation energy, and thus increasing the competitive diffusion process of hydrogen to go through the membrane. Another example can be seen in the case of ZIF-100 membrane, where the H_2/CO_2 separation is highly dependent on the retardation of the CO_2 permeation because of the strong adsorption, increasing the operating temperature from 25 to 150 °C results in the reduction of H_2/CO_2 selectivity from 70 to around 20.^[310] This is because less CO_2 is adsorbed at higher temperature and therefore it can permeate more freely resulting in lower H_2/CO_2 selectivity.

3.4.2. Covalent Organic Frameworks-Based Membranes

Differing from MOF, covalent organic frameworks (COF) is completely built from organic materials and thus does not contain any inorganic parts. As in MOF, the architecture of COF can also be rationally tuned and thus rendering it for principally having endless possible structure. There are a number of studies using different type of COFs investigated for hydrogen separation process such as ACOF-1,^[321] COF-300,^[322,323] COF-320,^[324] DMTA-TAM-COF,^[325] LZU-1,^[321,326] N-COF,^[323] TFB-BD,^[326] TpEBR,^[327] TpPaMe,^[328] and TpPa-SO₃Na.^[327]

As in the case of MOF membrane fabrication, the porous substrate for the COF membrane fabrication can also be modified using different approach in order to improve the attachment of the COF membrane such as by using 3-aminopropyltriethoxysilane^[321,324] and polyaniline.^[322,325] Such a stronger attachment is possible since a covalent bond can be established between one of the COF monomers and the modifier. For example, by using 3-aminopropyltriethoxysilane, the amino group of this molecule can react with the aldehyde group through imine condensation.^[324] In addition, the substrate can also be functionalized to control the orientation of the COF membrane as exemplified by the use of cobalt–aluminum-layer double hydroxide (CoAl-LDH) layer to vertically grow COF-LZU-1 and TFB-BD COF membranes.^[326] However, it is also possible to fabricate a self-standing COF membrane in the absence of a porous substrate as exemplified in the case of N-COF and COF-300.^[323] This strategy relies on molding the mixture of the COF building blocks and transforming them into a crystalline structure in an autoclave with the assistance of the vapor from the solvents.

Despite these numerous attempts, not all of them have shown an excellent performance for hydrogen separation because of their relatively big pore aperture. For example, COF-320 membrane with pore aperture around 0.8 nm also shows H_2 selectivity against N_2 and CH_4

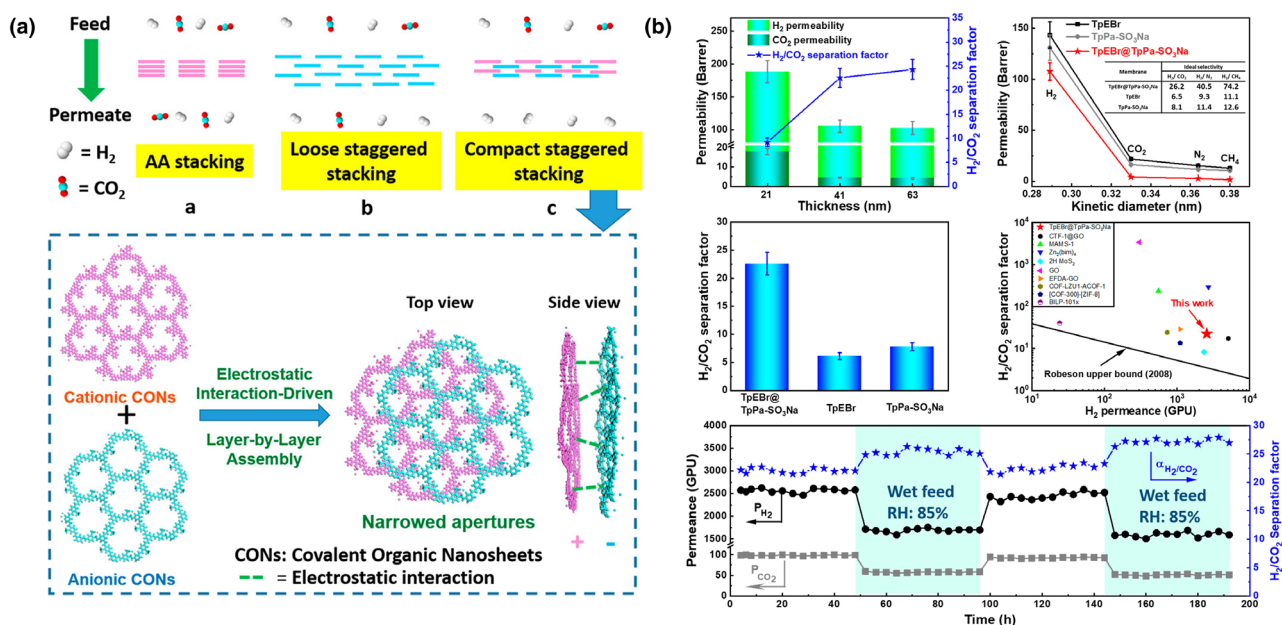


Figure 11. a) A schematic to improve the hydrogen molecular sieving in a COF membrane by alternately stacking cationic and anionic COF and b) the hydrogen separation performance of the resulting COF membrane. Reproduced with permission.^[327] Copyright 2020 American Chemical Society.

around 3.5 and 2.5, respectively.^[324] A better performance has then been shown by LZU-1 COF membrane with around 1.8 nm pore aperture that has moderate H₂ selectivity against CO₂, N₂, and CH₄ around 6, 8, and 9, respectively.^[321] However, it a rather sharp hydrogen molecular sieving cannot be seen in these cases.

There are, however, cases where a sharp hydrogen molecular sieving is observed in COF membranes. For example, in the case of N-COF and COF-300, the H₂/CO₂ separation factor is found to be around 13.8 and 11, respectively, while the H₂ permeance is around 4319 and 5160 GPU, respectively.^[323] In both cases, although the pore aperture of the COF is relatively big, the CO₂ molecules do have a tendency to get adsorbed in the COF's pores while the H₂ can diffuse freely resulting in high H₂ permeance and selectivity. Numerous studies have also been attempted to improve the molecular sieving capability of the COF membranes.

One possible strategy to improve the hydrogen molecular sieving in a COF membrane is to fabricate it as a dual-layer membrane as in the case of zeolite and MOF. In this case, a dual-layer LZU-1-ACOF-1 membrane has been successfully fabricated with H₂ permeability around 600 Barrer and has exhibited a high H₂ selectivity against CO₂, N₂, and CH₄ around 24, 84, and 100, respectively.^[321] Such a high hydrogen selectivity can be obtained because of the interlacing of the pore network at the interface between the COF layers resulting in improved molecular sieving. Another strategy is to vertically aligned the COF rather than conventionally aligning them horizontally. In this case, the separation process will take place through the interlayer spacing of the COF which is around 0.3–0.4 nm and thus can perform hydrogen molecular sieving.^[326] Using this strategy, the LZU-1 COF membrane has shown H₂ permeance around 3500 GPU with H₂/CO₂ and H₂/CH₄ selectivity around 30.

Another strategy is to stack the COF membrane with other materials with opposing charge to reduce its pore aperture. In this case, a combination of cationic TpEBr COF nanosheet and anionic TpPa-SO₃Na COF nanosheet has been studied for showing a great promise for hydrogen

separation.^[327] As illustrated in **Figure 11**, the rationale behind this strategy is to reduce the pore aperture of the COF's constituents by alternately stacking the cationic-anionic COFs on a porous alumina substrate using the Langmuir-Schaefer (LS) method. As a result, an ultrathin 41 nm COF composite membrane can be fabricated showing H₂ permeability around 108 Barrer and H₂ selectivity against CO₂, N₂, and CH₄ around 26, 40, and 74, respectively. This is in stark contrast to the H₂ selectivity of both COF constituents against CO₂, N₂, and CH₄ which is only found to be moderate in the range of 7, 10, and 12, respectively. Using the same strategy, the pore aperture of cationic TpPa-1 COF can also be reduced by stacking with non-porous anionic MXene Ti₃C₂T_x by utilizing the opposite charge of the two materials.^[329] Compared with the pure TpPa-1 COF membrane, the H₂ permeance of the composite decreases from $73.9 \times 10^{-8} \text{ mol m}^{-2} \text{ s}^{-1} \text{ Pa}^{-1}$ (2206 GPU) to $23.5 \times 10^{-8} \text{ mol m}^{-2} \text{ s}^{-1} \text{ Pa}^{-1}$ (702 GPU) but the H₂/CO₂ selectivity can be significantly improved almost six times to be 64.

As observed in the MOF membranes, the hydrogen separation performance in COF membranes can also be affected by the operating temperature considering the activated diffusion process of the hydrogen. It has been reported that increasing the operating temperature can improve the hydrogen selectivity toward the light gases.^[327] This can happen when the hydrogen permeation is more affected by the change of temperature in comparison to other gases, which might also be effectively blocked because of the molecular sieving effect.^[327] For some cases, the H₂ selectivity can also be unchanged or slightly drop.^[321,323] In these cases, the activated diffusion process of the light gases is in a strong competition with the hydrogen and thus resulting in unchanged hydrogen selectivity or a slight reduction since the hydrogen permeation will be slightly blocked.^[323]

A membrane for hydrogen separation can also be constructed from a composite containing both MOF and COF. The first strategy is to fabricate them as a bilayer membrane. This has been investigated by a

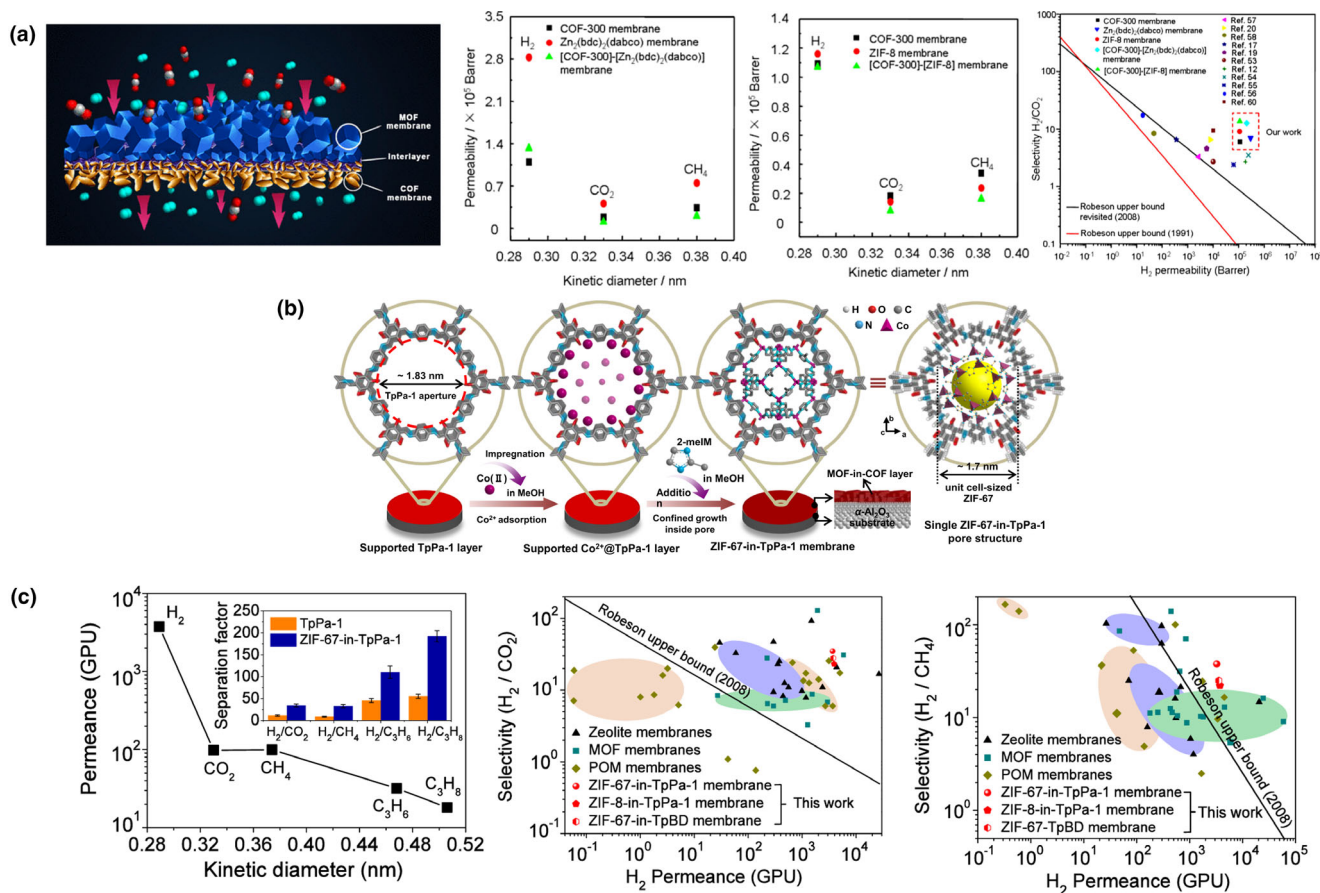


Figure 12. a) An illustration of a MOF-COF bilayer membrane fabricated using COF-300–Zn₂(bdc)₂(dabco) and COF-300–ZIF-8 and their corresponding hydrogen gas separation performance. b) A schematic of the ZIF-67-in-TpPa-1 MOF-in-COF membrane and c) its hydrogen gas separation performance. Figure a is reproduced with permission.^[322] Copyright 2016 American Chemical Society. Figures b and c are reproduced with permission.^[330] Copyright 2021 the authors and Springer Nature.

number of investigations involving COF-300–Zn₂(bdc)₂(dabco),^[322] COF-300–ZIF-8,^[322] and H₂P-DHPh COF–UiO-66.^[264] As can be seen in **Figure 12a**, the resulting COF-300–Zn₂(bdc)₂(dabco) and COF-300–ZIF-8 composite membranes have shown an increase in H₂/CO₂ selectivity to be around 12.6 and 9, respectively, from 6 that is observed in the pure COF-300 membrane. A better performance is obtained in H₂P-DHPh COF – UiO-66 where H₂ permeability and H₂/CO₂ selectivity around 109 000 Barrer and 33, respectively, can be obtained and is significantly better than the pure UiO-66 membrane.^[264] In these cases, the performance improvement could be attributed to the synergistic interaction occurring at the interlayer such as by acting as an anchor for other materials or to heal the defective sites. Another strategy to combine MOF and COF is to grow the former within the pore of the latter as exemplified in the case of ZIF-67 grown in TpPa-1 and is also illustrated in **Figure 12b,c**.^[330] Considering the relatively big pore size of the COF, such a space can actually be utilized to grow MOF which resulting in the establishment of a complex MOF-in-COF structure with improved hydrogen molecular sieving when compared with the pure COF membrane. The resulting composite membrane has then shown H₂ permeance around 3400 GPU with H₂/CO₂ and H₂/CH₄ in the range of 33–35. This strategy has also been successfully used to fabricate a free-standing ultrathin MOF-in-COF membrane utilizing ZIF-67 which is grown inside the

PBD COF membrane.^[331] Such a modification is highly effective to reduce the COF pore size from 2 nm to be around 0.3–0.6 nm and thus rendering the composite membrane to be suitable for hydrogen separation. The optimized synthesis condition can then result in a composite membrane with H₂ permeance around $73.9 \times 10^{-8} \text{ mol m}^{-2} \text{ s}^{-1} \text{ Pa}^{-1}$ (2206 GPU) and H₂/CH₄ selectivity around 34.

3.5. Microporous Polymeric Membranes

While the already discussed materials can be considered as inorganic, except MOFs which can be considered hybrid, there is also recently a significant advancement in the field of polymeric materials with promising hydrogen separation performance, particularly in the field of microporous polymeric membranes. Differing from the conventional polymeric materials, these microporous polymers have intrinsic microporosity that can be rationally tuned during the synthesis process. There are then two types of microporous polymers that have been recently developed as an advanced membrane material: polymer of intrinsic microporosity (PIM) and thermally rearranged (TR) polymers. Despite its huge potential as a material for gas separation processes, most of the studies using both microporous polymers are usually directed for CO₂

separation considering their high selectivity because they usually exhibit high solubility toward CO₂. Despite this, because of the possibility to rationally tune their property, a number of researches have also been directed to use both for hydrogen separation.

3.5.1. Polymer of Intrinsic Microporosity (PIM)

Polymers of intrinsic microporosity (PIM) was firstly discovered by Budd and McKeown in 2004.^[332,333] Differing from the already discussed materials previously, PIM is solution processable and therefore improving its ease of processing when it is going to be fabricated as a membrane. The high porosity and surface area of PIM is caused by the inability of the PIM polymer to efficiently pack and rotate because of the presence of the bulky contortion sites in the polymer backbone. PIM can then be generally classified into two main types: ladder PIMs and PIM-polyimide (PIM-PI).^[334] Ladder-PIM can be further grouped based on its site of contortion such as spiro-center, ethanoanthracene and Troger's base.^[334,335] Similarly, the PIM-PI can also be further grouped based on its contortion site either it is based on dianhydride or diamine.^[334]

The first PIMs that are investigated for hydrogen separation is PIM-1 and PIM-7 which are cast as a film with thickness around 46 and 28 μm, respectively.^[336] The H₂ permeability for PIM-1 and PIM-7 is found to be around 1300 Barrer and 860 Barrer, respectively. The H₂ selectivity against N₂ and CH₄ is reported to be around 14 and 10.4, respectively, for PIM-1 and 20.4 and 14, respectively, for PIM-7. Despite this satisfactory performance, the H₂/CO₂ selectivity of both PIMs is below 1 because of the high CO₂ solubility of the materials.

Afterward, several attempts have been conducted to improve the gas separation performance of PIMs, particularly focusing in enhancing the rigidity of PIM's structure and increasing the inefficiency of its chain packing to yield a membrane with more microporous structure. In the case of PIM-1, for instance, the chain rigidity can be improved through intramolecular locking mechanism of the spiro carbon resulting in the increase of H₂ permeability from 4270 to 9870 Barrer and H₂ selectivity against N₂ and CH₄ from 8 to 10 and 4.3 to 7.5, respectively.^[337] Another strategy that can be used is to co-polymerize PIM-1 using *p*-tert-butylcalix [4] arene to increase its chain packing inefficiency since the *p*-tert-butylcalix [4] arene has a bulky structure that can contribute in expanding the free volume of PIM-1.^[338] By optimizing the co-polymerization process, the H₂ permeability of the PIM-1 can be increased from 1738 to 2547 Barrer without sacrificing its selectivity against N₂ and CH₄ which is maintained be around 12 and 9, respectively. Meanwhile, for other cases, the most common employed strategy is by using monomers bearing different units such as hexaphenylbenzene (HPB),^[339] spirobifluorene (SBF),^[340–342] triptycene (Trip)^[343–346] and Tröger's base (TB)^[347–350] to rationally tune PIM microporous structure and its rigidity as illustrated in **Figure 13**.

Among this PIMs, there are several good candidates for hydrogen separation. TB-based PIMs such as PIM-EA-TB (EA = ethanoanthracene) looks promising because it has an unusual gas transport property since H₂ permeates faster than CO₂ and thus indicating the preference for the permeation of smaller gas molecule.^[347] As a result, PIM-EA-TB exhibits H₂/N₂ and H₂/CH₄ selectivity around 11, which is considerably higher than other PIMs and quite close to both PIM-1 and PIM-7, but with significantly higher H₂ permeability around 7700 Barrer, which is significantly higher than PIM-1 and PIM-7. A similar result is

also obtained by using methanopentacene (MP) as the bridged bicyclic structural unit in PIM-MP-TB.^[348] The H₂ permeability of this particular PIM is found to be around 4000 Barrer and its H₂ selectivity against N₂ and CH₄ is found to be around 20 and 15, respectively. Higher hydrogen separation performance can also be obtained using triptycene-based PIM such as PIM-Trip-TB that has comparable performance with PIM-EA-TB.^[346] A better hydrogen separation performance, however, can be obtained using another triptycene-based PIM called TPIM 1 utilizing the rigid and paddlewheel-structure of the bridgehead-substituted triptycene moiety.^[344] As a result, a PIM membrane with a more prominent ultramicroporous structure capable of enhanced hydrogen molecular sieving can be obtained as reflected by its H₂ permeability reaching 2666 Barrer and its H₂ selectivity against N₂ and CH₄ falling around 50.

PIM-PI is also another class of PIM that can be used for hydrogen purification. The first development of PIM-PI is initiated by the synthesis of the PIM-PI series 1–8^[351,352] with the further addition of PIM-PI series 9–11 a few years later.^[353] Compared with the ladder PIM, the H₂ selectivity of PIM-PI looks more promising. For example, the H₂/N₂ and H₂/CH₄ selectivity of PIM-PI-2 is found to be around 24 and its H₂ permeability is about 220 Barrer.^[351] Similarly, PIM-PI-4 and PIM-PI-7 have shown H₂/N₂ and H₂/CH₄ selectivity around 18 and 14, respectively, with H₂ permeability in the range of 300–350 Barrer.^[351] Later on, a series of KAUST-PI 1–7 were also developed.^[354] Differing from the PIM-PI series, except for KAUST-PI-7, the trend of the gas transport property of the KAUST-PI is similar with the PIM-EA-TB where hydrogen is the fastest permeating gas. Therefore, most of them can combine good H₂ permeability and selectivity. In particular, KAUST-PI-1 has exhibited H₂ permeability almost 4000 Barrer, which is about one order of magnitude higher than the best-performing PIM-PI series, and is also accompanied with relatively high H₂/N₂ and H₂/CH₄ selectivity around 38.^[354]

As in the case of ladder PIM, the dianhydride contortion site of the PIM-PI can also be constructed using spirobifluorene-based dianhydride (SBFDA) resulting in a PIM-PI called SBFDA-DMN (DMN = 3,3'-dimethylnaphthidine).^[355] However, the resulting H₂/N₂ and H₂/CH₄ selectivity is only around 10 and therefore very moderate. A slightly better result is reported using triptycene-based dianhydride with diamine as the monomers to construct both TDA-DMN1 and TDAi3-DMN (TDA and TDAi3 = dimethyl- and diisopropyl-triptycene-based dianhydride monomers).^[356] Both membranes show H₂ permeability in the range of 2200–3000 Barrer and H₂ selectivity against N₂ and CH₄ in the range of 14–18. As in the case of PIM, a quite promising result can also be obtained by using ethanoanthracene (EA) as exemplified by the fabrication of PIM EA-DMN and EAD-DMN (EAD = -dibenzodioxane-containing ethanoanthracene).^[357,358] By fabricating the PIM EA-DMN as a 15 μm film, the resulting membrane has H₂ permeability and H₂/N₂ and H₂/CH₄ selectivity around 1844 Barrer and more than 40, respectively. Meanwhile, the H₂ permeability of a 23 μm EAD-DMN membrane is around 1289 Barrer with H₂ selectivity against N₂ and CH₄ to be around 30 and 23, respectively.^[357] In addition, PIM-PI can also be constructed using a pseudo-TB-derived dianhydride and its dione-substituted resulting in PIM-PI called CTB1-DMN (CTB1 = 5,6,11,12-tetrahydro-5,11-methanodibenzo[a,e][8]annulene-2,3,8,9-tetracarboxylic anhydride) and CTB2-DMN (CTB2 = 6,12-dioxo5,6,11,12-tetrahydro-5,11-methanodibenzo[a,e][8]annulene-2,3,8,9-tetracarboxylic dianhydride), respectively.^[359] The latter performs better than the former with H₂ permeability around 1150 Barrer and both H₂/N₂ and H₂/CH₄ selectivity around 28.

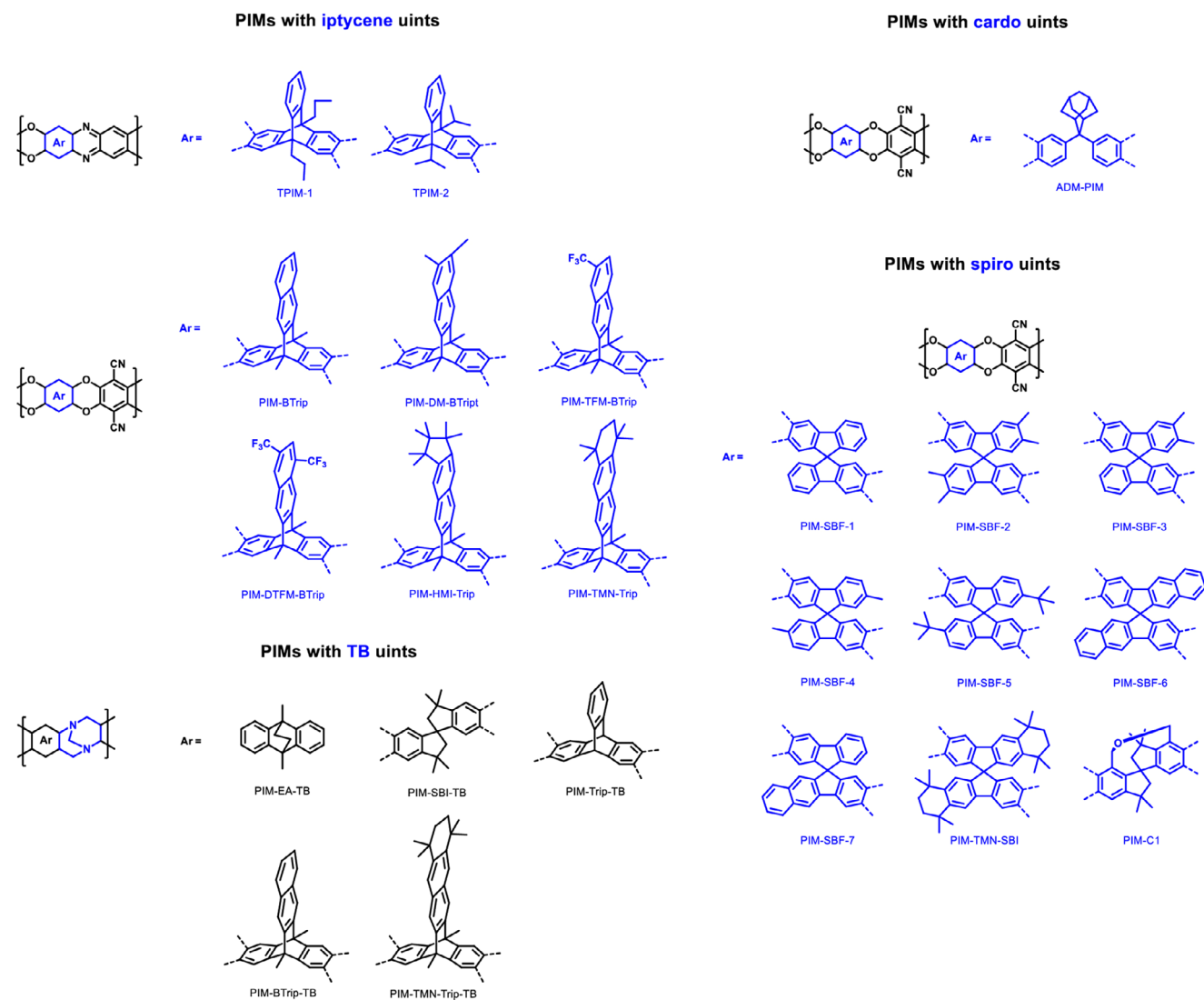


Figure 13. PIMs bearing different units to improve their microporosity and rigidity. Reproduced with permission.^[335] Copyright 2020 John Wiley and Sons, Inc.

Another strategy to fabricate PIM-PI membranes is to have contortion site in the diamine part of the PI and this can be constructed using spirobifluorene.^[360] Using (4,4'-hexafluoroisopropylidene) diphthalic anhydride (6FDA) as the dianhydride, it has H_2/N_2 and H_2/CH_4 selectivity around 30 and 37, respectively, but low H_2 permeability around 200 Barrer. Another possibility is to use TB-based diamines. However, some of them have still shown a similar performance as in the previous case, as exemplified in the PI-TB-1 to PI-TB-5.^[361,362] In this case, the H_2 permeability of PI-TB-3 is found to be around 300 Barrer with H_2/N_2 and H_2/CH_4 selectivity around 31 and 44, respectively.^[361] Also using two different TB-based diamine, namely 2,8-diamino-4,10-dimethyl-6H,12H5,11-methanodibenzo[1,5]diazocine (TBDA1) and 3,9-diamino-4,10-dimethyl-6H,12H-5,11-methanodibenzo[1,5]diazocine (TBDA2), a series of PIM-PI with significantly higher H_2/N_2 and H_2/CH_4 selectivity around 54 and 72, respectively, can be achieved but still with relatively low H_2 permeability around 159 Barrer.^[363,364] A PIM-PI membrane with H_2 permeability around 3300 Barrer is then

reported with methyl-substituted TB diamine (4MTBDA) combined with four different dianhydrides.^[365] However, this must also be compensated with relatively low H_2/N_2 and H_2/CH_4 selectivity around 11 and 9, respectively, in 4MTBDA-PMDA. A relatively good trade-off is reported in another TB-based PIM-PI-TB-1 and PIM-PI-TB-2 utilizing the di-ortho-substituted groups TB-based diamine with 6FDA as the dianhydride.^[366] The H_2 permeability of PIM-PI-TB-2 is found to be around 600 Barrer with H_2/N_2 and H_2/CH_4 selectivity around 17 and 19, respectively. Similarly, PIM-PIs using TB-based diamine with bio-dianhydride as the comonomer called Bio-TPBI-1, Bio-TPBI-2, Bio-PITB-1, and Bio-PITB-2 have also exhibited a good permeability-selectivity trade-off.^[367,368] The H_2 permeability and H_2/N_2 and H_2/CH_4 selectivity for these membranes is in the range between 700 and 1000 Barrer of 20–30, respectively. Iptycene family can also be used to construct the contortion site of the diamine side of the PIM-PI as exemplified by using substituted 1,4-triptycene,^[369] 2,6-diaminotriptycene and its extended version (DAT-1 and 2)^[370] and

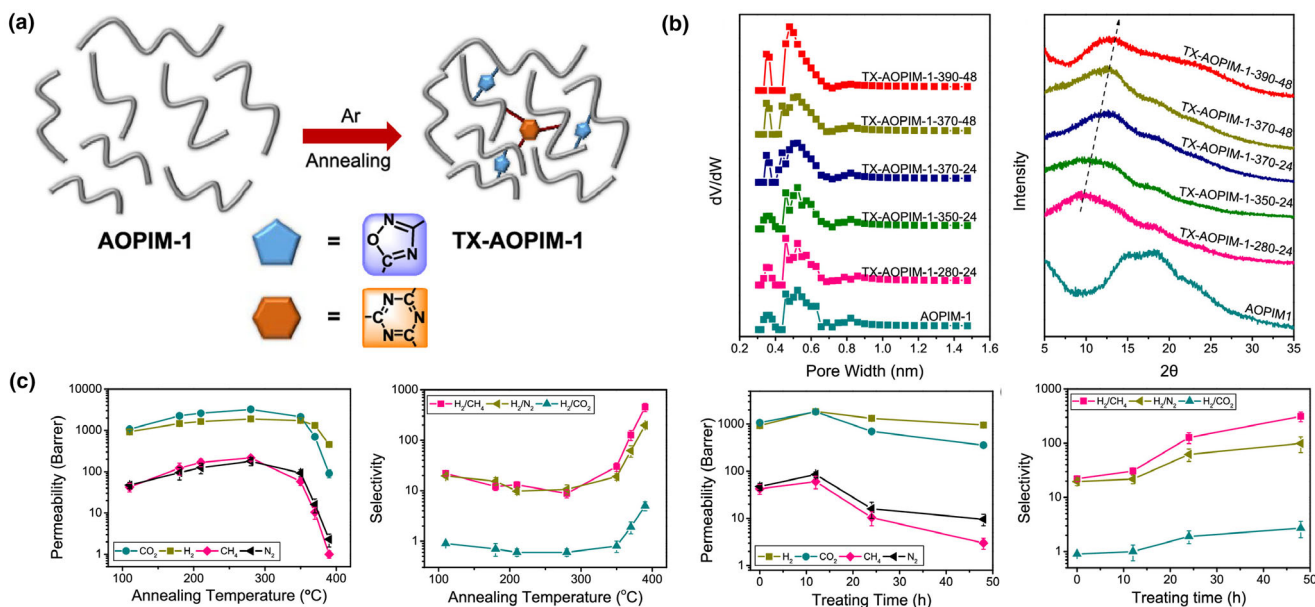


Figure 14. a) An illustration of the thermal treatment process to self-cross-link AO-PIM-1, b) the pore structure evolution of the AO-PIM-1 after the thermal treatment and c) the impact of various thermal treatment parameters on the hydrogen separation performance of thermally-treated AO-PIM-1. Reproduced with permission.^[379] Copyright 2021 American Chemical Society.

pentiptycene.^[371] For triptycene-based PIM-PI, even though a significantly high H_2/N_2 and H_2/CH_4 selectivity up to around 90 and 161 is reported for 6FDA-1,4-trip- CH_3 , all the membranes suffer from a relatively low H_2 permeability that is around 50 Barrer.^[369] Meanwhile, for pentiptycene PIM-PI, the H_2 permeability is generally slightly higher in the range of 100–190 Barrer accompanied with H_2/N_2 and H_2/CH_4 selectivity in the range of 26–42 and 34–52, respectively.^[371] A quite similar but better performance can be seen by combining 6FDA with 2,6-diaminotriptycene (DAT1) and its extended version (DAT2), resulting in 6FDA-DAT1 and 6FDA-DAT2, respectively. Since 6FDA-DAT2 is constructed using the extended version of DAT1 it has larger pore size. As a result, the H_2 permeability of 6FDA-DAT2 is higher than 6FDA-DAT1 (281 Barrer vs. 198 Barrer). Despite this, higher H_2 selectivity against N_2 and CH_4 is found in 6FDA-DAT1, which is around 42 and 62, respectively, in comparison to 6FDA-DAT2, which is reported to be around 31 and 40, respectively, as, with smaller pore size, the former has better molecular sieving ability than the latter.^[370]

Both ladder PIM and PIM-PI can also be functionalized with different functional groups to improve its hydrogen separation properties by introducing various functional groups such as amidoxime,^[372] carboxyl,^[373–375] hydroxyl,^[376] and thioamide.^[377] For example, as high as around 50 in H_2/N_2 selectivity is reported in PIM containing high carboxylate functional groups, even though the H_2 permeability decreases to be around 90 Barrer, which is caused by the shortening of the interchain distances and thus increasing the diffusivity selectivity.^[374] A rather high H_2 permeability around 900 Barrer can then be found in the case of amidoxime-functionalized PIM-1 (AO-PIM-1) with H_2/N_2 and H_2/CH_4 selectivity around 27, which is more than twice higher than the PIM-1, since this functional group enhances the rigidity of the PIM and shifts the PIM porosity to be in the ultramicroporous region resulting in a more enhanced molecular sieving.^[372] A better performance for hydrogen separation is then exhibited by a

combination of using carboxylate-containing PIM and cross-linking process as demonstrated in the C-CoPIM-TB-1 and C-CoPIM-TB-2.^[375] Both PIM membranes are obtained by cross-linking the carboxylate-containing triptycene-based copolymer named CoPIM-TB-1 and CoPIM-TB-2 using glycidol. The H_2 permeability of both membranes falls around 5000 Barrer, which is just slightly lower than their non-cross-linked counterparts, but they exhibit a relatively high H_2/N_2 and H_2/CH_4 selectivity around 30, which is almost a twofold improvement compared with the non-cross-linked ones.

In addition to the functionalization, PIM membranes can also be modified through various post-treatments to improve their hydrogen separation performance. In general, the function of such treatments is to increase the diffusive selectivity through the generation of ultramicropore and creation of a denser membrane structure suitable for molecular sieving.^[378,379] Therefore, the first consequence of such treatments is a significant drop in H_2 permeability. There are various techniques to accomplish this. For instance, by thermally treating AO-PIM-1 in argon atmosphere, the amidoxime group can be converted into oxadiazole and triazine rings in the interchains to self-cross-link the AO-PIM-1, as illustrated in **Figure 14**.^[379] Thermal treatment at 390 °C for 2 days results in a membrane with H_2 permeability around 300 Barrer and H_2 selectivity against CO_2 , N_2 and CH_4 around 16, 500, and 1000, respectively. Ozone can also be used to post-treat a PIM membrane. After a 5-min ozone treatment, the H_2 permeability of the treated membrane drops to 683 Barrer but its selectivity against CO_2 , N_2 , and CH_4 can be significantly improved to be around 5, 142, and 182, respectively.^[378] In another study, AO-PIM-1 membranes can also be post-treated by infiltrating their pores with 4-sulfocalix[4]arene (SCA4) macrocyclic molecule which also acts as a molecular gatekeeper to improve the molecular sieving capability of the membranes.^[380] At 2% infiltration of SCA4 in the AO-PIM-1, the H_2 permeability of the AO-PIM-1 drops around 16% to be around 781 Barrer but its

selectivity against CO₂, N₂ and CH₄ increases significantly from around 0.86; 19.6 and 22, respectively, to be around 3.1; 91 and 233, respectively.

For PIM-based membrane, increasing the operating temperature might negatively impact the separation performance. As has been studied in PIM-1, for instance, the H₂ permeation activation energy is -0.4 kJ mol^{-1} while the N₂ and CH₄ activation energy is 14.3 and 19.4 kJ mol^{-1} , respectively.^[381] This means that with increasing temperature, the H₂ permeance also gets lower while the N₂ and CH₄ permeance increases resulting in a decrease in selectivity. Similarly, in the case of PIM-Btrip, increasing the operating temperature from 25 to 55 °C decreases both the H₂ permeability from 8929 to 8649 Barrer and H₂ selectivity against N₂ and CH₄ from 22.2 to 11.1 and from 22 to 9, respectively.^[345] The PIM-TMN-Trip also faces similar condition in this condition since its H₂ permeability drops from 13 828 to 12 478 Barrer and its H₂ selectivity against N₂ and CH₄ drops from 9 to 7 and from 6 to 4, respectively. In both cases, the major cause is the negative activation energy of hydrogen resulting in a decrease of hydrogen permeability as the temperature increases.

One of the major drawbacks in the field of PIM membrane is the aging phenomenon experienced by PIM membranes. During the aging phase, the PIM polymeric chain undergoes rearrangement and as a result, the H₂ permeability usually goes down which is accompanied by the enhancement of the H₂ selectivity. Therefore, such a phenomenon could actually be exploited to improve the hydrogen separation performance as long as the permeability reduction is acceptable. For instance, a systematic study using PIM-SBF has shown that the H₂/N₂ selectivity of the PIM-SBF 2 increases from around 8 to 26 after around 3 years of aging.^[341] However, the permeability reduces from 9160 to 4240 Barrer. A more pronounced difference is also observed in PIM-MP-TB where after about 1 year of aging, the H₂ permeability decreases from 4000 Barrer to be around 800 Barrer but the H₂/N₂ and H₂/CH₄ selectivity can be significantly enhanced to be 61 and 55, respectively, from around 20 and 15, respectively.^[348]

This aging phenomenon might then be influenced by several factors. For instance, in a systematic study involving various PIMs, it has been observed that a very prominent aging phenomenon occurs in TPIM-1 and TPIM-2. In both cases, after around 720–780 days of aging, the H₂/N₂ selectivity increases almost 10-fold to be around 156 and 90 for TPIM-1 and TPIM-2, respectively.^[382] However, this must also be paid by almost 70% decrease of H₂ permeability to be 1105 and 354 Barrer for TPIM-1 and TPIM-2, respectively. When compared with PIM-1, the aging for both TPIM-1 and TPIM-2 is significantly faster which might be attributed to two major reasons, namely their initially higher free volume and their ribbon-like 2D geometry that is more prone to efficient chain packing. The aging phenomenon also depends on the membrane thickness. Usually, thinner PIM membranes experience faster rate of physical aging while also becoming less permeable and more selective toward hydrogen. For instance, after 50 days, the H₂ permeability of a 23 μm EAD-DMN drops from 1289 to 830 Barrer (35% lower) with an increase about 32% in H₂/N₂ selectivity to be around 40. Meanwhile, it takes around 180 days for a 172 μm EAD-DMN to have a comparable drop in H₂ permeability to be around 3476 Barrer with 13.3 H₂/N₂ selectivity.^[357] However, it also seems that post-treatment of a PIM-membrane might help to reduce the aging phenomenon. For instance, after 180 days, the thermally-cross-linked AO-PIM only shows a slight H₂ permeability reduction from 952 to 707 Barrer and thus increasing the H₂/CO₂ and H₂/CH₄ selectivity from 2.7 and 313 to 8.1 and 880, respectively.^[379] Similarly, the cross-linked c-CoPIM-

TB-1 and c-CoPIM-TB-2 shows a negligible reduction in performance after 40 days of aging and thus can maintain their H₂ permeability around 5000 Barrer and H₂ selectivity against N₂ and CH₄ to be in the range of 30–40. This could then be attributed to the effective impediment of the interchain mobility after the cross-linking process.^[375]

3.5.2. Thermally-Rearranged Polymers

In the TR polymers, the microporous structure is obtained through the spatial rearrangement of the rigid polymeric chains after experiencing heat treatment. Usually, TR polymers are rod-like and contain heterocyclic rings such as benzimidazole, benzoxazole, and benzothiazole which are obtained after thermally treating the precursors.^[335,383] For hydrogen separation process, these TR polymers can then be obtained by using poly(*o*-hydroxylamide)s,^[384–386] hydroxyl-containing polyimide,^[387–390] or poly(ether *o*-hydroxyimide)^[391] as the precursors which are thermally treated to improve their microporous structure. Some studies have investigated the use of TR polymers for hydrogen purification which can be synthesized from the precursors containing different units such as cardo,^[392] iptycene,^[393–397] and spiro^[398–400] to result TR polymers bearing these units as can be seen in **Figure 15**. The precursors can also be chosen from cross-linkable polyimides^[401,402] or already-functionalized precursors such as in the case of PIM-6FDA-OH.^[205]

In the TR polymers used for hydrogen separation, increasing the fractional free volume (FFV) in the TR polymer has to be optimized as this might negatively impact the hydrogen separation performance. For instance, in a study using poly(*o*-hydroxylamide)s as the precursor, which are synthesized by reacting 2,2-Bis(3-amino-4-hydroxyphenyl) hexafluoropropane and three different structures of diacid chlorides, it is found that the TR membrane with highest FFV, namely 6PBO (PBO = polybenzoxazole), is obtained when the reaction is carried out by using (4,4'-hexafluoroisopropylidene bis(benzoyl chloride)) (6FCl) as the diacid chloride. In this case, the FFV of 6PBO is found to be around 0.28 and its H₂ permeability and H₂/CH₄ selectivity is reported to be around 255 Barrer and 40, respectively.^[386] Meanwhile, the TR membranes which are constructed using *meta*-phenylene (mPBO) and *para*-phenylene (pPBO) have lower FFV value, namely around 0.24 and 0.2, respectively. As a result, in comparison to 6PBO, both mPBO and pPBO have lower H₂ permeability, namely around 60 and 85 Barrer, respectively, but higher H₂/CH₄ selectivity, namely around 115 and 59, respectively. In another study using spiro-based TR, spiroTR-PBO-6F with FFV around 0.27 shows the highest H₂ permeability around 430 Barrer but only moderate H₂/N₂ and H₂/CH₄ selectivity around 13.^[398] For this membrane, CO₂ is also the fastest permeating gas because the gas sorption is the predominant gas transport mechanism in TR with large microcavities. Meanwhile, spiroTR-PBO-BP with FFV around 0.2 shows H₂ permeability around 143 Barrer but with higher H₂/N₂ and H₂/CH₄ selectivity around 27. For this membrane, H₂ is the fastest permeating gas diffusion is now more restricted and thus the transport is governed by the kinetic diameter of the gases.

To further improve the performance of the TR polymers, the rigidity of the stiff segments of the TR polymers can also be enhanced. For instance, the synthesis of *ortho*-hydroxyl diamine with four methyl groups and a fixed biphenyl center as a precursor for polyimide can improve the polymer rigidity which are suitable to improve the molecular sieving ability for hydrogen separation.^[403] The performance of the TR polymers can also be enhanced by fabricating them from co-

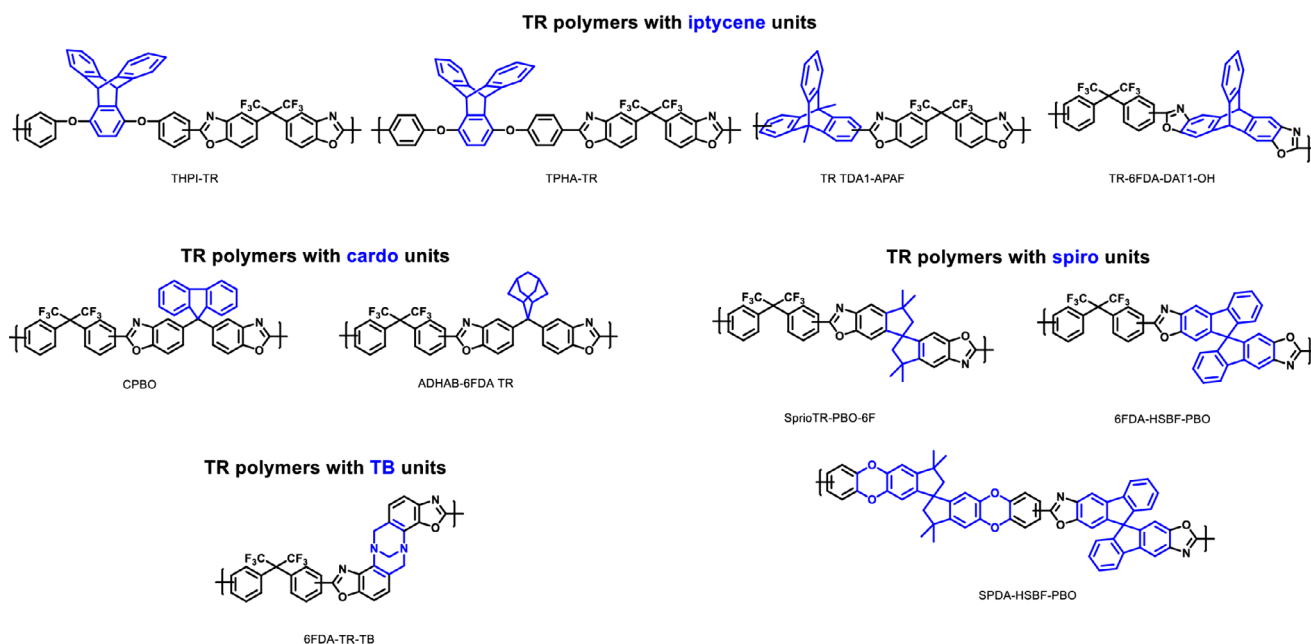


Figure 15. TR polymers containing different shape-persistent units. Reproduced with permission.^[335] Copyright 2020 John Wiley and Sons, Inc.

polymers.^[384,389,404,405] For example, by combining non-TR-able part in the precursors that has bulky non-polar side groups such as 2,4,5-trimethyl-*m*-phenylene diamine (DAM) and 4,4'-methylene-bis-(3-chloro-2,6-diethylaniline) (MCDEA) the chain packing can be more efficiently disrupted to increase the fractional free volume resulting in high gas permeability and better hydrogen selectivity.^[389] When compared with the TR polymer made from homo polymer, all the TR membranes show similar H_2 permeability around 44 Barrer but the ones with DAM and MCDEA show H_2/N_2 and H_2/CH_4 selectivity in the range of 70–80 and 106–120, respectively, while the normal TR polymer only exhibits around 36 and 26, respectively. In another study involving DAM and 4,4'-oxydianiline (ODA) as the non-TR-able part, as can be seen in **Figure 16A,B**, the H_2 permeability of the TR fabricated using this non-TR-able (TR-APAF-DAM and TR-APAF-ODA, APAF = 2,2'-bis(3-amino-4-hydroxyphenyl)-hexafluoropropane) part can be increased for the former up to 308.6 Barrer while the latter shows a decreasing trend up to 60.8 Barrer from 180 Barrer observed in the TR polymer without non-TR-able part.^[404] However, this must also be accompanied with decreasing H_2/N_2 selectivity in the former up to 20.3 while the latter shows an improvement up to 45 from 34 observed in the TR polymer without non-TR-able part. This is because DAM can increase the chain rigidity and is therefore more effective in disrupting the chain packing resulting during the thermal rearrangement process resulting in higher gas permeability while ODA increases the polymer flexibility and thus lowering the overall fractional free volume after thermal rearrangement process and could contribute in improving the molecular sieving effect.

During the fabrication of a TR membrane, the temperature for the thermal treatment has to be optimized by observing the weight loss trend obtained through gravimetric method, which is compared with the expected theoretical weight loss.^[393,397] Usually, treating the precursors at higher temperature than the theoretical or calculated temperature could be beneficial to constrain the chain relaxation and the

collapse of the microcavities.^[397] The optimization is required to balance the increase of H_2 permeability and the loss of H_2 selectivity—relative to the precursors—caused by the increase of the fractional free volume and the collapse of the microcavities.^[387,391,399] For instance, after thermally treating the polyetherimide at 450 °C, the H_2 permeability increases from 29.1 Barrer to 439 Barrer but its selectivity against CH_4 decreases from 223.8 to 25.8.^[391] In another study using spiro-based polyimide, 6FDA-HSBF, the H_2 permeability increases from 162 Barrer to 985 Barrer after the thermal treatment but the H_2 selectivity against N_2 and CH_4 decreases from 42.5 and 67.5, respectively, to 17.9 and 17.6, respectively.^[399] Such optimization also has to consider the chemistry of the precursors. For instance, in a systematic study involving two dianhydrides (6FDA and PMDA) and one diamine (3,3'-diamino-5,5',6,6'-tetramethyl-[1,1'-biphenyl]-2,2'-diol, TMBDA) and using both azeotropic and chemical imidization, four different PI precursor for TR membranes can be obtained, namely 6F-TM-Ac, 6F-TM-OH, PM-TM-Ac and PM-TM-OH. Once thermally treated, the maximum H_2/CH_4 selectivity observed for the first three TRs is found to be 50, 63, and 44, respectively, which is obtained by thermally treating the precursor at 425 °C.^[403] A further increase in the thermal treatment will only yield an increase in hydrogen permeability but a significant reduction in selectivity. Meanwhile, for the PM-TM-OH, the maximum selectivity of 77 is obtained by thermal treatment at 450 °C.

In addition, the content of the units inside the TR polymers should also be controlled since they can also influence the H_2 gas separation performance. For example, as illustrated in **Figure 16C,D**, in a study using triptycene-based poly(o-hydroxyimide) and triptycene-based poly(o-acetateimide) copolymer as precursors has shown that increasing the iptycene unit is beneficial to increase the number of microcavities in the resulting TR polymers so they can retain the permeability for small gases.^[394] The highest H_2/N_2 and H_2/CH_4 selectivity of the TR membranes fabricated with the highest triptycene loading is found to be around 96 and 203, respectively, for TPBO-1.0 and 70 and 125,

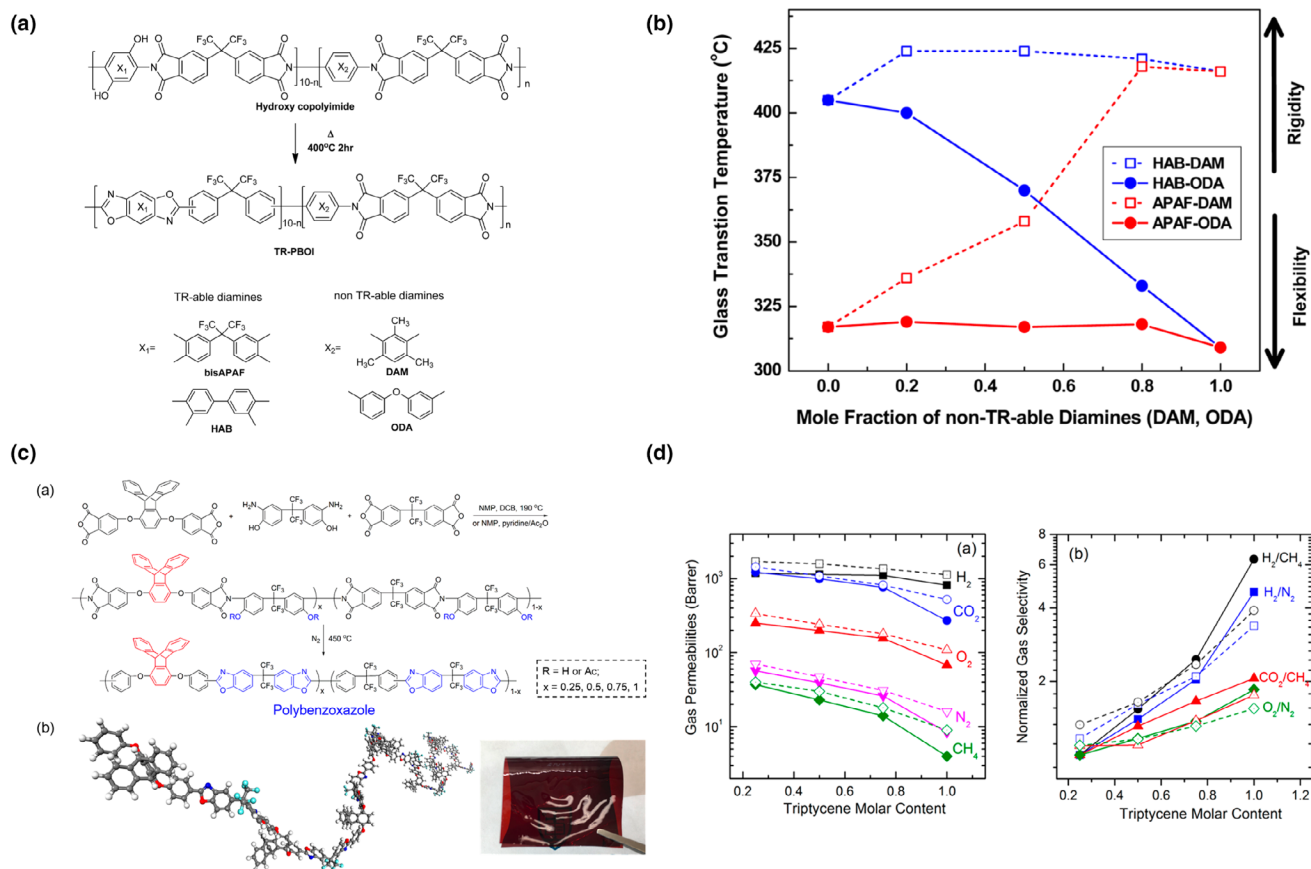


Figure 16. a) Scheme to fabricate a TR-polymer membrane with DAM and ODA as the non-TR-able parts and b) its impact on the rigidity and flexibility of the resulting membranes. c) An illustration to fabricate a TR polymer membrane with triptycene unit and d) the impact of the triptycene molar content on the gases permeability and selectivity. Figures a, b^[404] and Figures c, d^[394] are reproduced with permission. Copyright 2015 and 2018, respectively, American Chemical Society.

respectively, for TPBO-Ac-1.0. Meanwhile, the H₂ permeability of both TR membranes is also relatively high in the range of 800–1100 Barrer. However, in another study, it is also found that an optimization is required for the cardo-based TR membranes since incorporating too much cardo unit in the precursor does not linearly correlate with TR containing higher fractional free volume because of the repulsion effect.^[392] In the study, 5% of the cardo unit gives the best H₂ separation performance showing permeability around 1189 Barrer and H₂/N₂ and H₂/CH₄ selectivity around 21 and 29, respectively.

The hydrogen separation performance of TR polymers can also be further enhanced by embedding various additives such as functionalized boron nitride (BN).^[406] Compared with the pure TR membrane with H₂ permeability around 219 Barrer, the 1 wt% BN TR polymer shows a decrease in H₂ permeability to be around 97 Barrer but its H₂/CH₄ selectivity can be significantly increased from 24.6 to 322.3 because since the BN adds a more tortuous pathway for larger gas molecules to pass through.^[406]

As in the case with the PIM, TR polymers also suffer from the aging phenomenon. It has been observed that after 197 days, the H₂ permeability of PIM-PBO-3 decreases significantly from 768 to 277 Barrer. Meanwhile, the H₂ selectivity against N₂ and CH₄ selectivity increases from around 20 to be around 38.^[400]

3.6. Composites and Other Microporous Materials

In addition to the above materials, there are also other attempts to synthesize novel advanced microporous materials with a great promise for hydrogen purification. One of the common strategies to achieve this objective is by fabricating a composite of the above microporous materials.

In this case, a number of composite consisting of GO or rGO with MOFs such as HKUST-1,^[230,407] MIL-100,^[407] UiO-66-NH₂,^[408] ZIF-7,^[407] ZIF-8^[225,407,409] and Zn₂(bim)₄,^[410] and zeolite^[411] have been investigated to produce a membrane with excellent hydrogen separation performance. The improvement of the separation performance can result from the defects healing mechanism from one of the constituents. This is observed in the case where the GO acts a sealant to heal the intercrystalline defect of the MOF membranes and also to restrict the framework flexibility as owned by ZIF-8 and thus, when compared to the ZIF-8 membrane, resulting in about 4 times increase of H₂/CH₄ selectivity to be around 139.^[409] In another study, layering the GO after a porous substrate is coated with ZnO nanoparticles is not only helpful to heal the defects of the resulting Zn₂(bim)₄-GO composite membrane but also beneficial to guide the crystal orientation during the Zn₂(bim)₄ crystal growth.^[410] Through this bottom-up approach,

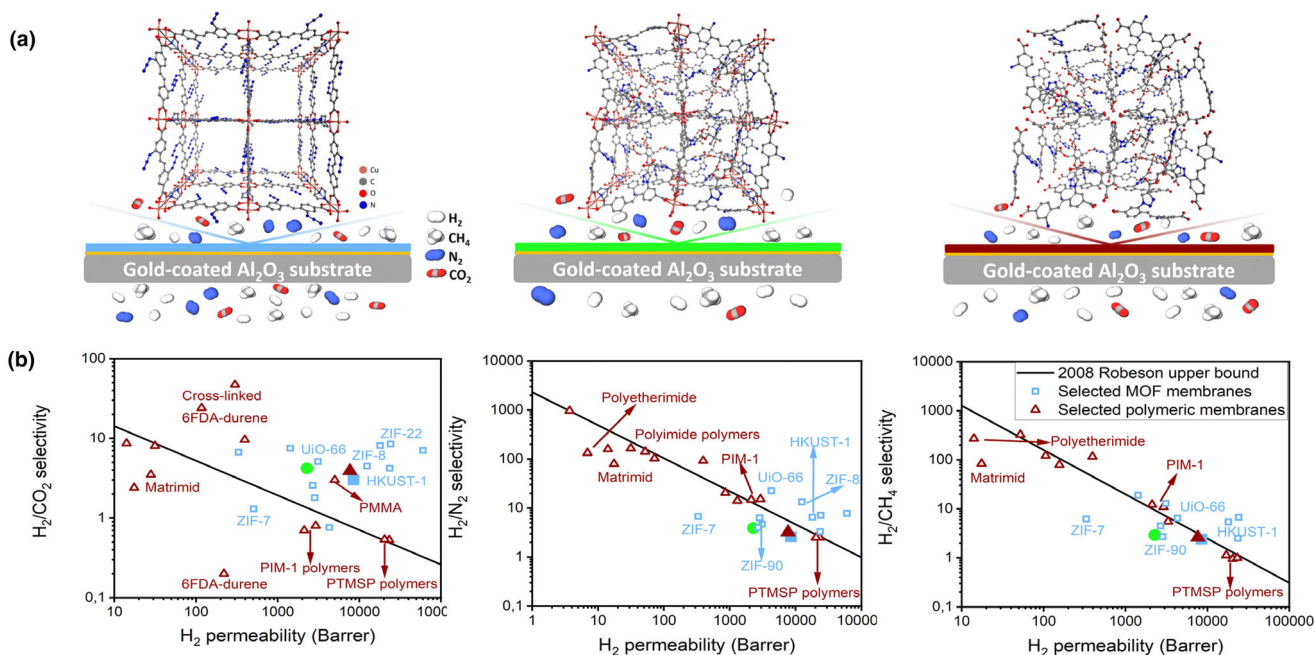


Figure 17. An illustration of the transformation from a, left) SURMOF to cross-linked a, middle) SURMOF to a, right) SURGEL and the hydrogen separation performance of the SURMOF (blue square), cross-linked SURMOF (green circle) and b) SURGEL (brown triangle). Reproduced with permission.^[418] Copyright 2023 Royal Society of Chemistry.

the resulting shows H₂ permeance around 1.5×10^{-7} mol m⁻² s⁻¹ Pa⁻¹ (447.7 GPU) and H₂ selectivity against CO₂, N₂ and CH₄ around 106, 126, and 256, respectively. Retrospectively, MOF can also contribute to cover the defective sites of a GO membrane and thus resulting in an increase of H₂/CO₂ selectivity from around 6 in a GO membrane to be around 400 in the ZIF-8-GO composite membrane.^[225]

Another synergistic effect can also be observed where the resulting new composites can combine the properties of its constituents and not just healing the defects. For instance, the use of HKUST-1 in a HKUST-1-GO composite can improve the CO₂ affinity of the resulting membrane.^[230] During the separation H₂/CO₂ process, this will then result in an improvement of H₂/CO₂ to be around 73 from 9 observed in GO membrane. This might be associated with the hindered CO₂ permeation as it now interacts more strongly with the composite. In another study using zeolite, it has also been observed that both the GO and the zeolite can work synergistically by contributing to ensure high hydrogen permeance up to 4900 GPU and high H₂/CO₂ selectivity up to 56, respectively, in the presence of steam.^[411] In another study, the MOF can also be used as a mean to control the interlayer spacing of the rGO membrane, which is not permeable to gases, as studied using four different MOFs, namely CuBTC, MIL-100, ZIF-7, and ZIF-8.^[407] As a result, the H₂ permeability for the CuBTC-rGO, MIL-100-rGO, ZIF-7-rGO, and ZIF-8-rGO composite membrane is found to be around 21 112, 311, 73, and 151 Barrer, respectively, with H₂/CO₂ selectivity around 10, 12, 25, and 20, respectively.

Another case of composite can also be seen in the form of a composite membrane combining microporous nanoparticles with PIM or TR polymers. The first simple strategy is to form a mixed matrix membrane (MMM) where microporous nanoparticles act as a discrete phase.

Various MOFs such as MIL-53,^[412] Mg-MOF-74,^[412] UiO-66-(OH)₂,^[413] TIFSIX3,^[412] ZIF-8^[387] and Zn₂(bim)₄,^[412] and silica nanoparticle^[388] have been incorporated in these microporous polymers as the nanofillers. One of the most important criteria to be fulfilled is to use MOF with suitable pore opening and to ensure the absence of interfacial defect in order to simultaneously enhance the H₂ permeability and selectivity. TIFSIX3/PIM-1 has shown an improvement both in the hydrogen permeability from 670 to 1010 Barrer and H₂/N₂ and H₂/CH₄ selectivity to be around 19 and 14, respectively, which are almost double the selectivity observed in the PIM-1.^[412] In another study using silica nanoparticle, the H₂ permeability and H₂/CH₄ selectivity of the TR polymers can be improved around 335 Barrer and 79, respectively, from 292 Barrer and 53, respectively, observed in the non-composite TR.^[388] In addition to MOF selection, establishing a good polymer-particle interaction is also paramount to obtain a good MMM. This can then be realized by modifying the nanoparticles such as by fabricating them as a gel^[414] or porous liquid.^[415] For example, by loading the AO-PIM with 5% of SOD zeolite type 1 porous liquid the H₂ permeability the H₂/N₂ selectivity can be improved from 400 to 1390 Barrer and from 15 to 34, respectively.^[415]

Another strategy to construct a composite membrane based on the microporous polymers and MOF is to construct a bilayer composite membrane. This is shown by growing ZIF-8 on AO-PIM-1 where the latter acts as a nucleation site for the former.^[416] After the ZIF-8 formation, AO-PIM-1 chain rigidification could occur and thus resulting in a composite membrane with H₂ permeability around 5700 Barrer and H₂/CO₂ selectivity around 12. This strategy can also be enhanced by firstly chelating the PIM with the metal ion corresponding to the MOF as exemplified in the case of ZIF-67 using Co²⁺-chelated PIM-1 as the interlayer for heterogeneous nucleation sites.^[417] The resulting

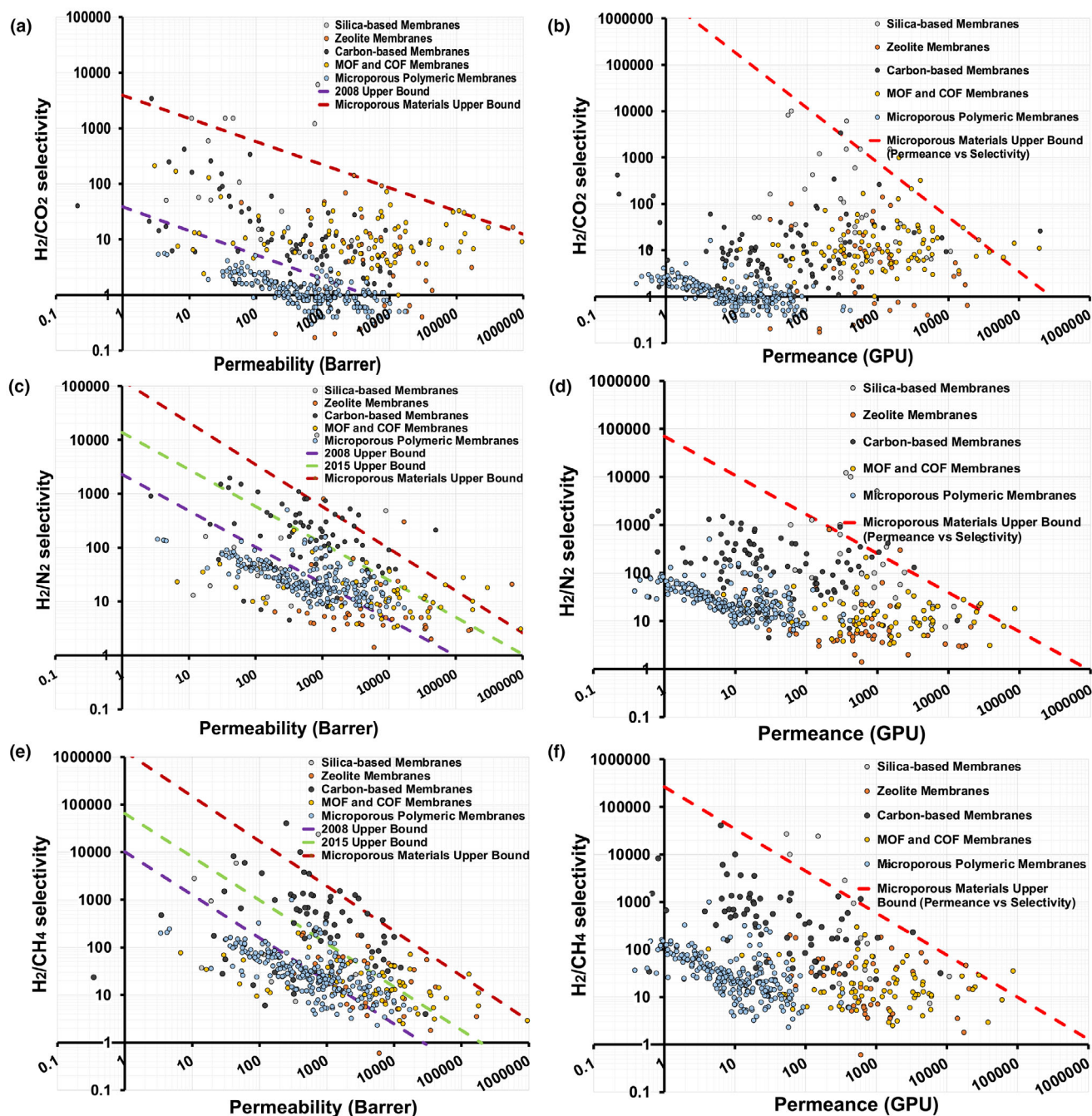


Figure 18. Hydrogen separation performance of the membranes fabricated from various microporous materials for a, b) H_2/CO_2 , c, d) H_2/N_2 , and e, f) H_2/CH_4 separation.

defect-free composite membrane shows H_2 permeance around $6.2 \times 10^{-7} \text{ mol m}^{-2} \text{ s}^{-1} \text{ Pa}^{-1}$ (1850.7 GPU) with selectivity against CO_2 and CH_4 around 15 and 52, respectively.

Recently, there is also a new research direction in fabricating a microporous polymeric membrane that is derived from surface mounted MOF (SURMOF) called SURGEL for hydrogen separation as illustrated in Figure 17a,b.^[418] The process is initiated by fabricating a

MOF membrane followed by cross-linking and the removal of the metal as the final step. Using this strategy, compared with commercial polymeric membranes, the SURGEL membrane exhibits a relatively higher H_2 permeance around $12.8 \times 10^{-7} \text{ mol m}^{-2} \text{ s}^{-1} \text{ Pa}^{-1}$ (3820.9 GPU and around 8000 Barrer) with satisfactory H_2/CO_2 separation performance around 3.9, which is close to the Knudsen selectivity value. In this case, the relatively high H_2 permeance and Knudsen

selectivity is inherited from the microporous structure of the SURMOF which is further constricted during the cross-linking process to improve the hydrogen selectivity.

4. Summary and Outlooks

Having extensively discussed the performance of various promising microporous materials, their hydrogen separation performance can then be summarized as shown in Figure 18 whose data is given in Table S1 in the Supporting Information. It should be noted that both the permeability (Barrer) and permeance (GPU) unit is used in Figure 18. This is mainly because the use of permeability unit is useful to obtain the insight regarding the intrinsic property of the material. Meanwhile, the use permeance unit can reflect better the membrane productivity for practical applications where a membrane with high permeance, rather than high permeability, is required which is usually achieved by forming it as a thin film with thickness less than 1 μm .^[419]

First, as can be seen in Figure 18a, in the field of H_2/CO_2 separation, the H_2 permeability of most of the microporous materials falls above 100 Barrer. For carbon-based membranes and microporous polymeric membranes this value falls in the range between 100 and 10 000 Barrer while the permeability of most of the zeolite and MOF-COF membranes falls above 1000 Barrer. Despite the comparable permeability performance of all microporous materials, as illustrated in Figure 18b, a further analysis on the membrane performance also shows that there are only three main clusters of microporous materials exhibiting relatively high permeance (more than 1000 GPU) with satisfactory selectivity (between 10 and 100): silica-based membranes, zeolite membranes, and MOF-COF membranes. Meanwhile, both the carbon-based membranes and microporous polymeric membranes suffer from relatively low gas permeance. This might then be caused by the fact that most research on both materials are carried out by fabricating them as a thick film rather than a thin film and thus resulting in a low permeance membrane. Moreover, it can also be seen from both Figure 18a,b, that the microporous polymeric membranes show relatively low H_2/CO_2 selectivity (below 10) than other microporous materials, which can satisfactorily surpass the 2008 Robeson Upper Bound. This is because microporous polymers usually have high CO_2 solubility and thus mostly used to separate CO_2 from other gases. Meanwhile, in the case for other microporous materials, the possibility to tailor their pore size and architecture might contribute in rendering them to have high H_2/CO_2 selectivity.

Differing from the case of H_2/CO_2 separation, low membrane selectivity observed in microporous polymeric membranes is not encountered when one looks into Figure 18c,d and Figure 18e,f for H_2/N_2 and H_2/CH_4 separation, respectively. In both cases, their selectivity falls within the range of 10–100. Combined with relatively high H_2 permeability which can go up to 10 000 Barrer, microporous polymeric membranes have then been used as a new benchmark to construct the new upper bound in 2015, as illustrated in Figure 18c,e.^[420] In this case, since the solubility of both N_2 and CH_4 is lower than CO_2 in microporous polymeric membranes, the molecular sieving ability of microporous polymeric membranes can be more pronounced than in the case for H_2/CO_2 separation and thus rendering them to be have more promising performance to separate H_2 from both N_2 and CH_4 .

Despite this positive feature, as depicted in Figure 18d,f, the membrane permeance of the microporous polymeric membranes is still lower in comparison to the other microporous materials, particularly

silica, zeolite, MOF, and COF. The H_2 permeance of microporous polymeric membranes is again comparable with carbon-based membranes which, as has been stated, might be caused as both materials are mostly studied as a dense film rather than a thin film. However, compared to the microporous polymeric membranes, the carbon-based membranes show a relatively higher hydrogen selectivity. They can then satisfactorily surpass the 2015 Upper Bound set by the microporous polymeric membranes and even have the potential to set the new upper bound for these hydrogen separation processes. This could be caused since the generation of ultramicropores in the carbon-based membranes could be carefully controlled through adjusting their pyrolysis condition and thus contributing in enhancing the hydrogen selectivity.

Differing from both carbon-based membranes and microporous polymeric membranes, it can be seen that membranes with higher permeance can be obtained when they are fabricated from silica, zeolite, or MOF-COF. Furthermore, it can also be observed that both zeolite and MOF-COF membranes have higher H_2 permeance trend than silica-based membranes albeit with slightly lower H_2 selectivity which falls in the range of 10–100. One of the main reasons of this phenomenon could be associated by the presence of both intra- and intercrystalline defects in both zeolite and MOF-COF membranes, which could be quite challenging to be completely eliminated during the manufacturing process. As a consequence, the gas selectivity of such membranes can be lower than their predicted values—which is based on their pore aperture/pore size—and their gas permeance increases because of the less-resistance gas pathway provided by the non-selective defects. Moreover, in the case of MOF, some MOFs such as ZIF-8 does also have the feature of framework flexibility which will also contribute in reducing the gas selectivity.

Having extensively discussed the performance of the microporous materials for hydrogen separation, some recommendations can then be proposed for future research. First, from Figure 18a,c,e, it can be seen that the hydrogen separation performance of the microporous materials has satisfactorily surpassed the 2008 and 2015 Upper Bound and set a new upper bound ($P = k\alpha^n$ where P , k , α , and n are the hydrogen permeability/permeance, front factor, hydrogen selectivity, and slope, respectively),^[211,21,420] as also tabulated in Table 1. Therefore, further research could be first directed to surpass the current upper bound. However, it should also not be forgotten that this upper bound is

Table 1. The upper bound parameters of membranes fabricated from microporous materials for hydrogen separations.

Separation process	Parameter					
	2008 ^[21]		2015 ^[420]		Current (Microporous Materials)	
	k	n	k	n	k	n
Upper bound (permeability)						
H_2/CO_2	4515	−2.302	–	–	410 000 000	−2.4
H_2/N_2	97 650	−1.4841	1 100 000	−1.46	3 435 500	−1.28
H_2/CH_4	27 200	−1.107	195 000	−1.1	3 045 800	−1.06
Upper bound (permeance)						
H_2/CO_2	–	–	–	–	285 800	−0.85
H_2/N_2	–	–	–	–	909 000	−1.23
H_2/CH_4	–	–	–	–	1 326 000	−1.13

related to the membrane permeability and thus might not reflect its true readiness of applicability. Therefore, as can also be seen in Figure 18b, d, f and Table 1, the target should also to surpass the upper bound that is based on the permeance.

Different strategies could then be considered to achieve this objective and the strategies could be different from one microporous material to another. This is because, as has been summarized in Table 2, each of the microporous material has its own challenges that have to be addressed in the future. However, there are some general recommendations that are valid for all of the microporous materials to significantly improve their hydrogen separation performance from light gases. First, from the perspective to increase the membrane permeance, the research could be aimed toward the fabrication of a thin film membrane with reduced thickness. Even though this research direction is particularly important for microporous polymeric materials—which are often fabricated as a thick film for research purposes—such a direction should also be extended to other microporous materials, namely to reduce their thickness and thus increasing their applicability. Second, more research

could also be directed in the field of composite microporous membranes because this approach might offer a more promising result for hydrogen separation by combining the advantage of at least two different microporous materials. However, this approach must also be backed up by rational selection of the constituents of the composite membranes to obtain composite membranes with excellent separation performance. Thirdly, it might also be worthwhile to further investigate the utilization of various metals in microporous materials. This strategy, for example, has been proven for being able to improve the CO₂ gas separation performance in mixed matrix membranes by increasing the gas affinity of the membranes.^[421] Therefore, this strategy should also be applicable to improve the hydrogen separation performance of the membranes fabricated from microporous materials, particularly when the metals can establish a good interaction with the hydrogen molecule.

In addition to continuously advancing the research to improve the membrane performance, the research could also be focused on the investigation of hydrogen separation that mimics the real conditions

Table 2. Advantageous features and future research direction of membranes fabricated from microporous materials for hydrogen separation from light gases.

Membrane type	Advantageous features	Challenges and future research direction
Microporous silica-based membranes	<ul style="list-style-type: none"> • One of the earliest investigated microporous materials for hydrogen separation membranes with high hydrogen selectivity • Can tolerate challenging operating conditions 	<ul style="list-style-type: none"> • Manufacture of silica membrane with reduced thickness • Improvement of the hydrothermal stability of the silica membranes and their resistance against densification
Zeolite-based membranes	<ul style="list-style-type: none"> • Well-defined pore size • Good chemical and physical stability • Good trade-off between H₂ permeance and selectivity • Post-modification possibility to improve the hydrogen separation performance 	<ul style="list-style-type: none"> • Some zeolites might undergo structural changes at challenging operating conditions • Large-scale and reproducible defect-free zeolite membranes manufacturing with reduced thickness • Finding alternative porous supports or lowering the production cost of ceramic supports to reduce the overall manufacturing cost of the zeolite membranes
Carbon-based membranes (CMS and graphene-based)	<ul style="list-style-type: none"> • Wide possibility to use different carbon sources to produce CMS membranes with promising H₂/N₂ and H₂/CH₄ separation performance • Simple fabrication of GO-based membrane through vacuum filtration and spin-coating • Can tolerate challenging operating conditions 	<ul style="list-style-type: none"> • Relatively moderate H₂/CO₂ separation performance and thus requiring advancements in this field • High pyrolysis temperature might be needed to obtain a CMS membrane with excellent molecular sieving ability • Investigations on the long-term hydrogen separation performance of CMS membranes, particularly to investigate their aging phenomenon • Reproducible control of the interlayer spacing in the GO-based membranes to obtain GO-based membranes with excellent separation performance
MOF- and COF-based membranes	<ul style="list-style-type: none"> • Tailorable architecture by carefully selecting their building blocks • Good trade-off between H₂ permeance and selectivity • Post-synthetic modifications possibility to improve their hydrogen separation performance • The possibility to use polymers as porous support to reduce the membrane manufacturing cost 	<ul style="list-style-type: none"> • Large-scale and simple manufacturing of defect-free MOF and COF membranes without the necessity to use costly building blocks to reduce the membrane production cost • Limited operating conditions because of the presence of the organic building blocks • Evaluation of the hydrogen separation performance in the long term, particularly in non-ideal situations considering the framework sensitivity of some of MOFs and COFs
Microporous polymeric membranes (PIM and TR)	<ul style="list-style-type: none"> • Tailorable architecture by judiciously selecting the precursors • PIMs and precursors of TR polymers are solution processable materials and thus offering ease of fabrication and could be more promising for large-scale fabrication • Higher hydrogen permeability and H₂/N₂ and H₂/CH₄ selectivity in comparison with other polymers • The possibility to be used as a continuous matrix to fabricate composite membranes 	<ul style="list-style-type: none"> • Might have limited operating conditions because of their organic-based building blocks • Low H₂/CO₂ selectivity which is caused by high CO₂ solubility and thus requiring significant advancements in this direction • Investigations in the form of thin film membranes and their aging phenomenon

such as to investigate their performance at relevant operating conditions (e.g., high temperature or pressure and in the presence of impurities), particularly with membranes that are fabricated from quite sensitive materials such as MOF and COF, and also to comprehensively evaluate their performance in the long term, particularly when they are prone to aging such as in the case of CMS and microporous polymeric membranes. Furthermore, a study regarding the impact of membrane geometry, namely in flat-sheet and hollow fiber form, on the membrane performance and applicability could also become a topic in the future research that is worthy for investigation. When these approaches are combined together, the research in the field of microporous material can be more advanced to further support and advance the hydrogen economy in the future.

5. Conclusions

As the energy source continues to transition from fossil-based fuels into a more sustainable ones, it cannot be doubted that hydrogen as an energy carrier will play a major role in this field. However, in order to use it effectively, it has to be separated from other light gases. In this regard, membrane technology will also play a significant role since it holds a great promise to effectively purify hydrogen without huge energy consumption. Differing from polymeric materials, microporous materials could be a better alternative as it can combine high hydrogen permeance and precise molecular sieving and thus surpassing the permeance-selectivity trade-off. In this article, we have then thoroughly reviewed the state of the arts of various promising microporous materials that can be used for hydrogen separation against light gases. As one of the earliest investigated materials, silica-based microporous membranes have actually held a good promise in this field as reflected by their high hydrogen selectivity. However, recent advances in the microporous materials have also shown the possibility to fabricate a membrane from other microporous materials including zeolite, carbon-based porous materials, metal organic frameworks, covalent organic frameworks, and microporous polymers. Some of these materials also offer a number of advantages including the possibility to rationally tailor their architecture or pore size to further improve the hydrogen separation performance, which contributes to further push the performance boundary of the hydrogen separation membranes. Despite their promising performance, some challenges related to membrane thickness reduction, scalability, and separation performance in the real conditions still have to be addressed before their practical employment. Once these issues have been satisfactorily addressed, it could then be expected that the membranes fabricated from these microporous materials could significantly support and accelerate the transition from the fossil fuel-based to hydrogen-based green economy.

Acknowledgments

N.P. acknowledges the funding from the Alexander von Humboldt Postdoctoral Fellowship (Ref – 3.3 – GBR – 1219268 – HFST-P). N.P. and B.P.L. also acknowledge the funding from the Paul Wurth Chair, University of Luxembourg.

Conflict of Interest

The authors declare no conflict of interest.

Supporting Information

Supporting Information is available from the Wiley Online Library or from the author.

Keywords

hydrogen separation, membranes, microporous materials

Received: August 1, 2024
Revised: September 19, 2024
Published online: September 23, 2024

- [1] G. Bernardo, T. Araújo, T. da Silva Lopes, J. Sousa, A. Mendes, *Int. J. Hydrog. Energy* **2020**, *45*, 7313.
- [2] H. Nazir, C. Louis, S. Jose, J. Prakash, N. Muthuswamy, M. E. Buan, C. Flox, S. Chavan, X. Shi, P. Kauranen, *Int. J. Hydrog. Energy* **2020**, *45*, 13777.
- [3] N. Prasetya, Z. Wu, A. G. Gil, K. Li, J. *Eur. Ceram. Soc.* **2017**, *37*, 5281.
- [4] N. Prasetya, N. F. Himm, P. D. Sutrisna, I. G. Wenten, B. P. Ladewig, *Chem. Eng. J.* **2020**, *391*, 123575.
- [5] C. A. Scholes, K. H. Smith, S. E. Kentish, G. W. Stevens, *Int. J. Greenhouse Gas Control* **2010**, *4*, 739.
- [6] M. Maarefian, S. Bandehali, S. Azami, H. Sanaeepur, A. Moghadassi, *Int. J. Energy Res.* **2019**, *43*, 8217.
- [7] S. Sircar, T. Golden, *Sep. Sci. Technol.* **2000**, *35*, 667.
- [8] G. Moral, R. Ortiz-Imedio, A. Ortiz, D. Gorri, I. Ortiz, *Ind. Eng. Chem. Res.* **2022**, *61*, 6106.
- [9] O. A. Ojelade, S. F. Zaman, B.-J. Ni, *J. Environ. Manag.* **2023**, *342*, 118348.
- [10] D. R. MacFarlane, P. V. Cherepanov, J. Choi, B. H. Suryanto, R. Y. Hodgetts, J. M. Bakker, F. M. F. Vallana, A. N. Simonov, *Joule* **2020**, *4*, 1186.
- [11] M. Yáñez, F. Relvas, A. Ortiz, D. Gorri, A. Mendes, I. Ortiz, *Sep. Purif. Technol.* **2020**, *240*, 116334.
- [12] O. C. David, D. Gorri, K. Nijmeijer, I. Ortiz, A. Urriaga, *J. Membr. Sci.* **2012**, *419*, 49.
- [13] W. Liemberger, D. Halmschlager, M. Miltner, M. Harasek, *Appl. Energy* **2019**, *233*, 747.
- [14] M. Nordio, S. A. Wassie, M. V. S. Annaland, D. A. P. Tanaka, J. L. V. Sole, F. Gallucci, *Int. J. Hydrog. Energy* **2021**, *46*, 23417.
- [15] L. Hu, S. Pal, H. Nguyen, V. Bui, H. Lin, *J. Polym. Sci.* **2020**, *58*, 2467.
- [16] D. Nikolic, A. Giovanoglou, M. C. Georgiadis, E. S. Kikkinides, *Computer Aided Chemical Engineering*, **2007**, *24*, 159.
- [17] M. Amin, A. S. Butt, J. Ahmad, C. Lee, S. U. Azam, H. A. Mannan, A. B. Naveed, Z. U. R. Farooqi, E. Chung, A. Iqbal, *Energy Rep.* **2023**, *9*, 894.
- [18] F. Feng, J. Wu, M. Weber, S. Zhang, T.-S. Chung, *J. Membr. Sci.* **2024**, *711*, 123217.
- [19] N. Pal, M. Agarwal, *Int. J. Hydrog. Energy* **2021**, *46*, 27062.
- [20] N. W. Ockwig, T. M. Nenoff, *Chem. Rev.* **2007**, *107*, 4078.
- [21] L. M. Robeson, *J. Membr. Sci.* **2008**, *320*, 390.
- [22] T. Graham, *Philos. Trans. R. Soc. Lond.* **1866**, *156*, 399.
- [23] E. Harrison, L. Hobbs, *Rev. Sci. Instrum.* **1955**, *26*, 305.
- [24] D. Juenker, M. Van Swaay, C. Birchenall, *Rev. Sci. Instrum.* **1955**, *26*, 888.
- [25] K. Landecker, A. Gray, *Rev. Sci. Instrum.* **1954**, *25*, 1151.
- [26] M. A. Habib, A. Harale, S. Paglieri, F. S. Alrashed, A. Al-Sayoud, M. V. Rao, M. A. Nemitallah, S. Hossain, M. Hussien, A. Ali, *Energy Fuel* **2021**, *35*, 5558.
- [27] S. Yun, S. T. Oyama, *J. Membr. Sci.* **2011**, *375*, 28.

- [28] M. L. Bosko, A. Dalla Fontana, A. Tarditi, L. Cornaglia, *Int. J. Hydrog. Energy* **2021**, 46, 15572.
- [29] A. W. Thornton, J. M. Hill, A. J. Hill, *Membrane Gas Separation*, **2010**, DOI: [10.1002/9780470665626.ch5](https://doi.org/10.1002/9780470665626.ch5).
- [30] C. Li, S. M. Meckler, Z. P. Smith, J. E. Bachman, L. Maserati, J. R. Long, B. A. Helms, *Adv. Mater.* **2018**, 30, 1704953.
- [31] T. Okubo, H. Inoue, *AICHE J.* **1989**, 35, 845.
- [32] B. Ballinger, J. Motuzas, S. Smart, J. C. D. da Costa, *J. Membr. Sci.* **2014**, 451, 185.
- [33] S. Smart, J. Vente, J. D. Da Costa, *Int. J. Hydrog. Energy* **2012**, 37, 12700.
- [34] R. Igi, T. Yoshioka, Y. H. Ikuhara, Y. Iwamoto, T. Tsuru, *J. Am. Ceram. Soc.* **2008**, 91, 2975.
- [35] M. Kanezashi, M. Asaeda, *J. Chem. Eng. Jpn* **2005**, 38, 908.
- [36] Y.-S. Kim, K. Kusakabe, S. Morooka, S.-M. Yang, *Korean J. Chem. Eng.* **2001**, 18, 106.
- [37] Y. Yoshino, T. Suzuki, B. N. Nair, H. Taguchi, N. Itoh, *J. Membr. Sci.* **2005**, 267, 8.
- [38] D.-W. Lee, B. Sea, K.-Y. Lee, K.-H. Lee, *Ind. Eng. Chem. Res.* **2002**, 41, 3594.
- [39] K. Kusakabe, F. Shibao, G. Zhao, K.-I. Sotowa, K. Watanabe, T. Saito, *J. Membr. Sci.* **2003**, 215, 321.
- [40] M. Kanezashi, M. Asaeda, *J. Membr. Sci.* **2006**, 271, 86.
- [41] S. Battersby, S. Smart, B. Ladewig, S. Liu, M. C. Duke, V. Rudolph, J. C. D. da Costa, *Sep. Purif. Technol.* **2009**, 66, 299.
- [42] D.-W. Lee, C.-Y. Yu, K.-H. Lee, *J. Colloid Interface Sci.* **2008**, 325, 447.
- [43] K. Yoshida, Y. Hirano, H. Fujii, T. Tsuru, M. Asaeda, *J. Chem. Eng. Jpn* **2001**, 34, 523.
- [44] E. J. Kappert, A. Nijmeijer, N. E. Benes, *Microporous Mesoporous Mater.* **2012**, 151, 211.
- [45] D. K. Wang, J. C. D. da Costa, S. Smart, *J. Membr. Sci.* **2014**, 456, 192.
- [46] Q. Wei, F. Wang, Z.-R. Nie, C.-L. Song, Y.-L. Wang, Q.-Y. Li, *J. Phys. Chem. B* **2008**, 112, 9354.
- [47] H. R. Lee, M. Kanezashi, T. Yoshioka, T. Tsuru, *Desalin. Water Treat.* **2010**, 17, 120.
- [48] H. R. Lee, M. Kanezashi, Y. Shimomura, T. Yoshioka, T. Tsuru, *AICHE J.* **2011**, 57, 2755.
- [49] H. R. Lee, T. Shibata, M. Kanezashi, T. Mizumo, J. Ohshita, T. Tsuru, *J. Membr. Sci.* **2011**, 383, 152.
- [50] H. Qi, H. Chen, L. Li, G. Zhu, N. Xu, *J. Membr. Sci.* **2012**, 421, 190.
- [51] H. F. Qureshi, A. Nijmeijer, L. Winnubst, *J. Membr. Sci.* **2013**, 446, 19.
- [52] H. Zhang, Y. Wei, H. Qi, *Microporous Mesoporous Mater.* **2020**, 305, 110279.
- [53] Y. Wei, H. Zhang, J. Lei, H. Song, H. Qi, *Chin. J. Chem. Eng.* **2019**, 27, 3036.
- [54] H. Song, Y. Wei, C. Wang, S. Zhao, H. Qi, *Chin. J. Chem. Eng.* **2018**, 26, 53.
- [55] H. H. Han, S. H. Ryu, S. Nakao, Y. T. Lee, *J. Membr. Sci.* **2013**, 431, 72.
- [56] D. Lee, L. Zhang, S. Oyama, S. Niu, R. Saraf, *J. Membr. Sci.* **2004**, 231, 117.
- [57] D. Lee, S. T. Oyama, *J. Membr. Sci.* **2002**, 210, 291.
- [58] Y. Gu, P. Hacarlioglu, S. T. Oyama, *J. Membr. Sci.* **2008**, 310, 28.
- [59] S. Nakao, T. Suzuki, T. Sugawara, T. Tsuru, S. Kimura, *Microporous Mesoporous Mater.* **2000**, 37, 145.
- [60] A. K. Prabhu, S. T. Oyama, *J. Membr. Sci.* **2000**, 176, 233.
- [61] K. Kuraoka, T. Kakitani, T. Suetsugu, T. Yazawa, *Sep. Purif. Technol.* **2001**, 25, 161.
- [62] R. Levy, E. Ramos, L. Krasnoperov, A. Datta, J. Grow, *J. Mater. Res.* **1996**, 11, 3164.
- [63] S.-W. Nam, H.-Y. Ha, S.-P. Yoon, J. Han, T.-H. Lim, I.-H. Oh, S.-A. Hong, *Korean Membr. J.* **2001**, 3, 69.
- [64] H. Y. Ha, J. S. Lee, S. W. Nam, I. W. Kim, S.-A. Hong, *J. Mater. Sci. Lett.* **1997**, 16, 1023.
- [65] H. Y. Ha, S. W. Nam, W. K. Lee, *J. Membr. Sci.* **1993**, 85, 279.
- [66] C. E. Megiris, J. H. Glezer, *Ind. Eng. Chem. Res.* **1992**, 31, 1293.
- [67] S. Jiang, Y. Yan, G. Gavalas, *J. Membr. Sci.* **1995**, 103, 211.
- [68] S. Kim, G. R. Gavalas, *Ind. Eng. Chem. Res.* **1995**, 34, 168.
- [69] M. Tsapatsis, G. Gavalas, *J. Membr. Sci.* **1994**, 87, 281.
- [70] S. Yan, H. Maeda, K. Kusakabe, S. Morooka, Y. Akiyama, *Ind. Eng. Chem. Res.* **1994**, 33, 2096.
- [71] S. Morooka, S. Yan, K. Kusakabe, Y. Akiyama, *J. Membr. Sci.* **1995**, 101, 89.
- [72] Y. Gu, S. T. Oyama, *J. Membr. Sci.* **2007**, 306, 216.
- [73] Y. Gu, S. T. Oyama, *J. Membr. Sci.* **2009**, 345, 267.
- [74] S. Gopalakrishnan, J. C. D. da Costa, *J. Membr. Sci.* **2008**, 323, 144.
- [75] B.-K. Sea, M. Watanabe, K. Kusakabe, S. Morooka, S.-S. Kim, *Gas Sep. Purif.* **1996**, 10, 187.
- [76] S.-S. Kin, B.-K. Sea, *Korean J. Chem. Eng.* **2001**, 18, 322.
- [77] B. Sea, K.-H. Lee, *J. Ind. Eng. Chem.* **2001**, 7, 417.
- [78] B. G. Sea, G. H. Lee, *Bull. Korean Chem. Soc.* **2001**, 22, 1400.
- [79] A. Nijmeijer, B. Bladergroen, H. Verweij, *Microporous Mesoporous Mater.* **1998**, 25, 179.
- [80] G.-J. Hwang, K. Onuki, S. Shimizu, H. Ohya, *J. Membr. Sci.* **1999**, 162, 83.
- [81] M. Nomura, K. Ono, S. Gopalakrishnan, T. Sugawara, S.-I. Nakao, *J. Membr. Sci.* **2005**, 251, 151.
- [82] Y. Gu, B. Vaezian, S. J. Khatib, S. T. Oyama, Z. Wang, L. Achenie, *Sep. Sci. Technol.* **2012**, 47, 1698.
- [83] K. Akamatsu, M. Nakane, T. Sugawara, T. Hattori, S. Nakao, *J. Membr. Sci.* **2008**, 325, 16.
- [84] S. Araki, N. Mohri, Y. Yoshimitsu, Y. Miyake, *J. Membr. Sci.* **2007**, 290, 138.
- [85] T. Nagano, S. Fujisaki, K. Sato, K. Hataya, Y. Iwamoto, M. Nomura, S. Nakao, *J. Am. Ceram. Soc.* **2008**, 91, 71.
- [86] A. Comite, in *Current Trends and Future Developments on (Bio-) Membranes* (Eds: A. Basile, K. Ghasemzadeh), Elsevier, Amsterdam **2017**, pp. 3–23.
- [87] C. Barboiu, B. Sala, S. Bec, S. Pavan, E. Petit, P. Colomban, J. Sanchez, S. de Perthuis, D. Hittner, *J. Membr. Sci.* **2009**, 326, 514.
- [88] J. Motuzas, A. Darmawan, M. Elma, D. K. Wang, in *Current Trends and Future Developments on (Bio-) Membranes* (Eds: A. Basile, K. Ghasemzadeh), Elsevier, Amsterdam **2019**, pp. 77–99.
- [89] S. J. Khatib, S. T. Oyama, *Sep. Purif. Technol.* **2013**, 111, 20.
- [90] B. Wang, N. Hu, H. Wang, Y. Zheng, R. Zhou, *J. Mater. Chem. A* **2015**, 3, 12205.
- [91] L. Yu, M. S. Nobandegani, A. Holmgren, J. Hedlund, *J. Membr. Sci.* **2019**, 588, 117224.
- [92] A. Bose, M. Sen, J. K. Das, N. Das, *RSC Adv.* **2014**, 4, 19043.
- [93] S. Himeno, T. Tomita, K. Suzuki, K. Nakayama, K. Yajima, S. Yoshida, *Ind. Eng. Chem. Res.* **2007**, 46, 6989.
- [94] M. Kanezashi, J. O'Brien-Abraham, Y. Lin, K. Suzuki, *AICHE J.* **2008**, 54, 1478.
- [95] Z. Zheng, A. S. Hall, V. V. Gulians, *J. Mater. Sci.* **2008**, 43, 2499.
- [96] T. Tomita, K. Nakayama, H. Sakai, *Microporous Mesoporous Mater.* **2004**, 68, 71.
- [97] L. Wang, C. Zhang, X. Gao, L. Peng, J. Jiang, X. Gu, *J. Membr. Sci.* **2017**, 539, 152.
- [98] S. Yang, Z. Cao, A. Arvanitis, X. Sun, Z. Xu, J. Dong, *J. Membr. Sci.* **2016**, 505, 194.
- [99] P. Du, J. Song, X. Wang, Y. Zhang, J. Xie, G. Liu, Y. Liu, Z. Wang, Z. Hong, X. Gu, *J. Membr. Sci.* **2021**, 636, 119546.
- [100] L. Sandström, M. Palomino, J. Hedlund, *J. Membr. Sci.* **2010**, 354, 171.
- [101] G. Zhu, Y. Li, H. Zhou, J. Liu, W. Yang, *Mater. Lett.* **2008**, 62, 4357.
- [102] A. Huang, N. Wang, J. Caro, *J. Membr. Sci.* **2012**, 389, 272.
- [103] C. Zhou, C. Yuan, Y. Zhu, J. Caro, A. Huang, *J. Membr. Sci.* **2015**, 494, 174.
- [104] A. Huang, Q. Liu, N. Wang, X. Tong, B. Huang, M. Wang, J. Caro, *J. Membr. Sci.* **2013**, 437, 57.
- [105] C. Yuan, Q. Liu, H. Chen, A. Huang, *RSC Adv.* **2014**, 4, 41982.

- [106] A. Huang, F. Liang, F. Steinbach, J. Caro, *J. Membr. Sci.* **2010**, 350, 5.
- [107] A. Huang, N. Wang, J. Caro, *Microporous Mesoporous Mater.* **2012**, 164, 294.
- [108] A. Huang, J. Caro, *J. Mater. Chem.* **2011**, 21, 11424.
- [109] Y. Li, H. Chen, J. Liu, W. Yang, *J. Membr. Sci.* **2006**, 277, 230.
- [110] X. Li, K. Li, S. Tao, H. Ma, R. Xu, B. Wang, P. Wang, Z. Tian, *Microporous Mesoporous Mater.* **2016**, 228, 45.
- [111] A. Huang, F. Liang, F. Steinbach, T. M. Gesing, J. Caro, *J. Am. Chem. Soc.* **2010**, 132, 2140.
- [112] A. Huang, J. Caro, *Chem. Commun.* **2010**, 46, 7748.
- [113] A. Huang, J. Caro, *Chem. Commun.* **2011**, 47, 4201.
- [114] T. Wu, C. Shu, S. Liu, B. Xu, S. Zhong, R. Zhou, *Energy Fuel* **2020**, 34, 11650.
- [115] K. Kida, Y. Maeta, K. Yogo, *J. Membr. Sci.* **2017**, 522, 363.
- [116] C. Algeri, P. Bernardo, G. Golemme, G. Barbieri, E. Drioli, *J. Membr. Sci.* **2003**, 222, 181.
- [117] W. Xiao, Z. Chen, L. Zhou, J. Yang, J. Lu, J. Wang, *Microporous Mesoporous Mater.* **2011**, 142, 154.
- [118] N. Kosinov, E. J. Hensen, *J. Membr. Sci.* **2013**, 447, 12.
- [119] X. Zhu, H. Wang, Y. Lin, *Ind. Eng. Chem. Res.* **2010**, 49, 10026.
- [120] Y. Zhang, Z. Wu, Z. Hong, X. Gu, N. Xu, *Chem. Eng. J.* **2012**, 197, 314.
- [121] Z. Tang, S.-J. Kim, G. K. Reddy, J. Dong, P. Smirniotis, *J. Membr. Sci.* **2010**, 354, 114.
- [122] Z. Hong, F. Sun, D. Chen, C. Zhang, X. Gu, N. Xu, *Int. J. Hydrog. Energy* **2013**, 38, 8409.
- [123] Z. Hong, Z. Wu, Y. Zhang, X. Gu, *Ind. Eng. Chem. Res.* **2013**, 52, 13113.
- [124] Z. Tang, J. Dong, T. M. Nenoff, *Langmuir* **2009**, 25, 4848.
- [125] T. Masuda, N. Fukumoto, M. Kitamura, S. R. Mukai, K. Hashimoto, T. Tanaka, T. Funabiki, *Microporous Mesoporous Mater.* **2001**, 48, 239.
- [126] X. Xu, W. Yang, J. Liu, L. Lin, *Microporous Mesoporous Mater.* **2001**, 43, 299.
- [127] X. Xu, Y. Bao, C. Song, W. Yang, J. Liu, L. Lin, *J. Membr. Sci.* **2005**, 249, 51.
- [128] K. P. Dey, D. Kundu, M. Chatterjee, M. K. Naskar, *J. Am. Ceram. Soc.* **2013**, 96, 68.
- [129] Y. M. Galeano, L. Cornaglia, A. M. Tarditi, *J. Membr. Sci.* **2016**, 512, 93.
- [130] S. Zhong, N. Bu, R. Zhou, W. Jin, M. Yu, S. Li, *J. Membr. Sci.* **2016**, 520, 507.
- [131] M. Hong, J. L. Falconer, R. D. Noble, *Ind. Eng. Chem. Res.* **2005**, 44, 4035.
- [132] J. K. Das, N. Das, S. Bandyopadhyay, *J. Mater. Chem. A* **2013**, 1, 4966.
- [133] J. K. Das, N. Das, S. N. Roy, S. Bandyopadhyay, *Ceram. Int.* **2012**, 38, 333.
- [134] J. C. Poshusta, V. A. Tuan, J. L. Falconer, R. D. Noble, *Ind. Eng. Chem. Res.* **1998**, 37, 3924.
- [135] J. C. Poshusta, V. A. Tuan, E. A. Pape, R. D. Noble, J. L. Falconer, *AICHE J.* **2000**, 46, 779.
- [136] Z. Jabbari, S. Fatemi, M. Davoodpour, *Adv. Powder Technol.* **2014**, 25, 321.
- [137] M. Yu, H. H. Funke, R. D. Noble, J. L. Falconer, *J. Am. Chem. Soc.* **2011**, 133, 1748.
- [138] L. Zhou, J. Yang, G. Li, J. Wang, Y. Zhang, J. Lu, D. Yin, *Int. J. Hydrog. Energy* **2014**, 39, 14949.
- [139] W. Mei, Y. Du, T. Wu, F. Gao, B. Wang, J. Duan, J. Zhou, R. Zhou, *J. Membr. Sci.* **2018**, 565, 358.
- [140] M. Hong, S. Li, J. L. Falconer, R. D. Noble, *J. Membr. Sci.* **2008**, 307, 277.
- [141] H. Kalipcilar, T. C. Bowen, R. D. Noble, J. L. Falconer, *Chem. Mater.* **2002**, 14, 3458.
- [142] N. Kosinov, C. Auffret, V. G. Sripathi, C. Gücüyener, J. Gascon, F. Kapteijn, E. J. Hensen, *Microporous Mesoporous Mater.* **2014**, 197, 268.
- [143] N. Kosinov, C. Auffret, C. Gücüyener, B. M. Szyja, J. Gascon, F. Kapteijn, E. J. Hensen, *J. Mater. Chem. A* **2014**, 2, 13083.
- [144] R. Zhou, H. Wang, B. Wang, X. Chen, S. Li, M. Yu, *Ind. Eng. Chem. Res.* **2015**, 54, 7516.
- [145] Y. Zheng, N. Hu, H. Wang, N. Bu, F. Zhang, R. Zhou, *J. Membr. Sci.* **2015**, 475, 303.
- [146] H. Tang, L. Bai, M. Wang, Y. Zhang, M. Li, M. Wang, L. Kong, N. Xu, Y. Zhang, P. Rao, *Int. J. Hydrog. Energy* **2019**, 44, 23107.
- [147] B. Wang, Y. Zheng, J. Zhang, W. Zhang, F. Zhang, W. Xing, R. Zhou, *Microporous Mesoporous Mater.* **2019**, 275, 191.
- [148] T. Zhou, M. Shi, L. Chen, C. Gong, P. Zhang, J. Xie, X. Wang, X. Gu, *Chem. Eng. J.* **2022**, 433, 133567.
- [149] T. Zhou, M. Zhu, Y. Dai, L. Chen, J. Xie, Y. Zhang, X. Wang, X. Gu, *J. Membr. Sci.* **2024**, 700, 122699.
- [150] X. Li, C. Zhou, Z. Lin, J. Rocha, P. F. Lito, A. S. Santiago, C. M. Silva, *Microporous Mesoporous Mater.* **2011**, 137, 43.
- [151] P. F. Lito, C. F. Zhou, A. S. Santiago, A. E. Rodrigues, J. Rocha, Z. Lin, C. M. Silva, *Chem. Eng. J.* **2010**, 165, 395.
- [152] V. Sebastián, Z. Lin, J. Rocha, C. Téllez, J. Santamaría, J. Coronas, *J. Membr. Sci.* **2008**, 323, 207.
- [153] V. Sebastián, Z. Lin, J. Rocha, C. Téllez, J. Santamaría, J. Coronas, *Chem. Commun.* **2005**, 43, 3036.
- [154] H. Wang, X. Dong, Y. Lin, *J. Membr. Sci.* **2014**, 450, 425.
- [155] H. Kalipcilar, S. K. Gade, R. D. Noble, J. L. Falconer, *J. Membr. Sci.* **2002**, 210, 113.
- [156] F. Bonhomme, M. E. Welk, T. M. Nenoff, *Microporous Mesoporous Mater.* **2003**, 66, 181.
- [157] Y. Li, J. Wang, J. Shi, X. Zhang, J. Lu, Z. Bao, D. Yan, *Sep. Purif. Technol.* **2003**, 32, 397.
- [158] Y. Cheng, J.-S. Li, L.-J. Wang, X.-Y. Sun, X.-D. Liu, *Sep. Purif. Technol.* **2006**, 51, 210.
- [159] A. Huang, N. Wang, J. Caro, *Chem. Commun.* **2012**, 48, 3542.
- [160] H. Wu, X. Liu, Y. Guo, *Chin. J. Chem. Eng.* **2024**, 72, 44.
- [161] L. Lei, A. Lindbräthen, M. Hillestad, X. He, *J. Membr. Sci.* **2021**, 627, 119241.
- [162] L. Lei, F. Pan, A. Lindbräthen, X. Zhang, M. Hillestad, Y. Nie, L. Bai, X. He, M. D. Guiver, *Nat. Commun.* **2021**, 12, 268.
- [163] D. Grainger, M.-B. Hägg, *J. Membr. Sci.* **2007**, 306, 307.
- [164] T. Araújo, G. Bernardo, A. Mendes, *J. Membr. Sci.* **2024**, 693, 122337.
- [165] J. A. Lie, M.-B. Hägg, *J. Membr. Sci.* **2006**, 284, 79.
- [166] M. Campo, F. D. Magalhães, A. Mendes, *J. Membr. Sci.* **2010**, 350, 180.
- [167] H. Richter, H. Voss, N. Kaltenborn, S. Kämnitz, A. Wollbrink, A. Feldhoff, J. Caro, S. Roitsch, I. Voigt, *Angew. Chem. Int. Ed.* **2017**, 56, 7760.
- [168] H. Hatori, H. Takagi, Y. Yamada, *Carbon* **2004**, 42, 1169.
- [169] I. Kumakiri, K. Tamura, Y. Sasaki, K. Tanaka, H. Kita, *Ind. Eng. Chem. Res.* **2018**, 57, 5370.
- [170] H. Kita, K. Nanbu, T. Hamano, M. Yoshino, K. Okamoto, M. Funaoka, *J. Polym. Environ.* **2002**, 10, 69.
- [171] T. Koga, H. Kita, T. Suzuki, K. Uemura, K. Tanaka, I. Kawafune, M. Funaoka, *Trans. Mater. Res. Soc. Japan* **2008**, 33, 825.
- [172] K. Briceno, D. Montané, R. Garcia-Valls, A. Iulianelli, A. Basile, *J. Membr. Sci.* **2012**, 415, 288.
- [173] C. Zhang, W. J. Koros, *Adv. Mater.* **2017**, 29, 1701631.
- [174] M. A. L. Tanco, J. A. Medrano, V. Cechetto, F. Gallucci, D. A. P. Tanaka, *Int. J. Hydrog. Energy* **2021**, 46, 19758.
- [175] M. Nordio, J. Melendez, M. van Sint Annaland, D. A. P. Tanaka, M. L. Tanco, F. Gallucci, *Int. J. Hydrog. Energy* **2020**, 45, 28876.
- [176] A. Rahimalimaghani, D. P. Tanaka, M. L. Tanco, F. N. D'Angelo, F. Gallucci, *Int. J. Hydrog. Energy* **2022**, 47, 14570.
- [177] M. A. L. Tanco, D. A. P. Tanaka, S. C. Rodrigues, M. Teixeira, A. Mendes, *Int. J. Hydrog. Energy* **2015**, 40, 5653.
- [178] W. Wei, G. Qin, H. Hu, L. You, G. Chen, *J. Membr. Sci.* **2007**, 303, 80.
- [179] R. Xu, L. He, L. Li, M. Hou, Y. Wang, B. Zhang, C. Liang, T. Wang, *J. Energy Chem.* **2020**, 50, 16.
- [180] G. M. Iyer, C. Zhang, *ACS Mater. Lett.* **2022**, 5, 243.

- [181] Y. Jiao, Q. Wu, W. Xu, W. Lai, L. Xiao, X. Mei, H. Zhang, S. Luo, *Sep. Purif. Technol.* **2023**, 315, 123691.
- [182] V. Pirouzfard, S. S. Hosseini, M. R. Omidkhan, A. Z. Moghaddam, *Polym. Eng. Sci.* **2014**, 54, 147.
- [183] L. Hu, V. T. Bui, A. Krishnamurthy, S. Fan, W. Guo, S. Pal, X. Chen, G. Zhang, Y. Ding, R. P. Singh, *Sci. Adv.* **2022**, 8, eabl8160.
- [184] R. Wu, W. Yue, Y. Li, A. Huang, *Mater. Lett.* **2021**, 295, 129863.
- [185] M. Hou, L. Li, Z. He, R. Xu, Y. Lu, T. Wang, *Carbon* **2023**, 205, 194.
- [186] Y.-T. Lin, J.-Y. Li, H.-H. Tseng, M.-Y. Wey, *ACS Appl. Mater. Interfaces* **2021**, 13, 5165.
- [187] H.-H. Tseng, A. K. Itta, *J. Membr. Sci.* **2012**, 389, 223.
- [188] H. Wang, L. Zhang, G. R. Gavalas, *J. Membr. Sci.* **2000**, 177, 25.
- [189] M. B. Shiflett, H. C. Foley, *J. Membr. Sci.* **2000**, 179, 275.
- [190] M. B. Shiflett, H. C. Foley, *Science* **1902**, 1999, 285.
- [191] C. Song, T. Wang, X. Wang, J. Qiu, Y. Cao, *Sep. Purif. Technol.* **2008**, 58, 412.
- [192] C. Song, T. Wang, J. Qiu, *Desalination* **2009**, 249, 486.
- [193] S. O. Lawal, K. Watanabe, R. Uchino, N. Moriyama, H. Nagasawa, T. Tsuru, M. Kanazashi, *Ind. Eng. Chem. Res.* **2024**, 63, 1554.
- [194] B. Zhang, T. Wang, S. Zhang, J. Qiu, X. Jian, *Carbon* **2006**, 44, 2764.
- [195] P. T. Ngamou, M. Ivanova, O. Guillon, W. A. Meulenber, *J. Mater. Chem. A* **2019**, 7, 7082.
- [196] M. Hou, L. Li, J. Song, R. Xu, Z. He, Y. Lu, Z. Pan, C. Song, T. Wang, *Sep. Purif. Technol.* **2022**, 301, 121982.
- [197] Y. M. Lee, Y. K. Kim, J. M. Lee, H. B. Park, *Membr. J.* **2004**, 14, 99.
- [198] J. Petersen, M. Matsuda, K. Haraya, *J. Membr. Sci.* **1997**, 131, 85.
- [199] J. Liang, Z. Wang, M. Huang, S. Wu, Y. Shi, Y. Zhang, J. Jin, *ChemSusChem* **2020**, 13, 5531.
- [200] Q. Wang, F. Huang, C. J. Cornelius, Y. Fan, *J. Membr. Sci.* **2021**, 621, 118785.
- [201] M. Hou, W. Qi, L. Li, R. Xu, J. Xue, Y. Zhang, C. Song, T. Wang, *J. Membr. Sci.* **2021**, 635, 119541.
- [202] Y. Wu, F. Wang, B. Zhang, D. Zhao, T. Wang, J. Qiu, *Asia-Pacific J. Chem. Eng.* **2018**, 13, e2251.
- [203] L. Shao, T.-S. Chung, K. Pramoda, *Microporous Mesoporous Mater.* **2005**, 84, 59.
- [204] B. T. Low, T. S. Chung, *Carbon* **2011**, 49, 2104.
- [205] X. Ma, R. Swaidan, B. Teng, H. Tan, O. Salinas, E. Litwiller, Y. Han, I. Pinnau, *Carbon* **2013**, 62, 88.
- [206] K. Okamoto, M. Yoshino, K. Noborio, H. Maeda, K. Tanaka, H. Kita, *ACS Symposium Series*, America Chemical Society, Washington, DC **1999**. DOI: [10.1021/bk-2000-0744.ch021](https://doi.org/10.1021/bk-2000-0744.ch021).
- [207] H. Li, Q. Zhang, Z. Xie, B. Zhao, Y. Yu, Y. Liu, *Carbon* **2023**, 203, 47.
- [208] Z. Dai, H. Guo, J. Deng, L. Deng, J. Yan, R. J. Spontak, *J. Membr. Sci.* **2023**, 680, 121731.
- [209] H. Guo, J. Wei, Y. Ma, Z. Qin, X. Ma, R. Selyanchyn, B. Wang, X. He, B. Tang, L. Yang, *Sep. Purif. Technol.* **2023**, 317, 123883.
- [210] K. Hazazi, Y. Wang, N. S. Bettahalli, X. Ma, Y. Xia, I. Pinnau, *J. Membr. Sci.* **2022**, 654, 120548.
- [211] J. Nie, F. Okada, H. Kita, K. Tanaka, T. Mihara, D. Kondo, Y. Yamashita, N. Yahagi, *Energy Fuel* **2022**, 36, 7147.
- [212] A. K. Itta, H.-H. Tseng, M.-Y. Wey, *J. Membr. Sci.* **2011**, 372, 387.
- [213] Y. K. Kim, H. B. Park, Y. M. Lee, *J. Membr. Sci.* **2005**, 251, 159.
- [214] S. S. Hosseini, T. S. Chung, *J. Membr. Sci.* **2009**, 328, 174.
- [215] N. Sazali, W. N. W. Salleh, A. F. Ismail, Y. Iwamoto, *Int. J. Hydrog. Energy* **2021**, 46, 24855.
- [216] M. Cai, H. Liu, J. Chen, J. Wu, Z. Han, Z. Chen, S. Zhang, Y. Min, *Microporous Mesoporous Mater.* **2024**, 365, 112889.
- [217] N. Widiastuti, A. R. Widyanto, I. S. Caralin, T. Gunawan, R. Wijiyanti, W. N. Wan Salleh, A. F. Ismail, M. Nomura, K. Suzuki, *ACS Omega* **2021**, 6, 15637.
- [218] Y. Zhang, M. Sun, L. Li, R. Xu, Y. Pan, T. Wang, *J. Membr. Sci.* **2022**, 660, 120869.
- [219] K. Shimizu, T. Ohba, *Phys. Chem. Chem. Phys.* **2017**, 19, 18201.
- [220] K. Celebi, J. Buchheim, R. M. Wyss, A. Droudian, P. Gasser, I. Shorubalko, J.-I. Kye, C. Lee, H. G. Park, *Science* **2014**, 344, 289.
- [221] S. Huang, M. Dakhchoune, W. Luo, E. Oveisi, G. He, M. Rezaei, J. Zhao, D. T. Alexander, A. Züttel, M. S. Strano, *Nat. Commun.* **2018**, 9, 2632.
- [222] T. Ashirov, A. Coskun, *Chem* **2021**, 7, 2385.
- [223] H. W. Kim, H. W. Yoon, S.-M. Yoon, B. M. Yoo, B. K. Ahn, Y. H. Cho, H. J. Shin, H. Yang, U. Paik, S. Kwon, *Science* **2013**, 342, 91.
- [224] H. Li, Z. Song, X. Zhang, Y. Huang, S. Li, Y. Mao, H. J. Ploehn, Y. Bao, M. Yu, *Science* **2013**, 342, 95.
- [225] X. Wang, C. Chi, J. Tao, Y. Peng, S. Ying, Y. Qian, J. Dong, Z. Hu, Y. Gu, D. Zhao, *Chem. Commun.* **2016**, 52, 8087.
- [226] J. Zhu, X. Meng, J. Zhao, Y. Jin, N. Yang, S. Zhang, J. Sunarso, S. Liu, *J. Membr. Sci.* **2017**, 535, 143.
- [227] C. Chi, X. Wang, Y. Peng, Y. Qian, Z. Hu, J. Dong, D. Zhao, *Chem. Mater.* **2016**, 28, 2921.
- [228] H. Lin, R. Liu, S. Dangwal, S.-J. Kim, N. Mehra, Y. Li, J. Zhu, *ACS Appl. Mater. Interfaces* **2018**, 10, 28166.
- [229] A. Ibrahim, Y. Lin, *J. Membr. Sci.* **2018**, 550, 238.
- [230] Z. Kang, S. Wang, L. Fan, M. Zhang, W. Kang, J. Pang, X. Du, H. Guo, R. Wang, D. Sun, *Commun. Chem.* **2018**, 1, 3.
- [231] S. Ma, Z. Tang, Y. Fan, J. Zhao, X. Meng, N. Yang, S. Zhuo, S. Liu, *Carbon* **2019**, 152, 144.
- [232] A. F. Ibrahim, F. Banihashemi, Y. Lin, *Chem. Commun.* **2019**, 55, 3077.
- [233] K. Huang, J. Yuan, G. Shen, G. Liu, W. Jin, *Chin. J. Chem. Eng.* **2017**, 25, 752.
- [234] L. Cheng, K. Guan, G. Liu, W. Jin, *J. Membr. Sci.* **2020**, 595, 117568.
- [235] C. Y. Chuah, L. Nie, J.-M. Lee, T.-H. Bae, *Sep. Purif. Technol.* **2020**, 246, 116933.
- [236] R. Zeynali, K. Ghasemzadeh, A. B. Sarand, F. Kheiri, A. Basile, *Sep. Purif. Technol.* **2018**, 200, 169.
- [237] X. Meng, Y. Fan, J. Zhu, Y. Jin, C. Li, N. Yang, J. Zhao, J. Sunarso, S. Liu, *Sep. Purif. Technol.* **2019**, 227, 115712.
- [238] J. Shen, G. Liu, K. Huang, Z. Chu, W. Jin, N. Xu, *ACS Nano* **2016**, 10, 3398.
- [239] K. Guan, J. Shen, G. Liu, J. Zhao, H. Zhou, W. Jin, *Sep. Purif. Technol.* **2017**, 174, 126.
- [240] G. Romanos, L. Pastrana-Martínez, T. Tsoufis, C. Athanasekou, E. Galata, F. Katsaros, E. Favvas, K. Beltsios, E. Siranidi, P. Falaras, *J. Membr. Sci.* **2015**, 493, 734.
- [241] R. Nair, H. Wu, P. N. Jayaram, I. V. Grigorieva, A. Geim, *Science* **2012**, 335, 442.
- [242] Y. Qian, F. Zhang, D. J. Kang, H. Pang, *Energy Environ. Mater.* **2023**, 6, e12414.
- [243] N. Prasetya, I. G. Wenten, M. Franzreb, C. Wöll, *Coord. Chem. Rev.* **2023**, 475, 214877.
- [244] L. E. Kreno, K. Leong, O. K. Farha, M. Allendorf, R. P. Van Duyne, J. T. Hupp, *Chem. Rev.* **2012**, 112, 1105.
- [245] Q. Qian, P. A. Asinger, M. J. Lee, G. Han, K. Mizrahi Rodriguez, S. Lin, F. M. Benedetti, A. X. Wu, W. S. Chi, Z. P. Smith, *Chem. Rev.* **2020**, 120, 8161.
- [246] S. Zhou, X. Zou, F. Sun, H. Ren, J. Liu, F. Zhang, N. Zhao, G. Zhu, *Int. J. Hydrog. Energy* **2013**, 38, 5338.
- [247] H. Jin, A. Wollbrink, R. Yao, Y. Li, J. Caro, W. Yang, *J. Membr. Sci.* **2016**, 513, 40.
- [248] C.-K. Chang, H. J. Yu, H. Jang, T.-H. Hung, J. Kim, J. S. Lee, D.-Y. Kang, *J. Membr. Sci. Lett.* **2021**, 1, 100005.
- [249] M. N. Shah, M. A. Gonzalez, M. C. McCarthy, H.-K. Jeong, *Langmuir* **2013**, 29, 7896.
- [250] W. Li, Z. Yang, G. Zhang, Z. Fan, Q. Meng, C. Shen, C. Gao, *J. Mater. Chem. A* **2014**, 2, 2110.
- [251] Y. Mao, J. Li, W. Cao, Y. Ying, L. Sun, X. Peng, *ACS Appl. Mater. Interfaces* **2014**, 6, 4473.

- [252] W. Li, Q. Meng, C. Zhang, G. Zhang, *Chem. Eur. J.* **2015**, *21*, 7224.
- [253] S. Zhou, X. Zou, F. Sun, F. Zhang, S. Fan, H. Zhao, T. Schiestel, G. Zhu, *J. Mater. Chem.* **2012**, *22*, 10322.
- [254] T. Ben, C. Lu, C. Pei, S. Xu, S. Qiu, *Chem. Eur. J.* **2012**, *18*, 10250.
- [255] S. Hurrle, S. Friebe, J. Wohlgemuth, C. Wöll, J. Caro, L. Heinke, *Chem. Eur. J.* **2017**, *23*, 2294.
- [256] H. Guo, G. Zhu, I. J. Hewitt, S. Qiu, *J. Am. Chem. Soc.* **2009**, *131*, 1646.
- [257] D. Nagaraju, D. G. Bhagat, R. Banerjee, U. K. Kharul, *J. Mater. Chem. A* **2013**, *1*, 8828.
- [258] Y. Mao, H. Huang, W. Cao, J. Li, L. Sun, X. Jin, X. Peng, *Chem. Commun.* **2013**, *49*, 5666.
- [259] Y. Hu, X. Dong, J. Nan, W. Jin, X. Ren, N. Xu, Y. M. Lee, *Chem. Commun.* **2011**, *47*, 737.
- [260] F. Zhang, X. Zou, X. Gao, S. Fan, F. Sun, H. Ren, G. Zhu, *Adv. Funct. Mater.* **2012**, *22*, 3583.
- [261] W. Li, P. Su, G. Zhang, C. Shen, Q. Meng, *J. Membr. Sci.* **2015**, *495*, 384.
- [262] N. Wang, A. Mundstock, Y. Liu, A. Huang, J. Caro, *Chem. Eng. Sci.* **2015**, *124*, 27.
- [263] D.-J. Lee, Q. Li, H. Kim, K. Lee, *Microporous Mesoporous Mater.* **2012**, *163*, 169.
- [264] S. Das, T. Ben, S. Qiu, V. Valtchev, *ACS Appl. Mater. Interfaces* **2020**, *12*, 52899.
- [265] S. Friebe, B. Geppert, F. Steinbach, J. Caro, *ACS Appl. Mater. Interfaces* **2017**, *9*, 12878.
- [266] H. Guo, J. Liu, Y. Li, J. Caro, A. Huang, *Microporous Mesoporous Mater.* **2021**, *313*, 110823.
- [267] F. Cacho-Bailo, S. Catalan-Aguirre, M. Etxeberria-Benavides, O. Karvan, V. Sebastian, C. Tellez, J. Coronas, *J. Membr. Sci.* **2015**, *476*, 277.
- [268] Y. Li, F. Liang, H. Bux, W. Yang, J. Caro, *J. Membr. Sci.* **2010**, *354*, 48.
- [269] V. M. A. Melgar, H. T. Kwon, J. Kim, *J. Membr. Sci.* **2014**, *459*, 190.
- [270] W. Li, Q. Meng, X. Li, C. Zhang, Z. Fan, G. Zhang, *Chem. Commun.* **2014**, *50*, 9711.
- [271] S. Zhang, Z. Wang, H. Ren, F. Zhang, J. Jin, *J. Mater. Chem. A* **1962**, *2017*, 5.
- [272] M. C. McCarthy, V. Varela-Guerrero, G. V. Barnett, H.-K. Jeong, *Langmuir* **2010**, *26*, 14636.
- [273] O. Shekhah, R. Swaidan, Y. Belmabkhout, M. Du Plessis, T. Jacobs, L. J. Barbour, I. Pinnau, M. Eddaoudi, *Chem. Commun.* **2014**, *50*, 2089.
- [274] X. Zhang, Y. Liu, L. Kong, H. Liu, J. Qiu, W. Han, L.-T. Weng, K. L. Yeung, W. Zhu, *J. Mater. Chem. A* **2013**, *1*, 10635.
- [275] V. Chernikova, O. Shekhah, M. Eddaoudi, *ACS Appl. Mater. Interfaces* **2016**, *8*, 20459.
- [276] Y. Liu, Y. Peng, N. Wang, Y. Li, J. H. Pan, W. Yang, J. Caro, *ChemSusChem* **2015**, *8*, 3582.
- [277] G. He, M. Dakhchoune, J. Zhao, S. Huang, K. V. Agrawal, *Adv. Funct. Mater.* **2018**, *28*, 1707427.
- [278] H. Yin, J. Shang, J. Choi, A. C. Yip, *Microporous Mesoporous Mater.* **2019**, *280*, 347.
- [279] P. Hu, Y. Yang, Y. Mao, J. Li, W. Cao, Y. Ying, Y. Liu, J. Lei, X. Peng, *CrystEngComm* **2015**, *17*, 1576.
- [280] M. Drobek, M. Bechelany, C. Vallicari, A. Abou Chaaya, C. Charmette, C. Salvador-Levehang, P. Miele, A. Julbe, *J. Membr. Sci.* **2015**, *475*, 39.
- [281] Y. Liu, N. Wang, J. H. Pan, F. Steinbach, J. Caro, *J. Am. Chem. Soc.* **2014**, *136*, 14353.
- [282] X. Zhang, Y. Liu, S. Li, L. Kong, H. Liu, Y. Li, W. Han, K. L. Yeung, W. Zhu, W. Yang, *Chem. Mater.* **1975**, *2014*, 26.
- [283] J. Li, W. Cao, Y. Mao, Y. Ying, L. Sun, X. Peng, *CrystEngComm* **2014**, *16*, 9788.
- [284] H. Chen, X. Wang, Y. Liu, T. Yang, N. Yang, B. Meng, X. Tan, S. Liu, *J. Membr. Sci.* **2021**, *640*, 119851.
- [285] Y. Pan, B. Wang, Z. Lai, *J. Membr. Sci.* **2012**, *421*, 292.
- [286] K. Huang, Z. Dong, Q. Li, W. Jin, *Chem. Commun.* **2013**, *49*, 10326.
- [287] X. Wang, M. Sun, B. Meng, X. Tan, J. Liu, S. Wang, S. Liu, *Chem. Commun.* **2016**, *52*, 13448.
- [288] E. Shamsaei, X. Lin, Z.-X. Low, Z. Abbasi, Y. Hu, J. Z. Liu, H. Wang, *ACS Appl. Mater. Interfaces* **2016**, *8*, 6236.
- [289] J. Hou, P. D. Sutrisna, Y. Zhang, V. Chen, *Angew. Chem. Int. Ed.* **2016**, *55*, 3947.
- [290] E. Shamsaei, X. Lin, L. Wan, Y. Tong, H. Wang, *Chem. Commun.* **2016**, *52*, 13764.
- [291] P. Su, W. Li, C. Zhang, Q. Meng, C. Shen, G. Zhang, *J. Mater. Chem. A* **2015**, *3*, 20345.
- [292] G. Zhang, K. Tang, X. Zhang, L. Xu, C. Shen, Q. Meng, *J. Membr. Sci.* **2021**, *617*, 118612.
- [293] Y. Li, C. Ma, P. Nian, H. Liu, X. Zhang, *J. Membr. Sci.* **2019**, *581*, 344.
- [294] J. Hao, D. J. Babu, Q. Liu, H.-Y. Chi, C. Lu, Y. Liu, K. V. Agrawal, *J. Mater. Chem. A* **2020**, *8*, 7633.
- [295] L. Kong, X. Zhang, H. Liu, J. Qiu, *J. Membr. Sci.* **2015**, *490*, 354.
- [296] H. Bux, F. Liang, Y. Li, J. Cravillon, M. Wiebcke, J. Caro, *J. Am. Chem. Soc.* **2009**, *131*, 16000.
- [297] W. Li, P. Su, Z. Li, Z. Xu, F. Wang, H. Ou, J. Zhang, G. Zhang, E. Zeng, *Nat. Commun.* **2017**, *8*, 406.
- [298] D. J. Babu, G. He, J. Hao, M. T. Vahdat, P. A. Schouwink, M. Mensi, K. V. Agrawal, *Adv. Mater.* **2019**, *31*, 1900855.
- [299] J. Liu, C. Liu, A. Huang, *Int. J. Hydrog. Energy* **2020**, *45*, 703.
- [300] P. Nian, Y. Li, X. Zhang, Y. Cao, H. Liu, X. Zhang, *ACS Appl. Mater. Interfaces* **2018**, *10*, 4151.
- [301] A. Knebel, P. Wulfert-Holzmann, S. Friebe, J. Pavel, I. Strauß, A. Mundstock, F. Steinbach, J. Caro, *Chem. Eur. J.* **2018**, *24*, 5728.
- [302] Z. Zhou, C. Wu, B. Zhang, *Ind. Eng. Chem. Res.* **2020**, *59*, 3182.
- [303] X. Dong, K. Huang, S. Liu, R. Ren, W. Jin, Y. Lin, *J. Mater. Chem.* **2012**, *22*, 19222.
- [304] A. Huang, W. Dou, J. Caro, *J. Am. Chem. Soc.* **2010**, *132*, 15562.
- [305] A. Huang, J. Caro, *Angew. Chem. Int. Ed.* **2011**, *21*, 4979.
- [306] A. Huang, N. Wang, C. Kong, J. Caro, *Angew. Chem. Int. Ed. Engl.* **2012**, *51*, 10551.
- [307] A. Huang, Y. Chen, N. Wang, Z. Hu, J. Jiang, J. Caro, *Chem. Commun.* **2012**, *48*, 10981.
- [308] X. Ma, Y. Li, A. Huang, *J. Membr. Sci.* **2020**, *597*, 117629.
- [309] X. Ma, Z. Wan, Y. Li, X. He, J. Caro, A. Huang, *Angew. Chem.* **2020**, *132*, 21044.
- [310] N. Wang, Y. Liu, Z. Qiao, L. Diestel, J. Zhou, A. Huang, J. Caro, *J. Mater. Chem. A* **2015**, *3*, 4722.
- [311] D. Zou, D. Liu, J. Zhang, *Energy Environ. Mater.* **2018**, *1*, 209.
- [312] F. Cacho-Bailo, I. Matito-Martos, J. Perez-Carabajo, M. Etxeberria-Benavides, O. Karvan, V. Sebastián, S. Calero, C. Tellez, J. Coronas, *Chem. Sci.* **2017**, *8*, 325.
- [313] Y. Song, Y. Sun, D. Du, M. Zhang, Y. Liu, L. Liu, T. Ji, G. He, *J. Membr. Sci.* **2021**, *634*, 119393.
- [314] Y. Peng, Y. Li, Y. Ban, H. Jin, W. Jiao, X. Liu, W. Yang, *Science* **2014**, *346*, 1356.
- [315] Y. Peng, Y. Li, Y. Ban, W. Yang, *Angew. Chem.* **2017**, *129*, 9889.
- [316] S. Song, W. Wang, Y. Zhao, W. Wu, Y. Wei, H. Wang, *Angew. Chem. Int. Ed.* **2023**, *62*, e202312995.
- [317] K. Yang, S. Hu, Y. Ban, Y. Zhou, N. Cao, M. Zhao, Y. Xiao, W. Li, W. Yang, *Sci. Bull.* **1869**, *2021*, 66.
- [318] P. Nian, H. Liu, X. Zhang, *J. Membr. Sci.* **2019**, *573*, 200.
- [319] H. Song, Y. Peng, C. Wang, L. Shu, C. Zhu, Y. Wang, H. He, W. Yang, *Angew. Chem. Int. Ed.* **2023**, *62*, e202218472.
- [320] Y. Wang, H. Jin, Q. Ma, K. Mo, H. Mao, A. Feldhoff, X. Cao, Y. Li, F. Pan, Z. Jiang, *Angew. Chem.* **2020**, *132*, 4395.
- [321] H. Fan, A. Mundstock, A. Feldhoff, A. Knebel, J. Gu, H. Meng, J. Caro, *J. Am. Chem. Soc.* **2018**, *140*, 10094.
- [322] J. Fu, S. Das, G. Xing, T. Ben, V. Valtchev, S. Qiu, *J. Am. Chem. Soc.* **2016**, *138*, 7673.

- [323] B. Li, Z. Wang, Z. Gao, J. Suo, M. Xue, Y. Yan, V. Valtchev, S. Qiu, Q. Fang, *Adv. Funct. Mater.* **2023**, 33, 2300219.
- [324] H. Lu, C. Wang, J. Chen, R. Ge, W. Leng, B. Dong, J. Huang, Y. Gao, *Chem. Commun.* **2015**, 51, 15562.
- [325] J. Fu, T. Ben, *Acta Chim. Sin.* **2020**, 78, 805.
- [326] H. Fan, M. Peng, I. Strauss, A. Mundstock, H. Meng, J. Caro, *J. Am. Chem. Soc.* **2020**, 142, 6872.
- [327] Y. Ying, M. Tong, S. Ning, S. K. Ravi, S. B. Peh, S. C. Tan, S. J. Pennycook, D. Zhao, *J. Am. Chem. Soc.* **2020**, 142, 4472.
- [328] W. Zheng, J. Hou, C. Liu, P. Liu, L. Li, L. Chen, Z. Tang, *Chem. Asian J.* **2021**, 16, 3624.
- [329] D. Xu, Y. Jin, C. Li, Y. Fan, S. Kawi, X. Meng, J. Song, N. Yang, *J. Membr. Sci.* **2024**, 700, 122678.
- [330] H. Fan, M. Peng, I. Strauss, A. Mundstock, H. Meng, J. Caro, *Nat. Commun.* **2021**, 12, 38.
- [331] K. Qi, J. Yu, Y. Gao, L. Shi, Q. Yi, X. Li, J. Zeng, L. Gao, L. Gao, *Langmuir* **2024**, 7, 330.
- [332] P. M. Budd, B. S. Ghanem, S. Makhseed, N. B. McKeown, K. J. Msayib, C. E. Tattershall, *Chem. Commun.* **2004**, DOI: [10.1039/B311764B](https://doi.org/10.1039/B311764B).
- [333] P. M. Budd, E. S. Elabas, B. S. Ghanem, S. Makhseed, N. B. McKeown, K. J. Msayib, C. E. Tattershall, D. Wang, *Adv. Mater.* **2004**, 16, 456.
- [334] Y. Wang, X. Ma, B. Ghanem, F. Alghunaimi, I. Pinnau, Y. Han, *Mater. Today Nano* **2018**, 3, 69.
- [335] W. H. Lee, J. G. Seong, X. Hu, Y. M. Lee, *J. Polym. Sci.* **2020**, 58, 2450.
- [336] P. M. Budd, K. J. Msayib, C. E. Tattershall, B. S. Ghanem, K. J. Reynolds, N. B. McKeown, D. Fritsch, *J. Membr. Sci.* **2005**, 251, 263.
- [337] J. Zhang, H. Kang, J. Martin, S. Zhang, S. Thomas, T. C. Merkel, J. Jin, *Chem. Commun.* **2016**, 52, 6553.
- [338] J. Wu, J. Liu, T. Chung, *Adv. Sustain. Syst.* **2018**, 2, 1800044.
- [339] M. Carta, P. Bernardo, G. Clarizia, J. C. Jansen, N. B. McKeown, *Macromolecules* **2014**, 47, 8320.
- [340] C. G. Bezzu, M. Carta, A. Tonkins, J. C. Jansen, P. Bernardo, F. Bazzarelli, N. B. McKeown, *Adv. Mater.* **2012**, 24, 5930.
- [341] C. G. Bezzu, M. Carta, M.-C. Ferrari, J. C. Jansen, M. Monteleone, E. Esposito, A. Fuoco, K. Hart, T. Liyana-Arachchi, C. M. Colina, *J. Mater. Chem. A* **2018**, 6, 10507.
- [342] B. S. Ghanem, N. B. McKeown, P. M. Budd, D. Fritsch, *Macromolecules* **2008**, 41, 1640.
- [343] I. Rose, C. G. Bezzu, M. Carta, B. Comesaña-Gándara, E. Lasseuguette, M. C. Ferrari, P. Bernardo, G. Clarizia, A. Fuoco, J. C. Jansen, *Nat. Mater.* **2017**, 16, 932.
- [344] B. S. Ghanem, R. Swaidan, X. Ma, E. Litwiller, I. Pinnau, *Adv. Mater.* **2014**, 26, 6696.
- [345] A. Fuoco, B. Comesaña-Gándara, M. Longo, E. Esposito, M. Monteleone, I. Rose, C. G. Bezzu, M. Carta, N. B. McKeown, J. C. Jansen, *ACS Appl. Mater. Interfaces* **2018**, 10, 36475.
- [346] M. Carta, M. Croad, R. Malpass-Evans, J. C. Jansen, P. Bernardo, G. Clarizia, K. Friess, M. Lanč, N. B. McKeown, *Adv. Mater.* **2014**, 26, 3526.
- [347] M. Carta, R. Malpass-Evans, M. Croad, Y. Rogan, J. C. Jansen, P. Bernardo, F. Bazzarelli, N. B. McKeown, *Science* **2013**, 339, 303.
- [348] R. Williams, L. A. Burt, E. Esposito, J. C. Jansen, E. Tocci, C. Rizzuto, M. Lanč, M. Carta, N. B. McKeown, *J. Mater. Chem. A* **2018**, 6, 5661.
- [349] M. Carta, M. Croad, J. C. Jansen, P. Bernardo, G. Clarizia, N. B. McKeown, *Polym. Chem.* **2014**, 5, 5255.
- [350] I. Rose, M. Carta, R. Malpass-Evans, M.-C. Ferrari, P. Bernardo, G. Clarizia, J. C. Jansen, N. B. McKeown, *ACS Macro Lett.* **2015**, 4, 912.
- [351] B. S. Ghanem, N. B. McKeown, P. M. Budd, N. M. Al-Harbi, D. Fritsch, K. Heinrich, L. Starannikova, A. Tokarev, Y. Yampolskii, *Macromolecules* **2009**, 42, 7881.
- [352] B. S. Ghanem, N. B. McKeown, P. M. Budd, J. D. Selbie, D. Fritsch, *Adv. Mater.* **2008**, 20, 2766.
- [353] Y. Rogan, L. Starannikova, V. Ryzhikh, Y. Yampolskii, P. Bernardo, F. Bazzarelli, J. C. Jansen, N. B. McKeown, *Polym. Chem.* **2013**, 4, 3813.
- [354] R. Swaidan, M. Al-Saeedi, B. Ghanem, E. Litwiller, I. Pinnau, *Macromolecules* **2014**, 47, 5104.
- [355] X. Ma, B. Ghanem, O. Salinas, E. Litwiller, I. Pinnau, *ACS Macro Lett.* **2015**, 4, 231.
- [356] B. Ghanem, F. Alghunaimi, X. Ma, N. Alaslai, I. Pinnau, *Polymer* **2016**, 101, 225.
- [357] X. Ma, I. Pinnau, *Macromolecules* **2018**, 51, 1069.
- [358] Y. Rogan, R. Malpass-Evans, M. Carta, M. Lee, J. C. Jansen, P. Bernardo, G. Clarizia, E. Tocci, K. Friess, M. Lanč, *J. Mater. Chem. A* **2014**, 2, 4874.
- [359] X. Ma, M. A. Abdulhamid, I. Pinnau, *Macromolecules* **2017**, 50, 5850.
- [360] X. Ma, O. Salinas, E. Litwiller, I. Pinnau, *Macromolecules* **2013**, 46, 9618.
- [361] Y. Zhuang, J. G. Seong, Y. S. Do, W. H. Lee, M. J. Lee, M. D. Guiver, Y. M. Lee, *J. Membr. Sci.* **2016**, 504, 55.
- [362] Y. Zhuang, J. G. Seong, Y. S. Do, H. J. Jo, Z. Cui, J. Lee, Y. M. Lee, M. D. Guiver, *Macromolecules* **2014**, 47, 3254.
- [363] Z. Wang, D. Wang, F. Zhang, J. Jin, *ACS Macro Lett.* **2014**, 3, 597.
- [364] Z. Wang, D. Wang, J. Jin, *Macromolecules* **2014**, 47, 7477.
- [365] M. Lee, C. G. Bezzu, M. Carta, P. Bernardo, G. Clarizia, J. C. Jansen, N. B. McKeown, *Macromolecules* **2016**, 49, 4147.
- [366] B. Ghanem, N. Alaslai, X. Miao, I. Pinnau, *Polymer* **2016**, 96, 13.
- [367] X. Hu, W. H. Lee, J. Zhao, J. Y. Bae, J. S. Kim, Z. Wang, J. Yan, Y. Zhuang, Y. M. Lee, *J. Membr. Sci.* **2020**, 610, 118255.
- [368] X. Hu, W. H. Lee, J. Y. Bae, J. Zhao, J. S. Kim, Z. Wang, J. Yan, Y. M. Lee, *J. Membr. Sci.* **2020**, 615, 118533.
- [369] J. R. Wiegand, Z. P. Smith, Q. Liu, C. T. Patterson, B. D. Freeman, R. Guo, *J. Mater. Chem. A* **2014**, 2, 13309.
- [370] F. Alghunaimi, B. Ghanem, N. Alaslai, R. Swaidan, E. Litwiller, I. Pinnau, *J. Membr. Sci.* **2015**, 490, 321.
- [371] S. Luo, Q. Liu, B. Zhang, J. R. Wiegand, B. D. Freeman, R. Guo, *J. Membr. Sci.* **2015**, 480, 20.
- [372] R. Swaidan, B. S. Ghanem, E. Litwiller, I. Pinnau, *J. Membr. Sci.* **2014**, 457, 95.
- [373] N. Du, G. P. Robertson, J. Song, I. Pinnau, M. D. Guiver, *Macromolecules* **2009**, 42, 6038.
- [374] J. W. Jeon, D.-G. Kim, E. Sohn, Y. Yoo, Y. S. Kim, B. G. Kim, J.-C. Lee, *Macromolecules* **2017**, 50, 8019.
- [375] C. Zhang, L. Fu, Z. Tian, B. Cao, P. Li, *J. Membr. Sci.* **2018**, 556, 277.
- [376] X. Ma, R. Swaidan, Y. Belmabkhout, Y. Zhu, E. Litwiller, M. Jouiad, I. Pinnau, Y. Han, *Macromolecules* **2012**, 45, 3841.
- [377] C. R. Mason, L. Maynard-Atem, N. M. Al-Harbi, P. M. Budd, P. Bernardo, F. Bazzarelli, G. Clarizia, J. C. Jansen, *Macromolecules* **2011**, 44, 6471.
- [378] W. Ji, H. Geng, Z. Chen, H. Dong, H. Matsuyama, H. Wang, H. Wang, J. Li, W. Shi, X. Ma, *J. Membr. Sci.* **2022**, 662, 120971.
- [379] M. Huang, K. Lu, Z. Wang, X. Bi, Y. Zhang, J. Jin, *ACS Sustain. Chem. Eng.* **2021**, 9, 9426.
- [380] J. Wu, S. Japip, T.-S. Chung, *J. Mater. Chem. A* **2020**, 8, 6196.
- [381] S. Thomas, I. Pinnau, N. Du, M. D. Guiver, *J. Membr. Sci.* **2009**, 333, 125.
- [382] R. Swaidan, B. Ghanem, E. Litwiller, I. Pinnau, *Macromolecules* **2015**, 48, 6553.
- [383] S. Bandehali, A. E. Amooghin, H. Sanaeepur, R. Ahmadi, A. Fuoco, J. C. Jansen, S. Shirazian, *Sep. Purif. Technol.* **2021**, 278, 119513.
- [384] Y. S. Do, J. G. Seong, S. Kim, J. G. Lee, Y. M. Lee, *J. Membr. Sci.* **2013**, 446, 294.
- [385] S. Kim, J. G. Seong, Y. S. Do, Y. M. Lee, *J. Membr. Sci.* **2015**, 474, 122.
- [386] S. H. Han, H. J. Kwon, K. Y. Kim, J. G. Seong, C. H. Park, S. Kim, C. M. Doherty, A. W. Thornton, A. J. Hill, Á. E. Lozano, *Phys. Chem. Chem. Phys.* **2012**, 14, 4365.
- [387] J. S. Kim, S. J. Moon, H. H. Wang, S. Kim, Y. M. Lee, *J. Membr. Sci.* **2019**, 582, 381.
- [388] H. D. Patel, N. K. Acharya, *Polym. Eng. Sci.* **2021**, 61, 2782.

- [389] C. Y. Soo, H. J. Jo, Y. M. Lee, J. R. Quay, M. K. Murphy, *J. Membr. Sci.* **2013**, *444*, 365.
- [390] S. H. Han, N. Misdan, S. Kim, C. M. Doherty, A. J. Hill, Y. M. Lee, *Macromolecules* **2010**, *43*, 7657.
- [391] M. Calle, Y. M. Lee, *Macromolecules* **2011**, *44*, 1156.
- [392] Y. F. Yeong, H. Wang, K. P. Pramoda, T.-S. Chung, *J. Membr. Sci.* **2012**, *397*, 51.
- [393] A. Yerzhankzy, B. S. Ghanem, Y. Wang, N. Alaslai, I. Pinnau, *J. Membr. Sci.* **2020**, *595*, 117512.
- [394] S. Luo, Q. Zhang, L. Zhu, H. Lin, B. A. Kazanowska, C. M. Doherty, A. J. Hill, P. Gao, R. Guo, *Chem. Mater.* **2018**, *30*, 5322.
- [395] S. Luo, Q. Zhang, T. K. Bear, T. E. Curtis, R. K. Roeder, C. M. Doherty, A. J. Hill, R. Guo, *J. Membr. Sci.* **2018**, *551*, 305.
- [396] F. Alghunaimi, B. Ghanem, Y. Wang, O. Salinas, N. Alaslai, I. Pinnau, *Polymer* **2017**, *121*, 9.
- [397] S. Luo, J. Liu, H. Lin, B. A. Kazanowska, M. D. Hunckler, R. K. Roeder, R. Guo, *J. Mater. Chem. A* **2016**, *4*, 17050.
- [398] S. Li, H. J. Jo, S. H. Han, C. H. Park, S. Kim, P. M. Budd, Y. M. Lee, *J. Membr. Sci.* **2013**, *434*, 137.
- [399] X. Ma, O. Salinas, E. Litwiller, I. Pinnau, *Polym. Chem.* **2014**, *5*, 6914.
- [400] H. Shamsipur, B. A. Dawood, P. M. Budd, P. Bernardo, G. Clarizia, J. C. Jansen, *Macromolecules* **2014**, *47*, 5595.
- [401] M. Calle, H. J. Jo, C. M. Doherty, A. J. Hill, Y. M. Lee, *Macromolecules* **2015**, *48*, 2603.
- [402] M. Calle, C. M. Doherty, A. J. Hill, Y. M. Lee, *Macromolecules* **2013**, *46*, 8179.
- [403] X. Hu, W. H. Lee, J. Zhao, J. S. Kim, Z. Wang, J. Yan, Y. Zhuang, Y. M. Lee, *J. Membr. Sci.* **2020**, *604*, 118053.
- [404] H. J. Jo, C. Y. Soo, G. Dong, Y. S. Do, H. H. Wang, M. J. Lee, J. R. Quay, M. K. Murphy, Y. M. Lee, *Macromolecules* **2015**, *48*, 2194.
- [405] Y. Zhuang, J. G. Seong, W. H. Lee, Y. S. Do, M. J. Lee, G. Wang, M. D. Guiver, Y. M. Lee, *Macromolecules* **2015**, *48*, 5286.
- [406] Y. Wang, Z. Low, S. Kim, H. Zhang, X. Chen, J. Hou, J. G. Seong, Y. M. Lee, G. P. Simon, C. H. Davies, *Angew. Chem.* **2018**, *130*, 16288.
- [407] W. Li, Y. Zhang, P. Su, Z. Xu, G. Zhang, C. Shen, Q. Meng, *J. Mater. Chem. A* **2016**, *4*, 18747.
- [408] M. Jia, Y. Feng, S. Liu, J. Qiu, J. Yao, *J. Membr. Sci.* **2017**, *539*, 172.
- [409] A. Huang, Q. Liu, N. Wang, Y. Zhu, J. Caro, *J. Am. Chem. Soc.* **2014**, *136*, 14686.
- [410] Y. Li, H. Liu, H. Wang, J. Qiu, X. Zhang, *Chem. Sci.* **2018**, *9*, 4132.
- [411] H. Guo, G. Kong, G. Yang, J. Pang, Z. Kang, S. Feng, L. Zhao, L. Fan, L. Zhu, A. Vicente, *Angew. Chem.* **2020**, *132*, 6343.
- [412] E. Aliyev, J. Warfsmann, B. Tokay, S. Shishatskiy, Y.-J. Lee, J. Lillepaerg, N. R. Champness, V. Filiz, *ACS Sustain. Chem. Eng.* **2020**, *9*, 684.
- [413] Y. Sun, F. Fan, L. Bai, T. Li, J. Guan, F. Sun, Y. Liu, W. Xiao, G. He, C. Ma, *Results Eng.* **2023**, *20*, 101398.
- [414] K. Zhang, X. Luo, S. Li, X. Tian, Q. Wang, C. Liu, Y. Tang, X. Feng, R. Zhang, S. Yin, *Chem. Eng. J.* **2024**, *484*, 149489.
- [415] S. Han, Z. Wang, J. Yu, F. Wang, X. Li, *J. Clean. Prod.* **2024**, *448*, 141737.
- [416] S. Xiong, C. Pan, G. Dai, C. Liu, Z. Tan, C. Chen, S. Yang, X. Ruan, J. Tang, G. Yu, *J. Membr. Sci.* **2022**, *645*, 120217.
- [417] R. Wu, Y. Li, A. Huang, *J. Membr. Sci.* **2021**, *620*, 118841.
- [418] L. Pilz, C. Natzeck, J. Wohlgemuth, N. Scheuermann, S. Spiegel, S. Oßwald, A. Knebel, S. Bräse, C. Wöll, M. Tsotsalas, N. Prasetya, *J. Mater. Chem. A* **2023**, *11*, 24724.
- [419] P. M. Budd, N. B. McKeown, *Polym. Chem.* **2010**, *1*, 63.
- [420] R. Swaidan, B. Ghanem, I. Pinnau, *ACS Macro Letters* **2015**, *4*.
- [421] N. Prasetya, H. C. Gülbalkan, S. Keskin, C. Wöll, *Carbon Capture Sci. Technol.* **2024**, *13*, 100252.